Particulate Rare Earth Element behavior in the North Atlantic (GEOVIDE cruise)

Marion Lagarde[1], Nolwenn Lemaitre[2], Hélène Planquette[3], Mélanie Grenier[1], Moustafa Belhadj[1], Pascale Lherminier[4], Catherine Jeandel[1]

[1] LEGOS, University of Toulouse, CNRS, CNES, IRD, UPS, Toulouse, 31400, France
[2] ETH, Zurich, IGP, Zurich, Switzerland
[3] LEMAR, University of Brest, CNRS, IRD, Ifremer, Plouzané, 29280, France
[4] LOPS, Ifremer, CNRS, IRD, UBO, Ifremer, Plouzané, 29280, France

Correspondence to: Marion Lagarde (marion.lagarde@legos.obs-mip.fr)

Abstract. Particulate concentrations of the fourteen Rare Earth Elements (PREE), yttrium and 232-thorium were measured in 200 samples collected in the epipelagic (ca 0-200 m) and the mesopelagic (ca 200-1500 m) zones of the North Atlantic, during the GEOVIDE cruise (May/June 2014, R/V Pourquoi Pas?, GEOTRACES GA01), providing the most detailed snapshot of the PREE distribution in the North Atlantic so far. Concentrations of particulate cerium (PCe) varied between 0.2 pmol L^{-1} and 16 pmol L^{-1}, while particulate neodymium (PNd) concentrations ranged between 0.1 pmol L^{-1} and 6.1 pmol L^{-1}. Particulate ytterbium (PYb) concentrations ranged between 0.01 pmol L^{-1} and 0.50 pmol L^{-1}. In addition, this study showed that PREE distributions were also controlled by the biological production in the upper sunlit ocean and by remineralization processes in the mesopelagic area. Low surface concentrations combined with normalized PREE patterns displaying a negative Ce anomaly and HREE enrichments pointed to freshly formed biogenic particles imprinting the seawater signature. A significant relationship between biogenic silica (BSi) and PHREE was also observed in the Labrador and Irminger Seas, due to the occurrence of strong diatom blooms at the sampling time. In order to identify dissolved-particulate processes independent of the ionic radius, we used PHo/PY ratios and showed that absorption processes were predominant in the upper ocean while adsorption processes dominated at deeper depths.

This study highlighted different lithogenic fractions of PREE and dispersion depending on the shelf: off the Iberian margin, up to 100% of the PREE were determined to have a lithogenic origin. This lithogenic input spread westward along an intermediate nepheloid layer (INL), following isopycnals up to 1700 km away from the margin. In contrast, along the Greenland and Newfoundland margins, the circulation maintained lithogenic inputs of PREE along the coasts.

1 Introduction

Particles and water mass circulation are the main vectors in transferring chemical species from the surface to the deep ocean (Gehlen et al., 2006; Kwon et al., 2009; Lam and Marchal, 2015; Ohnemus and Lam, 2015). Particles are abundant in the upper ocean (up to 1000 µg L^{-1}), where dust inputs or important blooms occur, and their concentration decrease with depth in the

subsurface and deep ocean (5 to 60 µg L^{-1} on average, McCave and Hall, 2002; Stemmann et al., 2002). Particles are usually divided in two classes: large sinking particles that dominate the vertical flux, and small particles that are in suspension in the water column. These small suspended particles represent over 80% of the total particle mass (Lam et al., 2015 and references therein). In addition, their higher surface to volume ratios make suspended particles the main drivers of dissolved-particulate exchanges (Crecelius, 1980; Trull and Armand, 2001). Elements are up to 1000 times more concentrated in particles than in the dissolved phase (Lam et al., 2015), and among them trace metals are especially enriched in particles. For example, in the subpolar North Atlantic, particulate iron (PFe) concentrations can reach 50 nmol L^{-1} while dissolved Fe concentrations does not exceed 2.5 nmol L^{-1} (Tonnard et al., 2020). As the size spectrum between the particulate and the dissolved phase is continuous, the separation between the two pools is truly operational, based on the porosity of the filters used to discriminate the two phases, usually 0.4 µm (Planquette and Sherrell, 2012). Concentrations may then depend on the choice of this limit.

In the ocean, three main sources of particles are distinguishable (Fowler and Knauer, 1986; Jeandel et al., 2015; Lam et al., 2015 and references therein). The first one is lithogenic, with inputs from the rivers, dust deposits, ice melting and resuspension of deposited sediments. The second is biogenic, and related to the production of fresh organic matter by photosynthetic activity followed by zooplankton grazing, and the following food web activity. The last one results from authigenic processes such as the precipitation and formation of red clays, oxides and hydroxides. All these sources and processes lead to a very heterogeneous pool, in time, space and composition, evolving throughout their stay in the ocean and controlling the density of particles, and consequently their fate in the water column. Then, exchanges between the particulate and dissolved phases determine the chemistry of seawater and the residence time of the chemical species in the ocean (Jeandel et al., 2015; Jeandel and Oelkers, 2015; Turekian, 1977).

Oceanic tracers such as rare earth elements (REE) are adapted to the study of these exchanges (Jeandel et al., 1995; Kuss et al., 2001; Tachikawa et al., 1999b). Rare earth elements form a homogenous family characterized by a gradual filling of the 4f orbital as their atomic number increase. Except for cerium (Ce), their external orbital comprises three electrons, rendering their chemical properties relatively similar. However, the increasing weight concomitant with an increasing atomic number and the decreasing ionic radius generates slight differences between the light and heavy REE behaviors (LREE and HREE respectively). In seawater REE are mostly complexed by carbonates, this complexation increasing with the atomic number: 86% of lanthanum (La, the first REE of the series) is found as carbonates complexes, while this proportion is 99% of lutetium (Lu, the last REE of the series) (Schijf et al., 2015). Thus, the REE will react differently in the water column depending on various physical and geochemical processes such as aggregation-disaggregation, dissolution, complexation, sorption, mineralization and scavenging. These processes will lead to a fractionation along the REE series. Consequently, measuring the distribution of REEs between the solid and dissolved phases can help tracing and quantifying these processes.

Documenting these exchanges in the subarctic North Atlantic using REE among other tracers was one of the goals of the GEOVIDE cruise (2014, GA01 GEOTRACES cruise; Fig. 1). The North Atlantic is a key region of the global ocean, as it is the most important oceanic sink of anthropogenic CO_2 (Khatiwala et al., 2013), and it is i) a major place of deep water formation, mainly by convection, which drives the Atlantic meridional overturning circulation (AMOC), and ii) a productive

area, representing up to 18% of the global oceanic primary production (Sanders et al., 2014). The GEOVIDE section investigated stations close to the Iberian, Greenland and Canadian coasts and crossed areas of contrasted surface productivity. This cruise was part of the GEOTRACES program, which aims to document trace elements cycles in the ocean by a better understanding of their sources and sinks, including their export by particles (Henderson et al., 2007). Constraining the drivers of the particle-solution exchanges is thus an important issue in this area.

In this context, we present the first basin scale section of PREE concentrations and fractionation patterns in suspended particles collected in the Subpolar North Atlantic (SPNA), along the GEOVIDE section, from the surface to 1500 m depth. In the following, we specifically discuss processes affecting the PREE distribution such as lithogenic inputs from the margins, influence of biological activity and the role of ionic radius on their fate in the water column.

2 Methods

2.1 Study area: hydrographical and biogeochemical context

Samples were collected in the epipelagic and mesopelagic zones (0 m – 1500 m) during the GEOVIDE cruise (16th of May 2014 to 30th of June 2014, R/V Pourquoi Pas?) along the transect presented in Fig. 1. This figure also presents the main surface currents, as described in details in Zunino et al. (2017) and García-Ibáñez et al. (2018), together with the three main biogeochemical provinces identified by Longhurst (1995) and described in details by Lemaitre et al. (2018b): the subtropical North Atlantic (NAST), the North Atlantic drift (NADR) and the Arctic (ARCT) regions. The location of the stations where suspended particles were sampled (Fig. 1) were chosen to be representative of the diversity of water masses (Fig. 2) and biogeochemical provinces (Sarthou et al., 2018). Warm and salty waters coming from the tropical Atlantic are advected towards the Arctic by the North Atlantic Current (NAC, see Table 1 for abbreviation list). In response to air-sea exchanges and mixing with polar waters, surface waters become colder and fresher, but more importantly, denser. Thus, they tend to mix with underlying waters, particularly during convection events triggered by storms. In the Nordic Seas (between 65°N and 80°N), the water column can be ventilated down to the bottom, while convection never exceeds 2000 m in the subpolar gyre. The freshly formed deep water then returns southwards mainly through western boundary currents (Daniault et al., 2016; García-Ibáñez et al., 2015, 2018; Zunino et al., 2017).

At the south east end of the section, the North Atlantic subtropical (NAST) province is characterized by warm and salty waters (García-Ibáñez et al., 2018; Longhurst, 1995; Reygondeau et al., 2018; Zunino et al., 2017). This province is depleted in nutrients despite being under influence of continental inputs, and was sampled during the declining stage of the cyanobacteria bloom (Lemaitre et al., 2018b). Stations #1 and #13 were sampled in the NAST. The North Atlantic Drift region (NADR) is located between the NAST and the Reykjanes ridge, with higher nutrient concentrations than in the NAST (Longhurst, 1995).

A strong bloom of coccolithophorids, with a maximum intensity in the Icelandic basin, was occurring during the sampling time, and was associated with the highest primary production rate determined during the GEOVIDE cruise (1740 molC m^{-2} d^{-1}, station #26, Fonseca-Batista et al., 2019) and with high carbon export (up to 80 molC m^{-2} d^{-1}, station #32, Lemaitre et al., 2018b). Four open ocean stations were sampled in this province: within the southern branch of the NAC (stations #21 and #32), at the Subpolar front (station #26) and above the Reykjanes Ridge (station #38).

West of the Reykjanes Ridge, the Irminger and Labrador Seas (Fig. 1) located in the Arctic region (ARCT) were nutrient-replete. Large blooms of diatoms occurred in this area, with a maximum of primary production at the end of May, three weeks before the GEOVIDE sampling in the Labrador Sea and one month before the sampling in the Irminger Sea (Lemaitre et al., 2018b). The western part of the ARCT region is under the influence of the Newfoundland margin. In this province, station #44 was sampled in the middle of the gyre, station #51 in the East Greenland Coastal Current (EGCC) and station #53 on the Greenland shelf. In the Labrador Sea, station #64 was influenced by the West Greenland Current (following the EGCC after it crossed Cape Farewell) while station #69 was located within the formation area of LSW, where strong convection events occurred the winter before GEOVIDE (García-Ibáñez et al., 2018; de Jong and de Steur, 2016). Westward, the station #77 was located close to the Newfoundland margin (ca 300 km).

2.2 Sampling at sea

Suspended particles were collected with 12 L Niskin bottles mounted on a standard rosette and samples were dedicated to the concentration analyses of particulate barium in excess (Ba_{xs}, biogenic Ba), dissolved and particulate REE (including Nd isotopic composition) and yttrium (often integrated to REE as chemical analogue, named YREE in such case) as well as ancillary parameter analyses, including particulate 232-thorium (^{232}Th). The description of the sampling and filtration methods for water collected with this rosette follows that of Lemaitre et al. (2018b). Briefly, sampling was focused on the epipelagic (0 m – 200 m) and mesopelagic zones (200 m – 1500 m). Sampling bottles were shaken three times as recommended in the GEOTRACES cookbook (https://geotracesold.sedoo.fr/Cookbook.pdf), to avoid the loss of particles by sticking to the walls or settling at the bottom of the bottle. Then, four to eight liters of seawater were filtered off-line using clean slightly air pressurized containers (Perspex®). Suspended particles were collected onto polycarbonate filters of 0.4 µm porosity (Nuclepore®, 47 mm or 90 mm of diameter). After sample filtration, the filter was rinsed with ≤5 mL of ultra-pure water (Milli-Q; 18.2 MΩ cm) to remove most of sea salts. Finally, filters were carefully removed using plastic tweezers and were dried under a laminar flow hood at ambient temperature then stored in clean Petri dishes. Samples were handled in line in order to avoid contamination.

Ba, ^{232}Th, yttrium Y and PREE digestion procedure were performed on the same sample and the resulting solution was shared between analysts. ^{232}Th and Ba (but not Y) were first measured at the Royal Museum for Central Africa (Tervuren, Belgium), then Ba, ^{232}Th, Y and PREE were later analyzed at LEGOS (Toulouse, France; this work). Details of this procedure are described in section 2.3.1.

A clean sampling system was also deployed at the same stations to collect suspended particles dedicated to the analysis of trace metals prone to contamination like iron (Fe) or zinc (Zn). It was composed of a clean rosette equipped with 12 L GO-FLO bottles. Suspended particulate samples were collected on paired polyethersulfone and mixed ester cellulose filters of 0.45 µm and 5 µm porosity, respectively. The sample digestion and the subsequent analytical work were conducted in LEMAR, Brest (Gourain et al., 2019). The digestion procedure was slightly different than the procedure used on filters collected with the standard rosette (see section 2.3.2). Ba and Y were also measured on these "clean samples" together with other trace metals, in Brest.

2.3 Sample preparation and analysis

2.3.1 Leaching procedure and analysis for the PYREE

Polycarbonate filters mounted on the Perspex® filtration units were first cut into two parts using a ceramic blade. One half was archived, while the other half was placed in a clean Teflon vial (Savillex®). The filter was then digested at Tervuren with a strong acid solution made of 1.5 mL HCl, 1 mL HNO_3 and 0.5 mL HF, all concentrated (Merck® Suprapur Grades) (Lemaitre et al., 2018b). Vials were left on hot plates at 90°C overnight. After this, the filter was fully digested, and the solution was then evaporated until near dryness. Finally, 13 mL of 0.32 mol L^{-1} HNO_3 (Merck® Suprapur Grades) were added in the Savillex® vials and the leaching solutions were transferred into clean polypropylene tubes (VWR™). Then, Y, Ba, ^{232}Th and REE concentrations were measured using 2 mL of these archive solutions. Only few samples required an additional dilution by a factor between 1.3 and 1.5 using HNO_3 0.32 mol L^{-1} (prepared from Merck® nitric acid 65%, EMSURE® distilled twice at LEGOS to get the purest product), because the archive solution volume was below 2mL, which is the volume required by the ICP-MS measurement. These aliquots were placed in clean 5 mL polypropylene tubes and doped with a solution containing In and Re (ca. 100 ppt of both tracers) in order to correct matrix effects and sensitivity shifts during analysis. Analyses were performed at the Observatoire Midi Pyrénées (Toulouse, France) using a high-resolution inductively coupled plasma mass spectrometer (SF-ICP-MS, Element XR, Thermo Fischer Scientific®) in low resolution mode. The SF-ICP-MS was coupled to a desolvating nebulizer (Aridus II, CETAC Technologies®) to minimize oxide and hydroxide production rates and thus (hydr)oxide interferences (Aries et al., 2000). Oxide production rates were determined at the beginning and the end of every session using a Ce solution (CeO<0.03%). Other REE (hydr)oxides rates were then determined using the constant proportionality factor between them, previously determined with the same analytical configuration (Aries et al., 2000). Oxide-hydroxide interferences represented 0.001% to 1% of the signal except for Eu (0.3% to 10%). Isobaric interferences were corrected directly by the software of the ICP-MS, and thoroughly checked before the session. A five-point calibration curve was established using a multi elemental standard solution at the beginning, the middle and the end of the analysis. The 20.10^{-12} g g^{-1} of REE standard was measured every 5 samples. Standards were prepared by the dilution of a multi element stock solution (SCP Science, PlasmaCAL, Custom standard) in 0.32 mol L^{-1} HNO_3 with ca 0.1 ppb of In and of Re, to match the relative concentrations measured in the samples. The certified reference material SLRS-5 (NRC Canada) was systematically

analyzed with the samples and their concentrations are within the error bar of the consensual values published by Yeghicheyan et al. (2013), with a smaller error (see Fig. S1). Reproducibility was assessed by measuring two or three times 2 mL of 23 samples from the same leaching solution. The difference between replicates varied from 0 % to 20%, and were mostly under 10%. The average percentage of difference between these analytical replicates is presented on Fig. S2. Procedural blanks have been estimated by conducting the same chemical procedure on clean, unused filters. The average chemical blank (n = 8) represented 0.01% to 5% of the sample concentrations, except for Y and Lu for which the contribution of the blank was generally higher (between 1% and 30%). Blanks were finally subtracted to the measured concentrations.

Four sources of errors could affect the final data: errors on i) the proportion of filter analyzed that comes from cutting the filters in halves; ii) the volume of leachate; iii) the volume taken in the archive for analysis; iv) the standard deviation associated with ICP-MS measurements. The final error was calculated by propagating the uncertainties of these different sources, except for the cutting error, which is rather theoretical than empirical and was impossible to evaluate at the time. We assumed that particles had a homogenous distribution on the filters as heterogeneity is difficult to assess. This hypothesis is supported by the good agreement of Y, Ba and ^{232}Th between the samples from Niskin bottles and the samples from GO-FLO bottles, which were not cut in halves (see section 2.3.2 below). The different errors, their method of calculation and their comparison are summarized in Fig. S3.

2.3.2 Laboratory to laboratory comparisons and validation of our data

Ba and ^{232}Th results were used to compare the data obtained between Tervuren and Toulouse in order to assess the consistency of the different ICP-MS analyses. Y was used to compare the consistency of data obtained between Brest and Toulouse using two different sampling systems, filtration, digestion and analytical procedures. Y concentrations were more specifically used to validate the YREE sampling with the standard rosette, which is less prone to contamination than Fe or Zn, as underlined by van de Flierdt et al. (2012).

Results are presented in Fig. S4. Analytical determination of Ba and ^{232}Th concentrations were performed in Toulouse and in Tervuren (Lemaitre et al., 2018b). In Tervuren, an inductively coupled plasma quadrupole mass spectrometer (ICP-QMS; X Series 2 Thermo Fischer®) was used, while a high-resolution mass spectrometer was used in Toulouse (HR-ICP-MS; Element XR Thermo Fischer®). “Toulouse” vs. “Tervuren” Ba concentrations show a regression slope of 0.86 (r^2=0.91, n=198). For ^{232}Th, “Toulouse” vs. “Tervuren” concentrations show a slope of 1.05 (r^2=0.98, n=198; Fig. S4).

The comparison between the two sampling and subsequent analytical procedures is illustrated by Y concentrations analyzed in “Brest” and “Toulouse”. In Brest, filters collected with the clean-rosette were leached with a mixture of HF and HNO_3 during 4 hours at 130°C before evaporation (for details see Gourain et al., 2019), while in Toulouse, filters collected with the standard rosette were digested with a HCl, HF and HNO_3 solution (see above section 2.3.1). The comparison shows an excellent consistency between both datasets: for Y, the regression slope is 0.93 (r^2=0.82, n=78; Figure S4). For Ba, the regression slope

is 0.86 (r^2=0.91, n=78). This intercomparison exercise supports the excellent reliability of our PREE data and allows us to discuss the PREE concentrations in the context of trace metal concentrations from Gourain et al. (2019) in the following parts.

3 Results

Concentrations of PY, PREE, PBa and P^{232}Th are compiled in Table 2. For sake of clarity, we only displayed PCe, PNd and PYb concentrations (Fig. 2 and 3) since these three REEs represent the light REE (Nd), heavy REE (Yb) and a specific behavior (Ce). Noteworthy, LREE and HREE are not equally influenced by dissolved-particulate exchanges (Koeppenkastrop et al., 1991; Koeppenkastrop and De Carlo, 1992, 1993; Sholkovitz, 1992; Sholkovitz et al., 1994). As free trivalent LREE are more abundant in seawater, they are more prone to adsorption on particles than HREE (Schijf et al., 2015). The specific behavior of Ce is due to the occurrence of its IV oxidation state in addition to the III oxidation state common to all the REE. Two mechanisms for Ce oxidation have been proposed so far: a microbially mediated oxidation in seawater under oxic conditions that leads to formation of insoluble CeO_2, more particle reactive than Ce(III) (Byrne and Kim, 1990; Elderfield, 1988; Moffett, 1990, 1994; Sholkovitz and Schneider, 1991) and an oxidative scavenging onto Mn oxides particles (De Carlo et al., 1997; Koeppenkastrop and De Carlo, 1992). These two processes act in addition to the general scavenging process that affects all the trivalent REE by surface complexation, thus leading to the Ce enrichment in particles and its stronger depletion in the dissolved phase compared to other REE.

Particulate Ce concentrations are higher than PNd concentrations (Fig. 2; Fig. 3 A and B), which are higher than PYb concentrations (Fig. 3 C and D), in agreement with the natural abundance and reactivity of these three REE: the light Ce and Nd are more abundant than the heavy Yb, and Ce is the most particle-reactive of the REE.

3.1 Cerium

As shown in Fig. 2, particulate Ce concentrations varied between 0.2 pmol L^{-1} (station #64) and 16.3 pmol L^{-1} (station #32; Fig. 2). They were higher close to the Iberian margin (station #1: 1 pmol L^{-1} < PCe < 9.4 pmol L^{-1}) and on the Greenland shelf (station #53: 5.7 pmol L^{-1} < PCe < 14.6 pmol L^{-1}). In the NAST (station #13) and the NADR (stations #21 to #38) regions, vertical profiles presented a surface or subsurface maximum at all stations. A second maximum was observed at 160 m at station #13 and in the NADR region (except close to the subarctic front, at station #26). Below 200 m depth, PCe concentrations decreased and reached a value of 2 pmol L^{-1} within the mesopelagic area. Particulate Ce concentrations were higher to the east of the subarctic front (stations #13 and #21) compared to the west (stations #26, #32 and #38). In the ARCT region, surface PCe concentrations were lower and increased between 80 m and 160 m, with all PCe > 1 pmol L^{-1} at all open-sea stations. Maximum concentrations were observed just below 200 m, at stations #44, #64 and #69. At depths greater than 200 m, PCe concentrations were more variable in the ARCT region than in the NADR region. They were higher than those observed at the surface except at station #69 where they remained between 1 pmol L^{-1} and 2 pmol L^{-1}. Particulate Ce profiles differed from that of PNd and PYb at two stations only: station #38, where higher concentrations were observed at 100 m and 800 m for PCe

only; station #44, where PCe concentrations were more variable in the epipelagic zone than PNd and PYb, with maxima located at 120 m and 160 m depth. These maxima were not observed for other PREE at this station.

3.2 Neodymium

As for PCe (and other PREE, see supplementary information and Table 2), PNd concentrations were the highest close to the Iberian and Greenland margins with values up to 4.5 pmol L^{-1} in the upper 100 m (Fig. 3 A and B). Concentrations decreased as the distance to margins increased, as seen at stations #13 where PNd were lower than 1 pmol L^{-1}. Low PNd values were also measured at station #77, which is relatively close to the Newfoundland margin, yet located outside of the continental shelf.

3.3 Ytterbium

Distributions of PNd and PYb differed in several ways (Fig. 3). Stations #13, #44 and #69 displayed a maximum in subsurface for PYb that was not observed for PNd. In contrast, a local maximum in PNd was identified at 160 m at stations #64 and #69, but not for PYb. In the open ocean, at stations #21, #26, #32 and #38, concentrations of both elements were higher in the surface layer than below. The highest PYb concentrations were determined in the NADR region, which was the most productive at the time of the cruise (Fonseca-Batista et al., 2019). Concentrations then decreased with depth to become constant, except at station #38 where they increased again in the mesopelagic zone (below 300 m). In the ARCT region, surface concentrations of PNd were lower at 100 m than at 250 m, similar to station #1 contrasting on this point with the NADR region.

3.4 PYb_N/PNd_N ratios

To highlight a possible fractionation between LREE and HREE, the PYb_N/PNd_N ratio is calculated from concentrations normalized to the Post Archean Australian Shale (PAAS), commonly used for REE normalization, in order to get rid of the natural abundance "zig zag distribution" of the REE (Piper and Bau, 2013). This normalization allows i) a better diagnostic of the fractionation between PREE and ii) comparison with patterns in the literature. Results are presented in Fig. 4. The PYb_N/PNd_N ratio varied between 0.2 and 4.5, with an outlier (9) at station #13 at 40 m. Lower ratios (< 1) were observed along the margins, increasing with the distance from the coast. In the open ocean, except at station #38, PYb_N/PNd_N was higher at the surface (> 1.4), and decreased in the subsurface layers, ranging between 1 and 1.4. At station# 38, it was smaller than 1 in the upper 100 m and around 1 below. The lowest PYb_N/PNd_N ratio was determined in the core of the epipelagic zone at station #21 at 100 m (Fig. 4), where high concentrations of PLa, PCe, PPr and PNd (in other words, LREE) were measured. However, for other stations with a similar enrichment, no low PYb_N/PNd_N ratios were observed (stations #21 at 600m, #32 at 450 m and #38 at 800 m).

4 Discussion

4.1 Comparison with other studies

Particulate REE data in suspended particles are very scarce in the literature. To our knowledge, for the North Atlantic, only one other set of concentrations was published by Kuss et al. (2001), who measured PREE in samples centrifuged from several m^3 of water at a depth of 7 m, collected along the 20°W meridian between 30°N and 60°N. Even though this study is located in a different area of the North Atlantic Ocean, and only in surface, similarities can be pointed out. Kuss et al. (2001) observed PCe concentrations ranging between 0.2 pmol L^{-1} and 4.9 pmol L^{-1} with higher concentrations close to the margins especially near the Iberian margin, consistent with our data. Their PNd concentrations of ca. 0.5 pmol L^{-1} to the south east of the NADR are also consistent with ours. The PNd concentrations reported by Tachikawa et al. (1999b) at a station located in a mesotrophic zone of the north-east tropical Atlantic and directly influenced by Saharan dust (6 g m^{-2} yr^{-1} to 15 g m^{-2} yr^{-1}, Rea, 1994) were almost 2 times higher than those reported here (PNd = 2.6 pmol L^{-1} at 10 m at station M, when PNd <1.4 pmol L^{-1} for GEOVIDE at 10 m; Fig. S5). The same authors measured lower concentrations than ours at the oligotrophic site of their study, where the dust flux was lower than at the mesotrophic site (4-5 g m^{-2} yr^{-1}, Rea, 1994) but higher than that found during the GEOVIDE cruise (2 ng m^{-3} to 500 ng m^{-3}, Shelley et al., 2017). Interestingly, PCe concentrations measured by these authors are similar to those reported in this study, for both the mesotrophic and oligotrophic sites. The difference of concentrations observed for the other PREE can be due to the fact that particle concentrations are usually higher in the subpolar North Atlantic than in the tropical Atlantic (Gehlen et al., 2006).

4.2 Lithogenic and authigenic PREE fractions

Particulate REE are found in both the lithogenic and authigenic phases of particles. Schematically, particles are often represented with a "lithogenic core" coated by authigenic material (Bayon et al., 2004; Sholkovitz et al., 1994). The "lithogenic core" has an external origin, product of the continental weathering transported by the winds or discharged by the rivers to the continental margins. The authigenic phases are produced in the water column, and particulate REE present in this phase can result from surface biological activity or scavenging by organic coatings and/or iron and manganese oxides and hydroxides (Bau, 1999; Bau and Koschinsky, 2009; Lam et al., 2015). Traces of the biological absorption can be found in inorganic planktonic tests ($CaCO_3$, Palmer, 1985; Roberts et al., 2012 and BSi, Akagi, 2013) or in biogenic byproducts like barite (Ba_{xs}, Garcia-Solsona et al., 2014; Guichard et al., 1979). The common view is that LREE are more sensitive to oxide phases of Fe and Mn, while HREE, more soluble, could preferentially react with biogenic phases (Akagi, 2013; Bertram and Elderfield, 1992; Grenier et al., 2018; Pham et al., 2019). In the Bering Strait, Akagi et al (2011) also observed a strong association between particulate HREE and biogenic silica collected in sediment traps. This specific BSi control on HREE behavior is discussed in section 4.6. Distribution coefficients also vary between HREE and LREE with depth and the nature of the particle phases (Schijf et al., 2015).

Thus, differentiating the distribution of REE between the lithogenic and authigenic phases can allow estimating the fraction implied in scavenging and/or absorption processes by the authigenic phase, while the lithogenic fraction can be used to picture continental inputs. The lithogenic REE fraction could also be estimated using conservative lithogenic tracers such as Al, ^{232}Th or Ti (e.g. Gourain et al., 2019; Tachikawa et al., 1997). These authors used Al as a lithogenic tracer while here we chose to use ^{232}Th. Indeed, the lithogenic fractions calculated from particulate Al (PAl) concentrations were often higher than 100% in surface waters close to the margins, revealing that a fraction of the total PAl is likely in the authigenic phase (Lerner et al., 2018; Van Beueskom et al., 1997). In addition, as Al is more prone to contamination, it was sampled with the clean rosette (Gourain et al., 2019), while ^{232}Th was measured in the same samples as PREE, collected with the standard rosette. The concentration of the lithogenic PREE fraction in particles is calculated by multiplying the ^{232}Th concentration in a given sample by the ratio of the considered REE on ^{232}Th in the upper continental crust (UCC, Rudnick and Gao, 2014, Eq. (1)), a value similar to the uniform ^{232}Th concentrations reported by Chase et al. (2001) in marine sediments from cores of the South Atlantic.

$$[REE_{litho}] = [^{232}Th] \times \left(\frac{[REE]}{[232Th]}\right)_{UCC} \quad (1)$$

$$\%REE_{litho} = \frac{[REE_{litho}]}{[REE]} \times 100 \quad (2)$$

$$\%REE_{authi} = 100 - \%REE_{litho} \quad (3)$$

These PREE lithogenic concentrations are then divided by the total PREE concentrations to obtain the fraction of particulate REE of lithogenic origin (Eq. (2)). The authigenic fraction is then obtained by subtracting the lithogenic fraction from 100 % (Eq. (3)).

The percentage of lithogenic PNd along the section is represented in Fig. 5. In this figure, we also chose to represent the average value of the lithogenic fractions of the remaining PREE for the PLREE at five selected stations, excepted for PCe because of its distinctive behavior that leads to higher affinity for particles. We also plotted the PHREE at the same stations (#1, #26, #51, #53 and #77). Error bars represent the standard deviation of the resulting averages. These five stations are representative of the three dominant biogeochemical contexts observed along the section: under lithogenic input influence (#1, #53), dominated by biological activity (#26, #51), and influenced by both (#77). Sometimes, the estimated Nd lithogenic fraction exceeded 100% (up to 550% at 20m at station #1, and up to 130% at 160 m at station #13 and at 200 m at station #32). This suggests an excess of ^{232}Th in the particles, likely authigenic, or a difference between the adsorption kinetics of ^{232}Th and REE, as reported by Hayes et al. (2015). In these cases, we capped the lithogenic proportion to 100%. The occurrence of an authigenic fraction of ^{232}Th may lead to a bias in the calculation of the lithogenic contribution and an overestimation of lithogenic contributions cannot be excluded at the surface. However, ^{232}Th remains predominantly lithogenic, and the comparison between the fractions calculated with Al and ^{232}Th provided in Fig. S6 for stations #1, #13, #32, #51 and #77 validates the use of ^{232}Th

315

4.3 PAAS normalization and REE patterns

The patterns of PAAS-normalized concentrations are represented in Fig. 5 together with the profiles for the same five stations as in 4.2. For ease of reading, patterns are averaged by depth intervals displaying similar values. Error bars represent the standard deviation of the concentration series. A dissolved REE pattern obtained in the North Atlantic Deep Water at 12°S at 2499 m (Zheng et al., 2016) is also represented, for comparison with a "typical" dissolved seawater pattern, marked by a negative Ce anomaly and a pronounced normalized HREE/LREE positive slope (De Baar et al., 1985; Elderfield, 1988; Elderfield and Greaves, 1982; Tachikawa et al., 1999a). The patterns of other stations are represented in Fig. S7.

The validity of using PAAS for normalization is assessed by the fact that PAAS does not present any significant difference in REE composition between shales and loess from Europe, North America and China (Rudnick and Gao, 2014), that are potential sources of lithogenic material for Europe and North America. The flat patterns obtained at stations #1, #13 and #53 validate a PAAS-like source of lithogenic material. Normalization to atmospheric depositions has been put aside as these inputs were very low during the cruise (Shelley et al., 2017), and the REE patterns of these dusts are not available. In addition, normalization to dusts would not have allowed us to compare our data with the REE patterns in the literature, which commonly uses PAAS to normalize.

4.4 Lithogenic supply at the margins

The high PREE concentrations close to the Iberian margin and on the Greenland shelf suggest that particulate material is released by the margins to the water column (Fig. 3 and Table 2), the highest concentrations being measured at station #1 (Fig. 5). At these stations, the lithogenic PREE fractions range between 50% and 100% (Fig. 3). The relatively flat total PREE patterns displayed at these stations show only a slight enrichment in LREE due to their preferential scavenging compared to the HREE (Fig. 5; Sholkovitz et al., 1994).

High percentages of lithogenic PREE were visible along two isopycnals (σ_0=27.05 and σ_0=27.4) visible from station #1 to station #32 (in other words beyond the Subpolar Front) spreading over 1700 km from the Iberian margin (Fig. 6). Similar maxima have been reported for lithogenic particulate iron (PFe) and particulate manganese (PMn) by Gourain et al., 2019 (their Fig. 6 B).

Above the Greenland shelf, at station #53, the fraction of lithogenic PREE was also high (55% to 86% for PNd), only slightly lower than at station #1, with a median lithogenic contribution of 59% for PLREE and 83% for PHREE (Fig. 5). Unlike what was observed to the south eastern end of GEOVIDE section from station #1 to #26, these lithogenic particles do not spread offshore. Indeed, except at the surface, the lithogenic fraction for LREE was lower than 50% at stations #51 and #64 in the Irminger Sea and in the Labrador Sea, respectively. This can be explained by the circulation: the East Greenland Irminger Current (EGIC) is a strong narrow current bypassing Greenland along its shelf (23.4 ± 1.9 Sv, Daniault et al., 2016), likely

preventing exchanges between the Irminger Subpolar Mode Water (IrSBPMW) and waters of the Greenland shelf, transported by the EGCC current which flows parallel to the coast (green and orange arrows around the Greenland southeastern tip in Fig. 1). Our observations are consistent with those of Lacan and Jeandel (2005), who showed that the Nd isotopic signatures (ε_{Nd}) of SPMW transported by the EGIC do not vary significantly along the Greenland shelf. In the same way, the lithogenic influence is moderate at station #77, where land-ocean exchanges are reduced due to the EGCC (1.5 ± 0.2 Sv, Daniault et al., 2016). While the lithogenic fraction is still relatively high at this station (50% < REE_{litho} <80% below 150m), the fractionated patterns indicate that other processes are at play (Fig. 5), like for example preferential scavenging of LREE on Mn and Fe oxyhydroxides (Bau, 1999) and/or fractionation by diatoms (Akagi et al., 2011). The roughly constant lithogenic contribution around 60% at station #77 indicates that like around Greenland, no nepheloid layers are spreading from the Newfoundland margin, at least at the time of the cruise.

Gourain et al. (2019) reported similar results for lithogenic PFe and PMn fractions estimated during the same cruise . These authors also observed a strong contribution of lithogenic material from the Iberian margin spreading until station #32, a lower contribution along the Newfoundland margin and almost no lithogenic contribution from the slope of the Greenland margin. Using lithogenic PMn as a tracer of sediment resuspension, they estimated that 100% of PMn was originating from sediment resuspension at station #1 between 250 m and 1000 m (their Fig. 4). Interestingly, E. Le Roy (Le Roy, 2019) observed an unexpected maximum of ^{227}Ac activity at 500 m at stations #1 and #21, indicating the influence of a sediment source, also consistent with the PREE lithogenic fraction. However, at station #13, the lithogenic PREE maximum was not found at the same depth as for ^{227}Ac (160 m instead of 200m). Unfortunately, the different sampling resolutions for PREE and ^{227}Ac did not permit to further compare data between these tracers except at the surface of station #1, where a maximum of ^{227}Ac was consistent with the lithogenic PREE signal.

These highly enriched depths in lithogenic tracers could be due to the formation of intermediate nepheloid layers (INL) at 250 m and 500 m along the Iberian margin, similar to those revealed slightly more north by McCave and Hall (2002). A contribution of the Mediterranean Water (MW) to these high concentrations and lithogenic proportions cannot be excluded, but the lack of data in the core of the MW (1000 m to 1500 m, García-Ibáñez et al., 2018) prevented us to conclude further.

A highly energetic process is needed to generate strong resuspension of lithogenic matter. It may result from the friction and energetic excitation of internal waves along the continental slope (Cacchione, 2002). Another possible source is the erosion of the coast by the strong current (from 0.05 m s^{-1} to 0.1 m s^{-1}) coming out from Gibraltar and flowing northward along the Iberian margin (Gourain et al., 2019; McCave and Hall, 2002; Zunino et al., 2017). A combination of all these dynamic processes, generating internal waves south of station #1 could have led to strong sediment resuspension, and subsequent advection of resulting particles northward by the current.

To sum up, margins can provide significant amounts of particulate lithogenic REE to the ocean that must be considered in the mass balance of REE. Occurrence and magnitude of these inputs depend on the morphology of the margin, the hydrodynamical forcing and the amount and composition of sediments leading (or not) to the formation of nepheloid layers.

4.5 Rare Earth Element fractionation: Ce anomalies

As briefly mentioned above, Ce presents a unique chemistry among REE elements with the coexistence of a trivalent and a tetravalent form. In seawater, the redox cycle of Ce and Mn are strongly linked (Bau and Dulski, 1996; Elderfield, 1988; Moffett, 1990, 1994). Biotic and abiotic oxidations of Ce have been previously reported. In seawater, the oxidation of Ce^{3+} in CeO_2 is microbially catalyzed and the resulting tetravalent CeO_2 is insoluble, and thus preferentially adsorbed by surface complexes of particles (Byrne and Kim, 1990; Elderfield, 1988; Moffett, 1990, 1994). This pattern of oxidation, which is similar to Mn oxidation, suggests a common mechanism and possible coprecipitation, yet with different kinetics (Moffett, 1990, 1994). Mn oxides can catalyze Ce abiotic oxidation at the surface of particles, leading to an oxidative scavenging of Ce by Mn oxides (Bau, 1999; Bau and Koschinsky, 2009; Byrne and Kim, 1990; De Carlo et al., 1997; Koeppenkastrop and De Carlo, 1992). Also, a Ce enrichment in Fe hydroxides by sequential leaching of ferromanganese crusts has also been reported (Bau and Koschinsky, 2009). In contrast, experiments of REE addition during Mn oxide and Fe hydroxide precipitation showed little (Davranche et al., 2004) or no evidence of a preferential Ce scavenging by Fe hydroxides unlike for Mn oxides (De Carlo et al., 1997; Koeppenkastrop and De Carlo, 1992; Ohta and Kawabe, 2001). Therefore, the preferential Ce scavenging onto Fe hydroxides is still under debate. This exceptional behavior among REE results in a Ce depletion in seawater.

Conversely, in particles, this leads to a "symmetrical" Ce enrichment compared to other REE when concentrations are normalized to a lithogenic reference as PAAS (Garcia-Solsona et al., 2014; Tachikawa et al., 1999a). This Ce enrichment is quantified using the Ce anomaly, calculated with the concentrations normalized to PAAS. The expression of Bolhar et al. (2004, Eq. 4) is used in this paper:

$$\frac{Ce}{Ce^*} = \frac{[Ce]}{2 * [Pr] - [Nd]} \quad (4)$$

This expression uses Pr and Nd concentrations and is preferred to the one using La and Nd concentrations, as La can also present anomalies in seawater (Bau and Dulski, 1996).

In this dataset, most of Ce/Ce* ratios are greater than one (i.e. positive anomaly). At stations #26, #32, #51 and #77 between the surface and ca. 100 m, PCe was depleted compared to other PREE, and (Ce/Ce*) < 1. This surface minimum was followed by a pronounced positive anomaly down to 200 m. At deeper depths, the anomaly was relatively higher in the NADR region compared to the NAST and ARCT regions, where they are around 1 when they are ≥1.2 in the NADR region (Fig. 7).

In the NADR, between the surface and 50 m (stations #26 and #32) and between 20 m and 60 m (station #38, which showed a surprising positive anomaly at the surface), the negative PCe anomaly was related to the seawater-like patterns, produced by REE uptake in seawater during formation of biogenic matter (Garcia-Solsona et al., 2014; Tachikawa et al., 1999b): all REEs were absorbed from seawater without fractionation. These PCe anomalies were rather constant or showed a slight increase with depth until 50 m or 100 m, depending on the stations. Below, the PCe anomalies increased with depth. These PCe anomaly variations were consistent with the high productivity and export characterizing this area (Lemaitre et al., 2018b). Indeed, if particles were removed faster than Ce is oxidized, the Ce anomaly would have been limited with depth (Moffett, 1990). Two

factors could explain the step in Ce/Ce* observed between 50 m and 100 m in the NADR: the beginning of remineralization in favor of the release of trivalent REE; and/or a decrease of the particle settling speed, in favor of CeO_2 adsorption from seawater and precipitation of Mn oxides which catalyzed Ce oxidation onto particles. Both factors could act simultaneously. The anomaly became even larger between 200 m and 400 m depending on the profiles, and was constant below 600 m, suggesting an equilibrium between Ce oxidation, trivalent REE desorption and remineralization processes. The behavior of PCe at station #21 was less clear, the profile displaying strong vertical variations (Fig. 7B): an important increase in Ce/Ce* was observed at 40 m depth, then Ce/Ce* decreased at 200m to a value similar to the surface one. These sharp variations suggested an influence of lithogenic particles, which was not observed at the other stations. A comparison between PCe lithogenic fractions and of the Ce anomaly vertical profiles showed mirror variations: less pronounced PCe anomalies were correlated to higher PCe lithogenic proportions (Fig. S8). This could be explained by advection of quite well preserved lithogenic material with smooth Ce anomaly. This is consistent with the spreading of nepheloid layers from the Iberian margin discussed above.

In the ARCT region, negative anomalies were also determined at the surface, but they were less pronounced than in the NADR region (Fig. 7). The PCe anomalies increased down to 200 m at stations #44, #51, #64 and #77 but remained lower than in the NADR region for the same depth range. These profiles could be compared to the profiles of stations #26 and #32, with a rather constant PCe anomaly in the first meters that increased after a "critical" depth (here about 40 m versus 100 m in the NADR). The PCe anomaly was then roughly constant below 200 m at stations #51, #64 and #69. At stations #44 and #77, the anomaly increased below 700 m and 1000 m, respectively. The weaker negative anomaly at the surface was consistent with a lower primary production (Lemaitre et al., 2018b). The roughly constant PCe anomaly at depths below 200m indicated that equilibrium between biotic and abiotic Ce oxidation, adsorption and remineralization of trivalent REE was reached faster in the ARCT region.

At station #69, high PCe positive anomalies were observed at the surface and there was no significant increase of the anomaly with depth. These variations were consistent with the fraction of lithogenic PCe but not as much as at station #21, where the lithogenic fraction was smaller (<60 %, Fig. S8). At this station, the equilibrium between the reactions leading to a PCe enrichment and adsorption-remineralization of all REE was reached at ca. 100 m, which was deeper than at the other stations of the region, suggesting a lower particle flux. At station #53, Ce anomaly was roughly constant (around 1), which is consistent with a station dominated by lithogenic inputs.

Four points displayed a Ce /Ce*>3 (station #32 at 140 m and 450 m, station #38 at 100 m and station #64 at 140 m). Although we cannot exclude punctual contamination in Ce during the sampling, we do not have a clear explanation and decided not to consider these data further. They are reported under brackets in Table 2 and not included in the figures.

4.6 The influence of biological activity on the PREE distributions

At stations #26, #32, #38 and #44 which displayed a seawater-like pattern at the surface, the formation of biogenic matter associated with high particle fluxes could explain the negative Ce anomaly and high PYb_N/PNd_N ratios (>1 and up to 4.5).

These patterns were progressively attenuating with depth due to the Ce oxidation discussed in the preceding section. However, the enrichment in HREE could reach 1000 m (Fig. 4), while the negative Ce anomaly was never observed at depths deeper than 100 m. Yet surprising, this could indicate that HREE are not fully associated with the soft tissues of the biogenic material. A LREE enrichment was simultaneously observed, consistent with the preferential scavenging of LREE onto solid phases.

When looking more closely to the authigenic phase of these samples, an uncommon enrichment of PHREE was observed, consistent with the total PREE patterns (Fig. 5 and S7). A strong primary production was determined at all these stations (Fonseca-Batista et al., 2019), so the preferential transfer of HREE from the dissolved phase to the authigenic particulate phase likely occurred when the biological stripping was active. This transfer seemed to have been even more important in the ARCT region, leading to more pronounced HREE enrichments, while the strongest bloom was observed in the NADR region. In the ARCT surface waters the PYb_N/PNd_N could reach 4.5, whereas PYb_N/PNd_N never exceeded 3 in the NADR region. In the ARCT region, the bloom was dominated by diatoms, still active at station #51 and #44, and declining at the others (Fonseca-Batista et al., 2019; Lemaitre et al., 2018b). This declining bloom led to a strong export, but high remineralization rates decreased the biological imprint in favor of the lithogenic signature at depth (Fig. 5). Thus, we suspect that biological uptake had a strong effect on the total and authigenic PREE patterns observed during GEOVIDE. A relationship between HREE and biogenic silica (BSi) was suggested by Akagi (2013), following thermodynamic calculations. According to this work, between 40% and 65% of REE form a $REE(H_3SiO_4)^{2+}$ could complex with silicic acid in the deep North Atlantic. Complexation of REE with silicates was further confirmed by Patten and Byrne (2017), although these authors estimated a lower complexation constant, and a smaller fraction of silica-complexed REE. In addition, significant correlations were observed between dissolved Si and dissolved HREE by Bertram and Elderfield (1992; western Indian Ocean), Stichel et al. (2012) and Garcia-Solsona et al. (2014, both in the Atlantic sector of Southern Ocean), Grenier et al. (2018; Kerguelen Islands) and Pham et al. (2019; Solomon Sea). Contrastingly, in other areas, Patten and Byrne (laboratory experiment, 2017, their Fig.7) and Zheng et al. (tropical South Atlantic, 2016, their Fig. 11) showed that the relationship between $SiOH_4$ and REE was either curvilinear or not significant. In our study, the highest surface authigenic PYb_N/PNd_N ratios were located in the Irminger and Labrador Seas, where the highest BSi concentrations of the GEOVIDE section were also measured (Sarthou et al., 2018) (Fig. S9A and B). A correlation between BSi and PHREE concentrations was detected although it remained weak, the highest correlation coefficient being R^2=0.4 for Lu. Interestingly, this correlation coefficient increased with the atomic mass number, confirming that BSi has a significant effect on authigenic PHREE distributions, from Tb to Lu, but not on lighter REE (Fig. S9 C). These correlations may indicate that in some areas characterized by high diatom blooms, the HREE distributions could be partly linked to the BSi formation, in agreement with Akagi's hypotheses. This relationship would depend on the abundance and the nature of particles (i.e. the occurrence of diatoms), and on the speciation of REE in the dissolved phase (de Baar et al., 2018). Akagi, (2013) suggested that silica-REEs complexes could be incorporated during frustule formation, but the mechanism underlying this enrichment during diatom blooms still has to be clarified. Linking it to what is known about complexation and adsorption processes of the REE is beyond the scope of this work. In addition, an effective relationship between BSi and PHREE can be

blurred by other scavenging processes involving particulate Mn and Fe (hydr)oxides, also known to influence the slope between LREE and HREE.

If diatoms are effectively preferentially incorporating the HREE, the high prevalence of coccolithophorids characterizing the NADR bloom (Lemaitre et al., 2018b) could explain the relatively low HREE enrichment in surface. Besides, patterns flatten with depth to present a quasi-lithogenic signature below 60 m, suggesting that particles with a strong organic signature did not reach this depth at the time of sampling.

4.7 The PAAS-normalized particulate Ho/Y ratio: a proxy of processes independent of the ionic radius

Yttrium (Y) and the lanthanide holmium (Ho) are characterized by roughly the same ionic radius and charge, making them "geochemical twins" (Bau, 1999). The PAAS-normalized particulate ratio (PHo_N/PY_N) highlights differences in their distributions, and therefore allows identifying radius-independent fractionation processes affecting YREE in seawater. We choose to normalize PHo/PY measured in our particulate samples to the PAAS ratio in order to reveal any relative loss or enrichment compared to continental material (Fig. 8). Because of different electron configurations, Ho is more prone to establish ionic bounds, and thus to be preferentially adsorbed onto (hydr)oxides like $FeOH_3$ and MnO_2. In comparison, Y preferentially establishes covalent bounds, and will be preferentially absorbed compared to Ho (Censi et al., 2007; Bau, 1999; Bau et al., 1995). Along the GEOVIDE section, PHo_N/PY_N ratio varied between 0.4 and 1.5, with most of the values being smaller than 1 (i.e. depleted in Ho compared to PAAS). To assess the influence of $FeOH_3$ and MnO_2 on PHo_N/PY_N distributions, we calculated their concentrations using the formula of Lam et al. (2015) and PMn and PFe data from Gourain et al. (2019). There was no obvious relationship between PHo_N/PY_N and $FeOH_3$ and MnO_2 (Fig. 9). Noteworthy, PHo_N/PY_N ratios were higher when $[Fe(OH)_3] > 10^{-2}$ µg L^{-1} and when MnO_2 content increased. However, the PHo_N/PY_N ratio was low (<0.6) in the Labrador Sea surface waters (station #69), the Irminger Sea (stations #44 and #51) and from the surface to 750 m depth in the NADR region (stations #21, #26 and #32; Fig. 8). This is consistent with the fact that both these locations are depleted in MnO_2 and $Fe(OH)_3$, leading to a weak adsorption of Ho (Fig. 9). All along the section, low PHo_N/PY_N ratios were observed from the surface to 800 m depth at productive stations (stations #21, #26 and #32, PHo_N/PY_N<0.9). This suggested a preferential absorption of Y during the formation of biogenic matter, as reported by Censi et al. (2007). In the NADR region, between 200 m and 600 m depth, PCe anomalies were positive (>1), PHREE were enriched, and PHo concentrations were relatively depleted at stations #26 and #21 (PHo_N/PY_N <1). The low remineralization rates observed in this area (Lemaitre et al., 2018a) could explain the enrichment of PY concentrations at the surface. At Station # 32, high PHo concentrations between 350 m and 600 m depth was concomitant with the largest PCe positive anomaly (>1.2), indicating intensive adsorption processes, leading to an enhanced scavenging of REE.

In the ARCT region, at station #69, slightly lower PHo_N/PY_N ratios were observed compared to the other stations of this region (0.5 at the surface, around 0.7 to 0.9 with depth). This station was characterized by a low primary production and the highest remineralization rates of the section (Fonseca-Batista et al., 2019; Lemaitre et al., 2018b, 2018a). This could have led to high

adsorption of Ho relative to Y. As Ho is more prone to be released from particles than Y, a lower PHo_N/PY_N ratio was observed. The higher PHo_N/PY_N ratios determined at the other ARCT stations point to scavenging by particles, although the Ce anomaly was lower than in the NADR region.

Although the PHo_N/PY_N ratios were not directly correlated to MnO_2 and $Fe(OH)_3$ estimated concentrations, this ratio was lower when the primary production was high, in agreement with a preferential incorporation of Y into the biogenic matter. The change of PHo_N/PY_N ratios with depth reflects a balance between two processes: the preferential scavenging of Ho by adsorption onto MnO_2 (identified with PCe anomalies) and remineralization.

5 Conclusion

Particulate concentrations of the fourteen Rare Earth Elements and ^{232}Th have been measured in 200 samples of suspended particles collected in the epipelagic and mesopelagic zones of the Subpolar North Atlantic during the GEOVIDE cruise (GEOTRACES GA01) during late spring - early summer of 2014, providing one of the only available PREE distribution snapshots in the North Atlantic. All PREE concentrations were higher close to the margins (stations #1 and #51), especially at the Iberian margin and on the Greenland shelf (station #53). These high concentrations contrasted with the low concentrations measured in the surface waters of the NADR region (stations #26, #32 and #38) and in the Irminger Sea (station #44).

The use of ^{232}Th as a lithogenic tracer allowed identifying the lithogenic and authigenic REE fractions. The greatest PREE lithogenic fractions were determined close to the Iberian margin, where 80 % to 100% of PREE have a lithogenic origin, in particular within two nepheloid layers located at 250 m and 500 m depth. These two nepheloid layers extended westward, mostly along isopycnals σ_0=27.05 and σ_0=27.4. This lithogenic signature was still visible at station #32, in other words at 1700 km from the margin, due to strong currents and energetic dynamics potentially enhanced by internal waves. Lower lithogenic fractions, between 50 and 80% of REE, were determined close to the Newfoundland margin, and on the Greenland shelf (station #53). No significant lithogenic inputs could be observed far from the Greenland shelf at stations #51 and #64. This is due to the strong EGIC current that prevents exchanges between the shelf and the open ocean.

The influence of biological activity on REE scavenging has also been evaluated. In areas of high biological productivity, the authigenic phase of particles was enriched in HREE compared to LREE. These particles also displayed negative PCe anomalies, as well as low PHo_N/Y_N ratios, suggesting recently formed particles with a preferential uptake of HREE and Y by absorption. In the NADR region, PCe anomaly and LREE enrichment increased with depth, while PHo_N/PY_N ratio remained low (<1). Low remineralization rates could maintain low PHo_N/PY_N ratios while promoting exchanges with the dissolved phase. This also led to the building of the PCe anomaly through sorption processes and to PLREE enrichment. In the Labrador Sea, remineralization rates were higher, moderate PCe positive anomalies were observed together with low PHo_N/PY_N ratios ($1< PCe/Ce^*<1.2$, $PHo_N/PY_N< 1$). High remineralization rates could have induced an increase in exchanges between particulate and the dissolved pools, leading to a lower number of adsorption sites on the authigenic coatings, and to subsequent lower PCe anomalies. The low PHo_N/PY_N ratios can also be attributed to these reduced exchanges. Thus, our results suggested

that the PHo_N/PY_N ratios were less controlled by MnO_2 and $Fe(OH)_3$ than previously proposed but more likely controlled by other processes such as absorption and adsorption that do not involve these two (hydr)oxides.

We also highlighted the importance of biogenic silica on HREE preferential scavenging, shown by a clear increase of the PHREE concentrations in the surface waters of the ARCT region, where a massive diatom bloom occurred. The correlation coefficient between BSi and REE concentrations showed no particular links with the atomic mass number from La to Gd, while it increased from Tb to Lu. This relationship was only observed for PHREE and the underlying mechanisms will have to be investigated in future studies.

Acknowledgments

We deeply thank the crew of the N/O Pourquoi Pas? whose implication was unvaluable during the cruise. Geraldine Sarthou, PI of GEOVIDE with Pascale Lherminier (co-author) is acknowledged for her serene management of this long cruise. We also thank Emmanuel de Saint-Léger and Fabien Perault from the DT INSU for their precious technical help all along the cruise.

We thank Aurelie Marquet, Camille Duquenoy and Jerome Chmeleff for making the (sometimes capricious) HR-ICP-MS operational. Many thanks to Michael Bau for the fruitful discussion we had during the Goldschmidt conference. This work was supported by the French National Research Agency (ANR-13-BS06-0014, ANR-12-PDOC-0025-01), the French National Centre for Scientific Research (CNRS-LEFECYBER, UMR 5566). The logistics were supported by DT-INSU and GENAVIR.

We also deeply acknowledge Rob Sherrell and one anonymous reviewer whose comments helped us to improve this manuscript.

References

Akagi, T.: Rare earth element (REE)–silicic acid complexes in seawater to explain the incorporation of REEs in opal and the "leftover" REEs in surface water: New interpretation of dissolved REE distribution profiles, Geochimica et Cosmochimica Acta, 113, 174–192, doi:10.1016/j.gca.2013.03.014, 2013.

Akagi, T., Fu, F., Hongo, Y. and Takahashi, K.: Composition of rare earth elements in settling particles collected in the highly productive North Pacific Ocean and Bering Sea: Implications for siliceous-matter dissolution kinetics and formation of two REE-enriched phases, Geochimica et Cosmochimica Acta, 75(17), 4857–4876, doi:10.1016/j.gca.2011.06.001, 2011.

Aries, S., Valladon, M., Polvé, M. and Dupré, B.: A Routine Method for Oxide and Hydroxide Interference Corrections in ICP-MS Chemical Analysis of Environmental and Geological Samples, Geostandards and Geoanalytical Research, 24(1), 19–31, doi:10.1111/j.1751-908X.2000.tb00583.x, 2000.

de Baar, H. J. W., Bruland, K. W., Schijf, J., van Heuven, S. M. A. C. and Behrens, M. K.: Low cerium among the dissolved rare earth elements in the central North Pacific Ocean, Geochimica et Cosmochimica Acta, 236, 5–40, doi:10.1016/j.gca.2018.03.003, 2018.

Bau, M.: Scavenging of dissolved yttrium and rare earths by precipitating iron oxyhydroxide: Experimental evidence for Ce oxidation, Y-Ho fractionation, and lanthanide tetrad effect, Geochim. Cosmochim. Ac., 63(1), 67–77, 1999.

Bau, M. and Dulski, P.: Distribution of yttrium and rare-earth elements in the Penge and Kuruman iron-formations, Transvaal Supergroup, South Africa, Precambrian Research, 79(1–2), 37–55, doi:10.1016/0301-9268(95)00087-9, 1996.

Bau, M. and Koschinsky, A.: Oxidative scavenging of cerium on hydrous Fe oxide: Evidence from the distribution of rare earth elements and yttrium between Fe oxides and Mn oxides in hydrogenetic ferromanganese crusts, Geochem. J., 43(1), 37–47, doi:10.2343/geochemj.1.0005, 2009.

Bayon, G., German, C. R., Burton, K. W., Nesbitt, R. W. and Rogers, N.: Sedimentary Fe–Mn oxyhydroxides as paleoceanographic archives and the role of aeolian flux in regulating oceanic dissolved REE, Earth and Planetary Science Letters, 224(3–4), 477–492, doi:10.1016/j.epsl.2004.05.033, 2004.

Bertram, C.J. and Elderfield, H.: The geochemical balance of the rare earth elements and neodymium isotopes in the oceans, Geochim. Cosmochim. Ac., 57, 1957–1986, 1992.

Bolhar, R., Kamber, B. S., Moorbath, S., Fedo, C. M. and Whitehouse, M. J.: Characterisation of early Archaean chemical sediments by trace element signatures, Earth and Planetary Science Letters, 222(1), 43–60, doi:10.1016/j.epsl.2004.02.016, 2004.

Byrne, R. H. and Kim, K.-H.: Rare earth element scavenging in seawater, Geochimica et Cosmochimica Acta, 54(10), 2645–2656, doi:10.1016/0016-7037(90)90002-3, 1990.

Cacchione, D. A.: The Shaping of Continental Slopes by Internal Tides, Science, 296(5568), 724–727, doi:10.1126/science.1069803, 2002.

Censi, P., Zuddas, P., Larocca, D., Saiano, F., Placenti, F. and Bonanno, A.: Recognition of water masses according to geochemical signatures in the Central Mediterranean sea: Y/Ho ratio and rare earth element behaviour, Chemistry and Ecology, 23(2), 139–153, doi:10.1080/02757540701197879, 2007.

Chase, Z., Anderson, R. F. and Fleisher, M. Q.: Evidence from authigenic uranium for increased productivity of the glacial subantarctic ocean, Paleoceanography, 16(5), 468–478, doi:10.1029/2000PA000542, 2001.

Crecelius, E. A.: The solubility of coal fly ash and marine aerosols in seawater, Marine Chemistry, 8(3), 245–250, doi:10.1016/0304-4203(80)90013-4, 1980.

Daniault, N., Mercier, H., Lherminier, P., Sarafanov, A., Falina, A., Zunino, P., Pérez, F. F., Ríos, A. F., Ferron, B., Huck, T., Thierry, V. and Gladyshev, S.: The northern North Atlantic Ocean mean circulation in the early 21st century, Progress in Oceanography, 146, 142–158, doi:10.1016/j.pocean.2016.06.007, 2016.

Davranche, M., Pourret, O., Gruau, G. and Dia, A.: Impact of humate complexation on the adsorption of REE onto Fe oxyhydroxide, Journal of Colloid and Interface Science, 277(2), 271–279, doi:10.1016/j.jcis.2004.04.007, 2004.

De Baar, H. J. W., Bacon, M. P., Brewer, P. G. and Bruland, K. W.: Rare earth elements in the Pacific and Atlantic Oceans, Geochimica et Cosmochimica Acta, 49(9), 1943–1959, doi:10.1016/0016-7037(85)90089-4, 1985.

De Carlo, E. H., Wen, X.-Y. and Irving, M.: The Influence of Redox Reactions on the Uptake of Dissolved Ce by Suspended Fe and Mn Oxide Particles, Aquatic Geochemistry, 3(4), 357–389, doi:10.1023/A:1009664626181, 1997.

Elderfield, H.: The oceanic chemistry of the rare-earth elements, Philosophical Transactions of the Royal Society of London, A(325), 105–126, 1988.

Elderfield, H. and Greaves, M. J.: The rare earth elements in seawater, Nature, 296(5854), 214–219, doi:10.1038/296214a0, 1982.

van de Flierdt, T., Pahnke, K., Amakawa, H., Andersson, P., Basak, C., Coles, B., Colin, C., Crocket, K., Frank, M., Frank, N., Goldstein, S. L., Goswami, V., Haley, B. A., Hathorne, E. C., Hemming, S. R., Henderson, G. M., Jeandel, C., Jones, K., Kreissig, K., Lacan, F., Lambelet, M., Martin, E. E., Newkirk, D. R., Obata, H., Pena, L., Piotrowski, A. M., Pradoux, C., Scher, H. D., Schöberg, H., Singh, S. K., Stichel, T., Tazoe, H., Vance, D. and Yang, J.: GEOTRACES intercalibration of neodymium isotopes and rare earth element concentrations in seawater and suspended particles. Part 1: reproducibility of results for the international intercomparison: Intercalibration of Seawater Nd Isotopes, Limnol. Oceanogr. Methods, 10(4), 234–251, doi:10.4319/lom.2012.10.234, 2012.

Fonseca-Batista, D., Li, X., Riou, V., Michotey, V., Deman, F., Fripiat, F., Guasco, S., Brion, N., Lemaitre, N., Tonnard, M., Gallinari, M., Planquette, H., Planchon, F., Sarthou, G., Elskens, M., LaRoche, J., Chou, L. and Dehairs, F.: Evidence of high N2 fixation rates in the temperate northeast Atlantic, Biogeosciences, 16(5), 999–1017, doi:10.5194/bg-16-999-2019, 2019.

Fowler, S. W. and Knauer, G. A.: Role of large particles in the transport of elements and organic compounds through the oceanic water column, Progress in Oceanography, 16(3), 147–194, doi:10.1016/0079-6611(86)90032-7, 1986.

García-Ibáñez, M. I., Pardo, P. C., Carracedo, L. I., Mercier, H., Lherminier, P., Ríos, A. F. and Pérez, F. F.: Structure, transports and transformations of the water masses in the Atlantic Subpolar Gyre, Progress in Oceanography, 135, 18–36, doi:10.1016/j.pocean.2015.03.009, 2015.

García-Ibáñez, M. I., Pérez, F. F., Lherminier, P., Zunino, P., Mercier, H. and Tréguer, P.: Water mass distributions and transports for the 2014 GEOVIDE cruise in the North Atlantic, Biogeosciences, 15(7), 2075–2090, doi:10.5194/bg-15-2075-2018, 2018.

Garcia-Solsona, E., Jeandel, C., Labatut, M., Lacan, F., Vance, D., Chavagnac, V. and Pradoux, C.: Rare earth elements and Nd isotopes tracing water mass mixing and particle-seawater interactions in the SE Atlantic, Geochim. Cosmochim. Ac., 125, 351–372, 2014.

Gehlen, M., Bopp, L., Emprin, N., Aumont, O., Heinze, C. and Ragueneau, O.: Reconciling surface ocean productivity, export fluxes and sediment composition in a global biogeochemical ocean model, 17, 2006.

Gourain, A., Planquette, H., Cheize, M., Lemaitre, N., Menzel Barraqueta, J.-L., Shelley, R., Lherminier, P. and Sarthou, G.: Inputs and processes affecting the distribution of particulate iron in the North Atlantic along the GEOVIDE (GEOTRACES GA01) section, Biogeosciences, 16(7), 1563–1582, doi:10.5194/bg-16-1563-2019, 2019.

Grenier, M.: Differentiating Lithogenic Supplies, Water Mass Transport, and Biological Processes On and Off the Kerguelen Plateau Using Rare Earth Element Concentrations and Neodymium Isotopic Compositions, Frontiers in Marine Science, 5, 30, 2018.

Guichard, F., Church, T. M., Treuil, M. and Jaffrezic, H.: Rare earths in barites: distribution and effects on aqueous partitioning, Geochimica et Cosmochimica Acta, 43(7), 983–997, doi:10.1016/0016-7037(79)90088-7, 1979.

Hayes, C. T., Anderson, R. F., Fleisher, M. Q., Vivancos, S. M., Lam, P. J., Ohnemus, D. C., Huang, K.-F., Robinson, L. F., Lu, Y., Cheng, H., Edwards, R. L. and Moran, S. B.: Intensity of Th and Pa scavenging partitioned by particle chemistry in the North Atlantic Ocean, Marine Chemistry, 170, 49–60, doi:10.1016/j.marchem.2015.01.006, 2015.

Henderson, G. M., Anderson, R. F., Adkins, J., Andersson, P., Boyle, E. A., Cutter, G., de Baar, H., Eisenhauer, A., Frank, M., Francois, R., Orians, K., Gamo, T., German, C., Jenkins, W., Moffett, J., Jeandel, C., Jickells, T., Krishnaswami, S., Mackey, D., Measures, C. I., Moore, J. K., Oschlies, A., Pollard, R., van der Loeff, M. R., Schlitzer, R., Sharma, M., von Damm, K., Zhang, J., Masque, P. and Grp, S. W.: GEOTRACES - An international study of the global marine biogeochemical cycles of trace elements and their isotopes, CHEMIE DER ERDE-GEOCHEMISTRY, 67(2), 85–131, doi:10.1016/j.chemer.2007.02.001, 2007.

Jeandel, C. and Oelkers, E. H.: The influence of terrigenous particulate material dissolution on ocean chemistry and global element cycles, Chemical Geology, 395, 50–66, doi:10.1016/j.chemgeo.2014.12.001, 2015.

Jeandel, C., Bishop, J. K. and Zindler, A.: Exchange of neodymium and its isotopes between seawater and small and large particles in the Sargasso Sea, Geochimica et Cosmochimica Acta, 59(3), 535–547, doi:10.1016/0016-7037(94)00367-U, 1995.

Jeandel, C., Rutgers van der Loeff, M., Lam, P. J., Roy-Barman, M., Sherrell, R. M., Kretschmer, S., German, C. and Dehairs, F.: What did we learn about ocean particle dynamics in the GEOSECS–JGOFS era?, Progress in Oceanography, 133, 6–16, doi:10.1016/j.pocean.2014.12.018, 2015.

de Jong, M. F. and de Steur, L.: Strong winter cooling over the Irminger Sea in winter 2014-2015, exceptional deep convection, and the emergence of anomalously low SST: Irminger sea cooling and convection, Geophys. Res. Lett., 43(13), 7106–7113, doi:10.1002/2016GL069596, 2016.

Khatiwala, S., Tanhua, T., Mikaloff Fletcher, S., Gerber, M., Doney, S. C., Graven, H. D., Gruber, N., McKinley, G. A., Murata, A., Ríos, A. F. and Sabine, C. L.: Global ocean storage of anthropogenic carbon, Biogeosciences, 10(4), 2169–2191, doi:10.5194/bg-10-2169-2013, 2013.

Koeppenkastrop, D. and De Carlo, E. H.: Sorption of rare-earth elements from seawater onto synthetic mineral particles: An experimental approach, Chemical Geology, 95(3), 251–263, doi:https://doi.org/10.1016/0009-2541(92)90015-W, 1992.

Koeppenkastrop, D. and De Carlo, E. H.: Uptake of rare earth elements from solution by metal oxides, Environ. Sci. Technol., 27(9), 1796–1802, doi:10.1021/es00046a006, 1993.

Koeppenkastrop, D., De Carlo, E. H. and Roth, M.: A method to investigate the interaction of rare earth elements in aqueous solution with metal oxides, Journal of Radioanalytical and Nuclear Chemistry, 152(2), 337–346, doi:10.1007/BF02104687, 1991.

Kuss, J., Garbe-Schönberg, C.-D. and Kremling, K.: Rare earth elements in suspended particulate material of North Atlantic surface waters, Geochimica et Cosmochimica Acta, 65(2), 187–199, doi:10.1016/S0016-7037(00)00518-4, 2001.

Kwon, E. Y., Primeau, F. and Sarmiento, J. L.: The impact of remineralization depth on the air–sea carbon balance, Nature Geoscience, 2(9), 630–635, doi:10.1038/ngeo612, 2009.

Lacan, F. and Jeandel, C.: Acquisition of the neodymium isotopic composition of the North Atlantic Deep Water: neodymium isotopic composition, Geochemistry, Geophysics, Geosystems, 6(12), n/a-n/a, doi:10.1029/2005GC000956, 2005.

Lam, P. J. and Marchal, O.: Insights into Particle Cycling from Thorium and Particle Data, Annual Review of Marine Science, 7(1), 159–184, doi:10.1146/annurev-marine-010814-015623, 2015.

Lam, P. J., Twining, B. S., Jeandel, C., Roychoudhury, A., Resing, J. A., Santschi, P. H. and Anderson, R. F.: Methods for analyzing the concentration and speciation of major and trace elements in marine particles, Progress in Oceanography, 133, 32–42, doi:10.1016/j.pocean.2015.01.005, 2015.

Le Roy, E.: Distribution des radionucléides naturels (226Ra et 227Ac) le long de la section GA01 dans l'Atlantique Nord., Université de Toulouse III – Paul Sabatier, Toulouse. [online] Available from: https://hal.archives-ouvertes.fr/tel-02454460 (Accessed 5 May 2020), 2019.

Lemaitre, N., Planchon, F., Planquette, H., Dehairs, F., Fonseca-Batista, D., Roukaerts, A., Deman, F., Tang, Y., Mariez, C. and Sarthou, G.: High variability of particulate organic carbon export along the North Atlantic GEOTRACES section GA01 as deduced from 234Th fluxes, Biogeosciences, 15(21), 6417–6437, doi:10.5194/bg-15-6417-2018, 2018a.

Lemaitre, N., Planquette, H., Sarthou, G., Jacquet, S., García-Ibáñez, M. I., Gourain, A., Cheize, M., Monin, L., André, L., Laha, P., Terryn, H., Dehairs, F. and Dehairs, F.: Particulate barium tracing of significant mesopelagic carbon remineralisation in the North Atlantic, Biogeosciences, 15(8), 2289–2307, doi:10.5194/bg-15-2289-2018, 2018b.

Lerner, P., Marchal, O., Lam, P. J. and Solow, A.: Effects of particle composition on thorium scavenging in the North Atlantic, Geochimica et Cosmochimica Acta, 233, 115–134, doi:10.1016/j.gca.2018.04.035, 2018.

Lherminier, P. and Sarthou, G.: The 2014 Greenland-Portugal GEOVIDE CTDO2 hydrographic and SADCP data (GO-SHIP A25 and GEOTRACES GA01), SEANOE, doi:https://doi.org/10.17882/52153, 2017.

Longhurst, A.: Seasonal cycles of pelagic production and consumption, Progress in Oceanography, 36(2), 77–167, doi:10.1016/0079-6611(95)00015-1, 1995.

McCave, I. . and Hall, I. .: Turbidity of waters over the Northwest Iberian continental margin, Progress in Oceanography, 52(2–4), 299–313, doi:10.1016/S0079-6611(02)00012-5, 2002.

Menzel Barraqueta, J.-L., Schlosser, C., Planquette, H., Gourain, A., Cheize, M., Boutorh, J., Shelley, R., Contreira Pereira, L., Gledhill, M., Hopwood, M. J., Lacan, F., Lherminier, P., Sarthou, G. and Achterberg, E. P.: Aluminium in the North Atlantic Ocean and the Labrador Sea (GEOTRACES GA01 section): roles of continental inputs and biogenic particle removal, Biogeosciences, 15(16), 5271–5286, doi:10.5194/bg-15-5271-2018, 2018.

Moffett, J. W.: Microbially mediated cerium oxidation in sea water, Nature, 345(6274), 421–423, doi:10.1038/345421a0, 1990.

Moffett, J. W.: The relationship between cerium and manganese oxidation in the marine environment, Limnol. Oceanogr., 39(6), 1309–1318, doi:10.4319/lo.1994.39.6.1309, 1994.

Ohnemus, D. C. and Lam, P. J.: Cycling of lithogenic marine particles in the US GEOTRACES North Atlantic transect, Deep Sea Research Part II: Topical Studies in Oceanography, 116, 283–302, doi:10.1016/j.dsr2.2014.11.019, 2015.

Ohta, A. and Kawabe, I.: REE(III) adsorption onto Mn dioxide (δ-MnO2) and Fe oxyhydroxide: Ce(III) oxidation by δ -MnO2, Geochimica and Cosmochimica Acta, 65(5), 695–703, 2001.

Palmer, M. R.: Rare earth elements in foraminifera tests, Earth and Planetary Science Letters, 73, 285–298, 1985.

Pham, V. Q., Grenier, M., Cravatte, S., Michael, S., Jacquet, S., Belhadj, M., Nachez, Y., Germineaud, C. and Jeandel, C.: Dissolved rare earth elements distribution in the Solomon Sea, Chemical Geology, 524, 11–36, doi:10.1016/j.chemgeo.2019.05.012, 2019.

Phoebe J. Lam, Jong-Mi Lee, Maija I. Heller, Sanjin Mehic, Yang Xiang and Nicholas R. Bates: Size-fractionated distributions of suspended particle concentration and major phase composition from the U.S. GEOTRACES Eastern Pacific Zonal Transect (GP16), Mar. Chem., doi:http://dx.doi.org/10.1016/j.marchem.2017.08.013, 2017.

Piper, D. Z. and Bau, M.: Normalized Rare Earth Elements in Water, Sediments, and Wine: Identifying Sources and Environmental Redox Conditions, AJAC, 04(10), 69–83, doi:10.4236/ajac.2013.410A1009, 2013.

Planquette, H. and Sherrell, R. M.: Sampling for particulate trace element determination using water sampling bottles: methodology and comparison to in situ pumps, Limnology and Oceanography: Methods, 10(5), 367–388, doi:10.4319/lom.2012.10.367, 2012.

R, S.: Ocean Data View, [online] Available from: http://odv.awi.de, 2016.

Rea, D. K.: The paleoclimatic record provided by eolian deposition in the deep sea: The geologic history of wind, Rev. Geophys., 32(2), 159, doi:10.1029/93RG03257, 1994.

Reygondeau, G., Guidi, L., Beaugrand, G., Henson, S. A., Koubbi, P., MacKenzie, B. R., Sutton, T. T., Fioroni, M. and Maury, O.: Global biogeochemical provinces of the mesopelagic zone, Journal of Biogeography, 45(2), 500–514, doi:10.1111/jbi.13149, 2018.

Roberts, N. L., Piotrowski, A. M., Elderfield, H., Eglinton, T. I. and Lomas, M. W.: Rare earth element association with foraminifera, Geochimica et Cosmochimica Acta, 94, 57–71, doi:10.1016/j.gca.2012.07.009, 2012.

Rudnick, R. L. and Gao, S.: Composition of the Continental Crust, in Treatise on Geochemistry, pp. 1–51, Elsevier., 2014.

Sanders, R., Henson, S. A., Koski, M., De La Rocha, C. L., Painter, S. C., Poulton, A. J., Riley, J., Salihoglu, B., Visser, A., Yool, A., Bellerby, R. and Martin, A. P.: The Biological Carbon Pump in the North Atlantic, Progress in Oceanography, 129, 200–218, doi:10.1016/j.pocean.2014.05.005, 2014.

Sarthou, G., Lherminier, P., Achterberg, E. P., Alonso-Pérez, F., Bucciarelli, E., Boutorh, J., Bouvier, V., Boyle, E. A., Branellec, P., Carracedo, L. I., Casacuberta, N., Castrillejo, M., Cheize, M., Contreira Pereira, L., Cossa, D., Daniault, N., De Saint-Léger, E., Dehairs, F., Deng, F., Desprez de Gésincourt, F., Devesa, J., Foliot, L., Fonseca-Batista, D., Gallinari, M., García-Ibáñez, M. I., Gourain, A., Grossteffan, E., Hamon, M., Heimbürger, L. E., Henderson, G. M., Jeandel, C., Kermabon, C., Lacan, F., Le Bot, P., Le Goff, M., Le Roy, E., Lefèbvre, A., Leizour, S., Lemaitre, N., Masqué, P., Ménage, O., Menzel Barraqueta, J.-L., Mercier, H., Perault, F., Pérez, F. F., Planquette, H. F., Planchon, F., Roukaerts, A., Sanial, V., Sauzède, R.,

Schmechtig, C., Shelley, R. U., Stewart, G., Sutton, J. N., Tang, Y., Tisnérat-Laborde, N., Tonnard, M., Tréguer, P., van Beek, P., Zurbrick, C. M. and Zunino, P.: Introduction to the French GEOTRACES North Atlantic Transect (GA01): GEOVIDE cruise, Biogeosciences, 15(23), 7097–7109, doi:10.5194/bg-15-7097-2018, 2018.

Schijf, J., Christenson, E. A. and Byrne, R. H.: YREE scavenging in seawater: A new look at an old model, Marine Chemistry, 177, 460–471, doi:10.1016/j.marchem.2015.06.010, 2015.

Shelley, R. U., Roca-Martí, M., Castrillejo, M., Sanial, V., Masqué, P., Landing, W. M., Beek, P. van, Planquette, H. and Sarthou, G.: Quantification of trace element atmospheric deposition fluxes to the Atlantic Ocean (>40°N; GEOVIDE, GEOTRACES GA01) during spring 2014, Deep Sea Research Part I: Oceanographic Research Papers, 119, 34–49, doi:https://doi.org/10.1016/j.dsr.2016.11.010, 2017.

Sholkovitz, E. R.: Chemical evolution of rare earth elements: fractionation between colloidal and solution phases of filtered river water, Earth and Planetary Science Letters, 114(1), 77–84, doi:10.1016/0012-821X(92)90152-L, 1992.

Sholkovitz, E. R. and Schneider, D. L.: Cerium redox cycles and rare earth elements in the Sargasso Sea, Geochimica et Cosmochimica Acta, 55(10), 2737–2743, doi:10.1016/0016-7037(91)90440-G, 1991.

Sholkovitz, E. R., Landing, W. M. and Lewis, B. L.: Ocean particle chemistry: The fractionation of rare earth elements between suspended particles and seawater, Geochimica et Cosmochimica Acta, 58(6), 1567–1579, doi:10.1016/0016-7037(94)90559-2, 1994.

Stemmann, L., Gorsky, G., Marty, J.-C., Picheral, M. and Miquel, J.-C.: Four-year study of large-particle vertical distribution (0–1000m) in the NW Mediterranean in relation to hydrology, phytoplankton, and vertical flux, Deep Sea Research Part II: Topical Studies in Oceanography, 49(11), 2143–2162, doi:10.1016/S0967-0645(02)00032-2, 2002.

Tachikawa, K., Handel, C. and Dupré, B.: Distribution of rare earth elements and neodymium isotopes in settling particulate material of the tropical Atlantic Ocean (EUMELI site), Deep Sea Research Part I: Oceanographic Research Papers, 44(11), 1769–1792, doi:10.1016/S0967-0637(97)00057-5, 1997.

Tachikawa, K., Jeandel, C. and Roy-Barman, M.: A new approach to the Nd residence time in the ocean: the role of atmospheric inputs, Earth and Planetary Science Letters, 170(4), 433–446, doi:10.1016/S0012-821X(99)00127-2, 1999a.

Tachikawa, K., Jeandel, C., Vangriesheim, A. and Dupré, B.: Distribution of rare earth elements and neodymium isotopes in suspended particles of the tropical Atlantic Ocean (EUMELI site), Deep Sea Research Part I: Oceanographic Research Papers, 46(5), 733–755, doi:10.1016/S0967-0637(98)00089-2, 1999b.

Tonnard, M., Planquette, H., Bowie, A. R., van der Merwe, P., Gallinari, M., Desprez de Gésincourt, F., Germain, Y., Gourain, A., Benetti, M., Reverdin, G., Tréguer, P., Boutorh, J., Cheize, M., Menzel Barraqueta, J.-L., Pereira-Contreira, L., Shelley, R., Lherminier, P. and Sarthou, G.: Dissolved iron in the North Atlantic Ocean and Labrador Sea along the GEOVIDE section (GEOTRACES section GA01), Biogeosciences Discussions, 1–53, doi:10.5194/bg-2018-147, 2018.

Trull, T. W. and Armand, L.: Insights into Southern Ocean carbon export from the C of particles and dissolved inorganic carbon during the SOIREE iron release experiment, 26, 2001.

Turekian, K. K.: The fate of metals in the oceans, Geochimica et Cosmochimica Acta, 41(8), 1139–1144, doi:https://doi-org-s.docadis.ups-tlse.fr/10.1016/0016-7037(77)90109-0, 1977.

Van Beueskom, J. E. E., Van Bennekom, A. J., Tréguer, P. and Morvan, J.: Aluminium and silicic acid in water and sediments of the Enderby and Crozet Basins, Deep Sea Research Part II: Topical Studies in Oceanography, 44(5), 987–1003, doi:10.1016/S0967-0645(96)00105-1, 1997.

Yeghicheyan, D., Bossy, C., Bouhnik Le Coz, M., Douchet, C., Granier, G., Heimburger, A., Lacan, F., Lanzanova, A., Rousseau, T. C. C., Seidel, J.-L., Tharaud, M., Candaudap, F., Chmeleff, J., Cloquet, C., Delpoux, S., Labatut, M., Losno, R., Pradoux, C., Sivry, Y. and Sonke, J. E.: A Compilation of Silicon, Rare Earth Element and Twenty-One other Trace Element Concentrations in the Natural River Water Reference Material SLRS-5 (NRC-CNRC), Geostandards and Geoanalytical Research, 37(4), 449–467, doi:10.1111/j.1751-908X.2013.00232.x, 2013.

Zheng, X.-Y., Plancherel, Y., Saito, M. A., Scott, P. M. and Henderson, G. M.: Rare earth elements (REEs) in the tropical South Atlantic and quantitative deconvolution of their non-conservative behavior, Geochimica et Cosmochimica Acta, 177, 217–237, doi:10.1016/j.gca.2016.01.018, 2016.

Zunino, P., Lherminier, P., Mercier, H., Daniault, N., García-Ibáñez, M. I. and Pérez, F. F.: The GEOVIDE cruise in May–June 2014 reveals an intense Meridional Overturning Circulation over a cold and fresh subpolar North Atlantic, Biogeosciences, 14(23), 5323–5342, doi:10.5194/bg-14-5323-2017, 2017.

Table 1: List of regions and water masses with their acronyms investigated in this study.

Regions	
SPNA	Subpolar North Atlantic
NAST	North Atlantic Subtropical
NADR	North Atlantic drift
ARCT	Arctic
Water masses	
ENACW	East North Atlantic Central Water
MW	Mediterranean Water
SAIW	Subarctic Intermediate Water
SPMW	Subpolar Mode Water
IrSPMW	Irminger Subpolar Mode Water
LSW	Labrador Sea Water
Currents	
NAC	North Atlantic Current
ERRC	East Reykjanes Ridge Current
IC	Irminger Current
EGIC	East Greenland Irminger Current
EGCC	East Greenland Coastal Current

Table 2: Particulate REE, Y, Ba and ^{232}Th concentrations in pmol L^{-1} with the corresponding 2σ error.

Particulate Rare Earth elements, yttrium, barium and 232-thorium concentrations and associated error (2σ) in pmol L^{-1}

Station	Longitude	Latitude	Depth [m]	La	Ce	Pr	Nd	Sm	Eu	Gd	Tb	Dy	Ho	Er	Tm	Yb	Lu	Y	Ba	Th
1	-10.0359	40.333	20	0.96 ± 0.04	2.00 ± 0.08	0.22 ± 0.01	0.76 ± 0.03	0.16 ± 0.01	0.032 ± 0.001	0.124 ± 0.007	0.018 ± 0.001	0.107 ± 0.004	0.020 ± 0.001	0.051 ± 0.004	0.0078 ± 0.0007	0.0495 ± 0.0021	0.0051 ± 0.0004	1.32 ± 0.06	168.7 ± 10.1	1.031 ± 0.051
1	-10.0359	40.333	40	1.73 ± 0.04	2.90 ± 0.07	0.37 ± 0.01	1.38 ± 0.06	0.33 ± 0.01	0.060 ± 0.002	0.238 ± 0.007	0.035 ± 0.002	0.192 ± 0.006	0.036 ± 0.001	0.097 ± 0.006	0.0130 ± 0.0008	0.0822 ± 0.0021	0.0077 ± 0.0003	2.91 ± 0.06	269.4 ± 7.1	0.150 ± 0.006
1	-10.0359	40.333	60	0.60 ± 0.01	1.10 ± 0.03	0.06 ± 0.00	0.22 ± 0.01	0.05 ± 0.00	0.011 ± 0.000	0.044 ± 0.001	0.007 ± 0.000	0.041 ± 0.001	0.008 ± 0.000	0.023 ± 0.001	0.0037 ± 0.0003	0.0212 ± 0.0007	0.0017 ± 0.0001	0.38 ± 0.01	246.9 ± 6.8	0.051 ± 0.002
1	-10.0359	40.333	79	1.01 ± 0.02	1.50 ± 0.03	0.16 ± 0.00	0.51 ± 0.01	0.11 ± 0.01	0.022 ± 0.001	0.095 ± 0.003	0.031 ± 0.001	0.071 ± 0.002	0.014 ± 0.000	0.039 ± 0.002	0.0065 ± 0.0002	0.0360 ± 0.0008	0.0037 ± 0.0002	0.95 ± 0.02	406.4 ± 8.1	0.113 ± 0.002
1	-10.0359	40.333	98	1.55 ± 0.06	2.85 ± 0.10	0.29 ± 0.02	1.06 ± 0.05	0.22 ± 0.02	0.044 ± 0.002	0.153 ± 0.010	0.020 ± 0.001	0.125 ± 0.005	0.023 ± 0.001	0.068 ± 0.006	0.0094 ± 0.0004	0.0575 ± 0.0032	0.0067 ± 0.0003	1.44 ± 0.07	501.4 ± 29.9	0.180 ± 0.008
1	-10.0359	40.333	119	1.25 ± 0.05	2.65 ± 0.11	0.27 ± 0.02	0.95 ± 0.06	0.23 ± 0.02	0.037 ± 0.002	0.147 ± 0.006	0.020 ± 0.001	0.116 ± 0.005	0.022 ± 0.001	0.058 ± 0.003	0.0084 ± 0.0005	0.0557 ± 0.0022	0.0070 ± 0.0003	1.32 ± 0.06	384.7 ± 23.4	0.187 ± 0.009
1	-10.0359	40.333	139	1.30 ± 0.04	3.18 ± 0.09	0.26 ± 0.01	0.96 ± 0.03	0.21 ± 0.01	0.036 ± 0.001	0.147 ± 0.003	0.057 ± 0.003	0.111 ± 0.003	0.020 ± 0.000	0.058 ± 0.003	0.0071 ± 0.0005	0.0494 ± 0.0010	0.0061 ± 0.0002	0.99 ± 0.03	346.1 ± 14.1	0.203 ± 0.005
1	-10.0359	40.333	160	1.47 ± 0.08	3.94 ± 0.19	0.32 ± 0.02	1.12 ± 0.06	0.23 ± 0.03	0.046 ± 0.002	0.172 ± 0.012	0.022 ± 0.002	0.126 ± 0.008	0.023 ± 0.001	0.062 ± 0.004	0.0085 ± 0.0008	0.0571 ± 0.0027	0.0069 ± 0.0004	1.64 ± 0.10	323.7 ± 25.6	0.221 ± 0.011
1	-10.0359	40.333	200	2.59 ± 0.06	6.04 ± 0.13	0.58 ± 0.02	2.09 ± 0.05	0.36 ± 0.01	0.077 ± 0.002	0.282 ± 0.009	0.038 ± 0.002	0.213 ± 0.006	0.038 ± 0.001	0.104 ± 0.003	0.0139 ± 0.0004	0.0931 ± 0.0028	0.0121 ± 0.0004	1.85 ± 0.05	400.1 ± 11.0	0.475 ± 0.014
1	-10.0359	40.333	249	3.46 ± 0.23	7.93 ± 0.43	0.77 ± 0.06	2.82 ± 0.15	0.54 ± 0.05	0.105 ± 0.006	0.392 ± 0.020	0.057 ± 0.004	0.286 ± 0.016	0.050 ± 0.003	0.133 ± 0.010	0.0186 ± 0.0018	0.1239 ± 0.0064	0.0166 ± 0.0010	2.46 ± 0.16	619.0 ± 46.9	0.573 ± 0.034
1	-10.0359	40.333	299	3.73 ± 0.15	8.83 ± 0.35	0.90 ± 0.06	3.00 ± 0.19	0.44 ± 0.03	0.109 ± 0.004	0.401 ± 0.015	0.053 ± 0.003	0.301 ± 0.011	0.053 ± 0.002	0.133 ± 0.006	0.0204 ± 0.0012	0.1296 ± 0.0044	0.0166 ± 0.0006	2.56 ± 0.11	428.5 ± 26.4	0.684 ± 0.023
1	-10.0359	40.333	309	2.55 ± 0.09	5.69 ± 0.17	0.60 ± 0.03	2.14 ± 0.17	0.63 ± 0.02	0.077 ± 0.002	0.308 ± 0.009	0.041 ± 0.002	0.234 ± 0.016	0.043 ± 0.001	0.118 ± 0.007	0.0166 ± 0.0009	0.1065 ± 0.0031	0.0138 ± 0.0004	2.22 ± 0.08	326.5 ± 17.4	0.433 ± 0.010
1	-10.0359	40.333	499	2.82 ± 0.10	6.22 ± 0.22	0.65 ± 0.05	2.43 ± 0.16	0.48 ± 0.04	0.090 ± 0.004	0.338 ± 0.032	0.047 ± 0.003	0.253 ± 0.023	0.046 ± 0.002	0.122 ± 0.009	0.0179 ± 0.0014	0.1110 ± 0.0042	0.0145 ± 0.0006	2.22 ± 0.09	397.4 ± 17.1	0.500 ± 0.019
1	-10.0359	40.333	597	3.39 ± 0.07	7.10 ± 0.14	0.73 ± 0.02	2.59 ± 0.06	0.50 ± 0.02	0.097 ± 0.002	0.330 ± 0.016	0.081 ± 0.002	0.259 ± 0.006	0.047 ± 0.001	0.127 ± 0.004	0.0181 ± 0.0006	0.1132 ± 0.0022	0.0153 ± 0.0003	2.35 ± 0.06	589.4 ± 13.3	0.484 ± 0.012
1	-10.0359	40.333	702	5.73 ± 0.14	9.61 ± 0.23	1.23 ± 0.03	4.50 ± 0.12	0.83 ± 0.03	0.184 ± 0.004	0.656 ± 0.033	0.103 ± 0.003	0.610 ± 0.014	0.121 ± 0.003	0.333 ± 0.011	0.0454 ± 0.0010	0.2801 ± 0.0066	0.0389 ± 0.0008	7.73 ± 0.19	244.0 ± 5.9	0.719 ± 0.018
1	-10.0359	40.333	800	2.55 ± 0.05	5.30 ± 0.10	0.56 ± 0.01	1.98 ± 0.04	0.37 ± 0.01	0.070 ± 0.001	0.239 ± 0.010	0.036 ± 0.001	0.200 ± 0.004	0.037 ± 0.001	0.103 ± 0.003	0.0139 ± 0.0004	0.0910 ± 0.0016	0.0121 ± 0.0003	1.99 ± 0.04	231.3 ± 4.1	0.417 ± 0.010
1	-10.0359	40.333	1000	2.56 ± 0.04	5.14 ± 0.07	0.56 ± 0.01	1.99 ± 0.03	0.38 ± 0.02	0.090 ± 0.001	0.276 ± 0.004	0.041 ± 0.002	0.222 ± 0.005	0.041 ± 0.000	0.112 ± 0.003	0.0155 ± 0.0006	0.0983 ± 0.0014	0.0129 ± 0.0002	3.59 ± 0.05	237.6 ± 3.4	0.374 ± 0.006
1	-10.0359	40.333	1505	3.64 ± 0.16	7.40 ± 0.29	0.84 ± 0.05	2.85 ± 0.12	0.50 ± 0.02	0.071 ± 0.003	0.286 ± 0.015	0.041 ± 0.003	0.221 ± 0.009	0.040 ± 0.001	0.108 ± 0.008	0.0145 ± 0.0009	0.0939 ± 0.0038	0.0124 ± 0.0005	2.22 ± 0.10	210.2 ± 11.2	0.361 ± 0.012
13	-13.8877	41.383	20	1.38 ± 0.07	3.33 ± 0.15	0.29 ± 0.02	1.11 ± 0.04	0.42 ± 0.02	0.061 ± 0.003	0.182 ± 0.007	0.026 ± 0.002	0.138 ± 0.005	0.026 ± 0.001	0.080 ± 0.006	0.0104 ± 0.0007	0.0648 ± 0.0023	0.0081 ± 0.0004	1.38 ± 0.06	385.2 ± 20.4	0.176 ± 0.006
13	-13.8877	41.383	40	1.22 ± 0.03	1.04 ± 0.03	0.19 ± 0.00	0.78 ± 0.02	0.20 ± 0.01	0.057 ± 0.001	0.254 ± 0.007	0.050 ± 0.002	0.403 ± 0.010	0.106 ± 0.002	0.388 ± 0.010	0.0689 ± 0.0015	0.4958 ± 0.0110	0.0818 ± 0.0018	6.31 ± 0.17	217.1 ± 5.3	0.069 ± 0.002
13	-13.8877	41.383	60	1.00 ± 0.03	0.89 ± 0.02	0.12 ± 0.00	0.41 ± 0.01	0.09 ± 0.01	0.023 ± 0.001	0.099 ± 0.003	0.018 ± 0.001	0.109 ± 0.004	0.026 ± 0.001	0.090 ± 0.002	0.0150 ± 0.0007	0.1075 ± 0.0026	0.0162 ± 0.0004	1.48 ± 0.04	179.2 ± 4.7	0.071 ± 0.001
13	-13.8877	41.383	78	0.92 ± 0.02	1.47 ± 0.03	0.14 ± 0.00	0.5 ± 0.01	0.10 ± 0.01	0.023 ± 0.001	0.100 ± 0.003	0.021 ± 0.001	0.104 ± 0.003	0.024 ± 0.001	0.080 ± 0.003	0.0132 ± 0.0005	0.0984 ± 0.0021	0.0152 ± 0.0004	2.45 ± 0.06	247.7 ± 6.1	0.080 ± 0.002
13	-13.8877	41.383	100	0.61 ± 0.01	1.00 ± 0.02	0.12 ± 0.00	0.43 ± 0.01	0.09 ± 0.01	0.020 ± 0.001	0.091 ± 0.004	0.013 ± 0.000	0.081 ± 0.002	0.017 ± 0.000	0.055 ± 0.001	0.0082 ± 0.0003	0.0624 ± 0.0013	0.0093 ± 0.0002	0.99 ± 0.02	280.9 ± 4.9	0.074 ± 0.001
13	-13.8877	41.383	120	0.85 ± 0.02	1.37 ± 0.03	0.12 ± 0.00	0.46 ± 0.01	0.08 ± 0.00	0.020 ± 0.001	0.088 ± 0.002	0.012 ± 0.000	0.079 ± 0.003	0.016 ± 0.000	0.049 ± 0.002	0.0076 ± 0.0004	0.0531 ± 0.0016	0.0076 ± 0.0003	0.87 ± 0.04	302.2 ± 6.2	0.071 ± 0.002
13	-13.8877	41.383	140	0.78 ± 0.01	1.36 ± 0.03	0.15 ± 0.00	0.54 ± 0.01	0.12 ± 0.00	0.025 ± 0.001	0.098 ± 0.003	0.014 ± 0.001	0.082 ± 0.002	0.017 ± 0.000	0.050 ± 0.002	0.0075 ± 0.0003	0.0525 ± 0.0012	0.0073 ± 0.0002	1.04 ± 0.03	358.5 ± 7.0	0.095 ± 0.002
13	-13.8877	41.383	160	1.26 ± 0.03	3.92 ± 0.10	0.22 ± 0.01	0.82 ± 0.02	0.16 ± 0.01	0.035 ± 0.001	0.166 ± 0.010	0.025 ± 0.001	0.169 ± 0.004	0.036 ± 0.001	0.111 ± 0.003	0.0170 ± 0.0007	0.1153 ± 0.0030	0.0171 ± 0.0004	1.90 ± 0.05	455.7 ± 11.7	0.345 ± 0.008
13	-13.8877	41.383	200	0.74 ± 0.04	1.07 ± 0.05	0.14 ± 0.01	0.56 ± 0.03	0.12 ± 0.01	0.033 ± 0.003	0.114 ± 0.006	0.015 ± 0.001	0.095 ± 0.007	0.018 ± 0.001	0.054 ± 0.004	0.0079 ± 0.0006	0.0520 ± 0.0024	0.0072 ± 0.0004	1.03 ± 0.07	411.9 ± 27.6	0.076 ± 0.004
13	-13.8877	41.383	250	1.42 ± 0.07	2.44 ± 0.12	0.24 ± 0.02	1.03 ± 0.06	0.21 ± 0.02	0.067 ± 0.004	0.178 ± 0.009	0.052 ± 0.004	0.145 ± 0.009	0.030 ± 0.001	0.085 ± 0.006	0.0120 ± 0.0008	0.0870 ± 0.0042	0.0119 ± 0.0006	1.69 ± 0.10	532.8 ± 31.4	0.185 ± 0.008
13	-13.8877	41.383	300	1.83 ± 0.07	2.87 ± 0.10	0.28 ± 0.01	0.89 ± 0.03	0.10 ± 0.01	0.052 ± 0.003	0.110 ± 0.004	0.018 ± 0.001	0.113 ± 0.006	0.024 ± 0.001	0.078 ± 0.004	0.0103 ± 0.0005	0.0697 ± 0.0022	0.0095 ± 0.0004	1.30 ± 0.05	575.2 ± 26.3	0.077 ± 0.003
13	-13.8877	41.383	400	0.98 ± 0.02	1.61 ± 0.03	0.19 ± 0.00	0.73 ± 0.01	0.14 ± 0.01	0.030 ± 0.001	0.128 ± 0.003	0.018 ± 0.001	0.102 ± 0.003	0.019 ± 0.000	0.050 ± 0.002	0.0074 ± 0.0005	0.0486 ± 0.0012	0.0063 ± 0.0001	0.95 ± 0.02	941.8 ± 16.3	0.098 ± 0.002
13	-13.8877	41.383	500	0.96 ± 0.05	2.32 ± 0.10	0.20 ± 0.01	0.78 ± 0.03	0.29 ± 0.01	0.043 ± 0.002	0.127 ± 0.005	0.018 ± 0.001	0.096 ± 0.004	0.018 ± 0.001	0.056 ± 0.004	0.0073 ± 0.0005	0.0452 ± 0.0016	0.0056 ± 0.0002	0.96 ± 0.04	269.0 ± 14.2	0.123 ± 0.004
13	-13.8877	41.383	600	0.77 ± 0.03	2.11 ± 0.07	0.16 ± 0.01	0.90 ± 0.02	0.13 ± 0.01	0.025 ± 0.001	0.107 ± 0.003	0.014 ± 0.001	0.088 ± 0.003	0.017 ± 0.001	0.048 ± 0.003	0.0074 ± 0.0005	0.0465 ± 0.0016	0.0054 ± 0.0002	0.86 ± 0.04	302.6 ± 16.2	0.144 ± 0.004
13	-13.8877	41.383	700	0.81 ± 0.02	2.07 ± 0.05	0.16 ± 0.00	0.60 ± 0.02	0.12 ± 0.00	0.026 ± 0.001	0.113 ± 0.005	0.016 ± 0.001	0.090 ± 0.004	0.018 ± 0.000	0.050 ± 0.002	0.0074 ± 0.0003	0.0463 ± 0.0011	0.0057 ± 0.0002	1.06 ± 0.03	311.1 ± 8.3	0.107 ± 0.003
13	-13.8877	41.383	800	0.92 ± 0.02	2.19 ± 0.04	0.20 ± 0.00	0.74 ± 0.01	0.15 ± 0.00	0.030 ± 0.001	0.125 ± 0.003	0.017 ± 0.001	0.098 ± 0.003	0.019 ± 0.000	0.052 ± 0.002	0.0077 ± 0.0003	0.0492 ± 0.0010	0.0061 ± 0.0002	0.94 ± 0.02	264.8 ± 4.4	0.135 ± 0.002
13	-13.8877	41.383	1000	0.98 ± 0.05	2.36 ± 0.10	0.21 ± 0.01	0.76 ± 0.03	0.15 ± 0.01	0.043 ± 0.002	0.129 ± 0.005	0.018 ± 0.001	0.097 ± 0.006	0.018 ± 0.001	0.057 ± 0.003	0.0074 ± 0.0005	0.0457 ± 0.0016	0.0057 ± 0.0002	0.98 ± 0.04	272.6 ± 14.4	0.124 ± 0.005
13	-13.8877	41.383	1501	1.03 ± 0.06	2.38 ± 0.13	0.21 ± 0.01	0.78 ± 0.04	0.15 ± 0.01	0.032 ± 0.002	0.142 ± 0.011	0.022 ± 0.002	0.094 ± 0.005	0.018 ± 0.001	0.047 ± 0.004	0.0071 ± 0.0006	0.0459 ± 0.0024	0.0055 ± 0.0004	1.72 ± 0.10	192.7 ± 13.7	0.154 ± 0.008
21	-19.6724	46.544	10	0.98 ± 0.03	1.19 ± 0.03	0.15 ± 0.00	0.56 ± 0.01	0.11 ± 0.01	0.030 ± 0.001	0.113 ± 0.003	0.020 ± 0.001	0.123 ± 0.004	0.028 ± 0.001	0.094 ± 0.003	0.0151 ± 0.0006	0.1154 ± 0.0035	0.0192 ± 0.0006	2.16 ± 0.06	228.2 ± 6.4	0.076 ± 0.002
21	-19.6724	46.544	20	3.84 ± 0.15	7.28 ± 0.29	0.26 ± 0.01	0.86 ± 0.03	0.17 ± 0.01	0.051 ± 0.002	0.214 ± 0.016	0.043 ± 0.002	0.175 ± 0.008	0.037 ± 0.001	0.112 ± 0.006	0.0183 ± 0.0011	0.1296 ± 0.0049	0.0209 ± 0.0008	3.11 ± 0.14	609.8 ± 28.9	0.150 ± 0.005
21	-19.6724	46.544	40	0.76 ± 0.02	0.81 ± 0.02	0.09 ± 0.00	0.32 ± 0.01	0.07 ± 0.00	0.017 ± 0.001	0.069 ± 0.002	n.d.	0.065 ± 0.003	0.014 ± 0.000	0.042 ± 0.002	0.0063 ± 0.0003	0.0473 ± 0.0014	0.0072 ± 0.0003	1.13 ± 0.04	333.5 ± 9.9	0.060 ± 0.002
21	-19.6724	46.544	60	0.96 ± 0.03	1.43 ± 0.04	0.19 ± 0.01	0.76 ± 0.02	0.15 ± 0.01	0.026 ± 0.001	0.148 ± 0.006	0.023 ± 0.001	0.147 ± 0.006	0.029 ± 0.001	0.081 ± 0.002	0.0111 ± 0.0006	0.0715 ± 0.0021	0.0095 ± 0.0003	1.46 ± 0.04	213.9 ± 7.5	0.074 ± 0.002
21	-19.6724	46.544	76	0.99 ± 0.04	1.82 ± 0.07	0.17 ± 0.01	0.65 ± 0.03	0.12 ± 0.01	0.032 ± 0.001	0.118 ± 0.004	0.016 ± 0.001	0.097 ± 0.005	0.02 ± 0.001	0.057 ± 0.003	0.0084 ± 0.0005	0.0584 ± 0.0026	0.0065 ± 0.0004	1.10 ± 0.05	551.7 ± 25.1	0.088 ± 0.003
21	-19.6724	46.544	100	9.59 ± 0.28	(15.59 ± 0.36)	0.92 ± 0.03	2.87 ± 0.09	0.13 ± 0.00	0.028 ± 0.001	0.120 ± 0.004	0.018 ± 0.002	0.093 ± 0.003	0.018 ± 0.001	0.051 ± 0.002	0.0072 ± 0.0004	0.0456 ± 0.0013	0.0060 ± 0.0003	0.95 ± 0.03	477.5 ± 13.9	0.076 ± 0.002
21	-19.6724	46.544	120	0.79 ± 0.02	1.31 ± 0.03	0.16 ± 0.01	0.68 ± 0.01	0.12 ± 0.01	0.032 ± 0.001	0.110 ± 0.002	0.016 ± 0.001	0.083 ± 0.003	0.016 ± 0.000	0.044 ± 0.002	0.0057 ± 0.0002	0.0399 ± 0.0007	0.0052 ± 0.0002	0.82 ± 0.02	495.6 ± 11.8	0.058 ± 0.001
21	-19.6724	46.544	140	1.05 ± 0.02	2.46 ± 0.06	0.19 ± 0.01	0.74 ± 0.03	0.11 ± 0.01	0.034 ± 0.001	0.123 ± 0.003	0.017 ± 0.001	0.090 ± 0.004	0.017 ± 0.000	0.045 ± 0.002	0.0070 ± 0.0004	0.0424 ± 0.0012	0.0057 ± 0.0002	0.95 ± 0.02	516.0 ± 16.5	0.096 ± 0.002
21	-19.6724	46.544	160	0.40 ± 0.01	0.77 ± 0.02	0.09 ± 0.00	0.33 ± 0.01	0.08 ± 0.00	0.028 ± 0.001	0.069 ± 0.001	0.010 ± 0.001	0.057 ± 0.003	0.011 ± 0.000	0.031 ± 0.002	0.0041 ± 0.0003	0.0297 ± 0.0008	0.0034 ± 0.0001	0.66 ± 0.02	352.3 ± 13.6	0.051 ± 0.001
21	-19.6724	46.544	200	0.63 ± 0.02	1.07 ± 0.03	0.13 ± 0.00	0.52 ± 0.02	0.11 ± 0.00	0.028 ± 0.001	0.099 ± 0.003	0.014 ± 0.001	0.078 ± 0.004	0.015 ± 0.000	0.041 ± 0.002	0.0060 ± 0.0004	0.0359 ± 0.0013	0.0047 ± 0.0002	0.78 ± 0.03	354.6 ± 13.4	0.053 ± 0.001
21	-19.6724	46.544	300	0.75 ± 0.02	2.12 ± 0.04	0.15 ± 0.00	0.57 ± 0.01	0.11 ± 0.01	0.033 ± 0.001	0.110 ± 0.002	0.016 ± 0.001	0.090 ± 0.004	0.017 ± 0.000	0.050 ± 0.003	0.0066 ± 0.0003	0.0433 ± 0.0011	0.0056 ± 0.0002	1.02 ± 0.02	517.1 ± 15.6	0.065 ± 0.001
21	-19.6724	46.544	400	1.02 ± 0.02	1.77 ± 0.03	0.10 ± 0.00	0.39 ± 0.02	0.09 ± 0.00	0.030 ± 0.001	0.076 ± 0.002	0.01 ± 0.001	0.059 ± 0.001	0.011 ± 0.000	0.032 ± 0.002	0.0044 ± 0.0003	0.0284 ± 0.0005	0.0033 ± 0.0001	0.61 ± 0.01	396.8 ± 13.0	0.044 ± 0.001
21	-19.6724	46.544	500	0.86 ± 0.02	1.66 ± 0.04	0.17 ± 0.01	0.65 ± 0.02	0.14 ± 0.00	0.039 ± 0.002	0.111 ± 0.003	0.035 ± 0.002	0.090 ± 0.006	0.017 ± 0.000	0.046 ± 0.002	0.0064 ± 0.0004	0.0401 ± 0.0013	0.0056 ± 0.0002	1.17 ± 0.03	545.3 ± 17.9	0.142 ± 0.003
21	-19.6724	46.544	600	1.68 ± 0.04	3.23 ± 0.06	0.22 ± 0.00	0.74 ± 0.02	0.09 ± 0.00	0.023 ± 0.001	0.088 ± 0.002	0.015 ± 0.000	0.073 ± 0.003	0.015 ± 0.001	0.040 ± 0.002	0.0059 ± 0.0002	0.0366 ± 0.0010	0.0048 ± 0.0001	0.74 ± 0.02	437.2 ± 10.7	0.072 ± 0.002
21	-19.6724	46.544	700	1.09 ± 0.03	2.09 ± 0.05	0.28 ± 0.01	1.15 ± 0.03	0.46 ± 0.01	0.064 ± 0.002	0.184 ± 0.005	0.027 ± 0.001	0.139 ± 0.007	0.025 ± 0.001	0.068 ± 0.003	0.0097 ± 0.0005	0.0577 ± 0.0015	0.0076 ± 0.0003	1.15 ± 0.03	383.4 ± 13.5	0.135 ± 0.003
21	-19.6724	46.544	800	0.81 ± 0.02	2.19 ± 0.04	0.14 ± 0.00	0.52 ± 0.01	0.11 ± 0.01	0.030 ± 0.001	0.097 ± 0.002	0.013 ± 0.001	0.079 ± 0.003	0.015 ± 0.000	0.042 ± 0.002	0.0062 ± 0.0004	0.0367 ± 0.0010	0.0050 ± 0.0002	1.02 ± 0.03	319.1 ± 9.9	0.073 ± 0.002
21	-19.6724	46.544	1000	1.01 ± 0.03	1.95 ± 0.05	0.26 ± 0.01	1.03 ± 0.04	0.21 ± 0.01	0.059 ± 0.002	0.171 ± 0.004	0.025 ± 0.001	0.129 ± 0.006	0.023 ± 0.001	0.063 ± 0.003	0.0090 ± 0.0005	0.0536 ± 0.0014	0.0071 ± 0.0003	1.07 ± 0.03	356.2 ± 12.5	0.125 ± 0.003
21	-19.6724	46.544	1200	0.53 ± 0.01	1.36 ± 0.03	0.12 ± 0.00	0.45 ± 0.01	0.09 ± 0.00	0.020 ± 0.001	0.081 ± 0.002	0.011 ± 0.001	0.068 ± 0.004	0.013 ± 0.000	0.037 ± 0.001	0.0052 ± 0.0003	0.0348 ± 0.0010	0.0044 ± 0.0001	0.68 ± 0.02	242.2 ± 7.7	0.079 ± 0.002
26	-22.6046	50.278	20	0.99 ± 0.03	0.64 ± 0.01	0.16 ± 0.00	0.61 ± 0.02	0.13 ± 0.01	0.028 ± 0.001	0.127 ± 0.004	0.018 ± 0.001	0.109 ± 0.004	0.022 ± 0.001	0.065 ± 0.003	0.0092 ± 0.0005	0.0647 ± 0.0016	0.0077 ± 0.0003	2.06 ± 0.05	1047.0 ± 21.4	0.048 ± 0.003
26	-22.6046	50.278	50	2.31 ± 0.12	1.35 ± 0.06	0.38 ± 0.03	1.52 ± 0.07	0.32 ± 0.03	0.085 ± 0.005	0.307 ± 0.013	0.082 ± 0.006	0.253 ± 0.018	0.049 ± 0.002	0.144 ± 0.014	0.0203 ± 0.0015	0.1364 ± 0.0058	0.0206 ± 0.0010	2.88 ± 0.17	1921.2 ± 129.8	0.072 ± 0.003
26	-22.6046	50.278	75	0.88 ± 0.02	0.95 ± 0.02	0.17 ± 0.01	0.64 ± 0.02	0.12 ± 0.01	0.035 ± 0.003	0.125 ± 0.004	0.018 ± 0.001	0.104 ± 0.004	0.021 ± 0.001	0.060 ± 0.002	0.0083 ± 0.0004	0.0565 ± 0.0016	0.0077 ± 0.0003	1.24 ± 0.03	362.3 ± 11.7	0.058 ± 0.002
26	-22.6046	50.278	99	0.55 ± 0.02	0.35 ± 0.01	0.10 ± 0.00	0.37 ± 0.01	0.08 ± 0.00	0.019 ± 0.001	0.090 ± 0.005	0.011 ± 0.000	0.063 ± 0.003	0.013 ± 0.000	0.036 ± 0.002	0.0052 ± 0.0002	0.0326 ± 0.0009	0.0045 ± 0.0001	0.72 ± 0.03	159.3 ± 4.9	0.030 ± 0.001
26	-22.6046	50.278	200	0.35 ± 0.01	0.57 ± 0.02	0.05 ± 0.00	0.19 ± 0.01	0.04 ± 0.00	0.010 ± 0.000	0.049 ± 0.003	0.007 ± 0.000	0.037 ± 0.003	0.007 ± 0.000	0.019 ± 0.001	0.0028 ± 0.0002	0.0181 ± 0.0005	0.0018 ± 0.0001	0.50 ± 0.02	424.0 ± 16.4	0.032 ± 0.001
26	-22.6046	50.278	400	0.41 ± 0.01	0.77 ± 0.02	0.07 ± 0.00	0.28 ± 0.01	0.05 ± 0.00	0.021 ± 0.001	0.056 ± 0.002	0.008 ± 0.000	0.047 ± 0.002	0.009 ± 0.000	0.027 ± 0.002	0.0036 ± 0.0002	0.0231 ± 0.0007	0.0025 ± 0.0001	0.58 ± 0.02	404.0 ± 14.9	0.042 ± 0.001
26	-22.6046	50.278	599	0.45 ± 0.02	1.59 ± 0.05	0.10 ± 0.00	0.36 ± 0.01	0.08 ± 0.00	0.023 ± 0.001	0.072 ± 0.002	0.011 ± 0.000	0.061 ± 0.002	0.012 ± 0.000	0.033 ± 0.002	0.0047 ± 0.0002	0.0313 ± 0.0010	0.0039 ± 0.0001	0.69 ± 0.02	356.9 ± 12.9	0.044 ± 0.001
26	-22.6046	50.278	800	0.65 ± 0.02	1.78 ± 0.04	0.13 ± 0.00	0.51 ± 0.02	0.1 ± 0.01	0.029 ± 0.001	0.092 ± 0.002	0.014 ± 0.001	0.074 ± 0.003	0.014 ± 0.000	0.039 ± 0.003	0.0056 ± 0.0003	0.0361 ± 0.0008	0.0045 ± 0.0001	0.72 ± 0.02	366.4 ± 12.8	0.073 ± 0.002
26	-22.6046	50.278	1000	0.49 ± 0.01	1.56 ± 0.03	0.10 ± 0.00	0.41 ± 0.01	0.09 ± 0.00	0.029 ± 0.001	0.079 ± 0.002	0.011 ± 0.000	0.062 ± 0.002	0.012 ± 0.000	0.034 ± 0.002	0.0046 ± 0.0002	0.0286 ± 0.0006	0.0034 ± 0.0001	0.67 ± 0.01	300.2 ± 12.4	0.064 ± 0.002
32	-26.703	55.515	10	1.26 ± 0.03	0.69 ± 0.01	0.22 ± 0.01	0.82 ± 0.02	0.16 ± 0.01	0.038 ± 0.001	0.165 ± 0.003	0.023 ± 0.001	0.143 ± 0.005	0.029 ± 0.001	0.087 ± 0.005	0.0131 ± 0.0009	0.0839 ± 0.0020	0.0126 ± 0.0003	1.65 ± 0.03	80.3 ± 2.6	0.044 ± 0.001
32	-26.703	55.515	20	3.48 ± 0.3	1.46 ± 0.12	0.45 ± 0.05	1.71 ± 0.14	0.34 ± 0.02	0.079 ± 0.007	0.345 ± 0.068	0.051 ± 0.008	0.320 ± 0.041	0.066 ± 0.005	0.200 ± 0.030	0.0292 ± 0.0054	0.1960 ± 0.0162	0.0300 ± 0.0026	4.20 ± 0.27	203.1 ± 16.5	0.071 ± 0.005

Station	Longitude	Latitude	Depth [m]	La	Ce	Pr	Nd	Sm	Eu	Gd	Tb	Dy	Ho	Er	Tm	Yb	Lu	Y	Ba	Th
32	-26.703	55.515	40	1.14 ± 0.03	0.75 ± 0.02	0.20 ± 0.01	0.75 ± 0.02	0.15 ± 0.01	0.035 ± 0.001	0.154 ± 0.002	0.023 ± 0.001	0.141 ± 0.007	0.029 ± 0.001	0.090 ± 0.003	0.0131 ± 0.0006	0.0910 ± 0.0013	0.0136 ± 0.0003	1.63 ± 0.05	101.8 ± 3.2	0.053 ± 0.001
32	-26.703	55.515	60	0.59 ± 0.02	0.40 ± 0.01	0.11 ± 0.00	0.43 ± 0.02	0.09 ± 0.01	0.021 ± 0.001	0.090 ± 0.003	0.013 ± 0.001	0.079 ± 0.003	0.016 ± 0.000	0.048 ± 0.003	0.0068 ± 0.0005	0.0470 ± 0.0013	0.0064 ± 0.0003	0.85 ± 0.03	105.4 ± 3.6	0.034 ± 0.001
32	-26.703	55.515	80	0.83 ± 0.04	0.61 ± 0.02	0.14 ± 0.01	0.54 ± 0.02	0.12 ± 0.01	0.027 ± 0.001	0.108 ± 0.004	0.014 ± 0.001	0.084 ± 0.007	0.016 ± 0.001	0.043 ± 0.003	0.0057 ± 0.0003	0.0384 ± 0.0017	0.0048 ± 0.0002	0.88 ± 0.04	113.1 ± 5.9	0.028 ± 0.002
32	-26.703	55.515	100	0.63 ± 0.02	0.36 ± 0.01	0.12 ± 0.00	0.43 ± 0.01	0.09 ± 0.01	0.021 ± 0.001	0.085 ± 0.002	0.012 ± 0.001	0.067 ± 0.004	0.013 ± 0.000	0.035 ± 0.002	0.0043 ± 0.0002	0.0315 ± 0.0005	0.0039 ± 0.0001	0.76 ± 0.02	140.8 ± 5.1	0.023 ± 0.001
32	-26.703	55.515	120	0.56 ± 0.02	0.40 ± 0.01	0.09 ± 0.00	0.34 ± 0.01	0.08 ± 0.00	0.018 ± 0.001	0.071 ± 0.002	0.009 ± 0.000	0.060 ± 0.004	0.012 ± 0.000	0.032 ± 0.002	0.0050 ± 0.0003	0.0300 ± 0.0011	0.0036 ± 0.0002	0.70 ± 0.03	311.3 ± 11.9	0.031 ± 0.001
32	-26.703	55.515	140	0.38 ± 0.01	(2.51 ± 0.06)	0.07 ± 0.00	0.27 ± 0.01	0.06 ± 0.00	0.013 ± 0.000	0.056 ± 0.001	0.008 ± 0.000	0.044 ± 0.002	0.009 ± 0.000	0.023 ± 0.001	0.0031 ± 0.0002	0.0201 ± 0.0005	0.0022 ± 0.0001	0.69 ± 0.02	277.2 ± 12.6	0.029 ± 0.001
32	-26.703	55.515	161	0.65 ± 0.02	0.90 ± 0.03	0.09 ± 0.00	0.33 ± 0.01	0.07 ± 0.00	0.031 ± 0.001	0.071 ± 0.002	0.033 ± 0.002	0.048 ± 0.003	0.010 ± 0.000	0.027 ± 0.002	0.0041 ± 0.0002	0.0251 ± 0.0007	0.0029 ± 0.0001	0.57 ± 0.02	418.7 ± 16.0	0.055 ± 0.001
32	-26.703	55.515	200	0.31 ± 0.01	0.43 ± 0.01	0.05 ± 0.00	0.19 ± 0.00	0.05 ± 0.00	0.013 ± 0.000	0.039 ± 0.001	0.006 ± 0.000	0.035 ± 0.001	0.007 ± 0.000	0.021 ± 0.001	0.0029 ± 0.0002	0.0197 ± 0.0006	0.0022 ± 0.0001	0.46 ± 0.03	647 ± 41.8	0.124 ± 0.005
32	-26.703	55.515	300	0.59 ± 0.01	1.14 ± 0.02	0.10 ± 0.00	0.38 ± 0.01	0.07 ± 0.01	0.026 ± 0.001	0.069 ± 0.001	0.013 ± 0.001	0.058 ± 0.003	0.011 ± 0.000	0.031 ± 0.002	0.0044 ± 0.0002	0.0281 ± 0.0008	0.0032 ± 0.0001	0.68 ± 0.01	497.8 ± 19.3	0.054 ± 0.001
32	-26.703	55.515	380	0.54 ± 0.01	0.98 ± 0.03	0.09 ± 0.00	0.35 ± 0.01	0.07 ± 0.00	0.017 ± 0.001	0.066 ± 0.002	0.012 ± 0.001	0.057 ± 0.004	0.011 ± 0.000	0.031 ± 0.002	0.0042 ± 0.0003	0.0263 ± 0.0006	0.0030 ± 0.0001	0.56 ± 0.02	463.7 ± 16.6	0.065 ± 0.002
32	-26.703	55.515	450	11.42 ± 0.36	(16.27 ± 0.59)	0.14 ± 0.00	0.43 ± 0.02	0.09 ± 0.00	0.024 ± 0.001	0.099 ± 0.004	0.010 ± 0.000	0.060 ± 0.003	0.012 ± 0.001	0.033 ± 0.002	0.0045 ± 0.0002	0.0308 ± 0.0012	0.0034 ± 0.0001	0.60 ± 0.06	590.9 ± 15.5	0.060 ± 0.005
32	-26.703	55.515	500	0.54 ± 0.01	1.37 ± 0.03	0.11 ± 0.00	0.42 ± 0.01	0.09 ± 0.01	0.023 ± 0.001	0.081 ± 0.002	0.013 ± 0.001	0.064 ± 0.003	0.012 ± 0.000	0.035 ± 0.002	0.0047 ± 0.0004	0.0300 ± 0.0009	0.0037 ± 0.0001	0.61 ± 0.02	357.1 ± 14.5	0.054 ± 0.002
32	-26.703	55.515	598	0.47 ± 0.01	1.20 ± 0.03	0.10 ± 0.00	0.39 ± 0.01	0.07 ± 0.00	0.021 ± 0.001	0.070 ± 0.001	0.010 ± 0.000	0.060 ± 0.003	0.011 ± 0.000	0.032 ± 0.002	0.0045 ± 0.0002	0.0303 ± 0.0006	0.0037 ± 0.0001	0.67 ± 0.02	310.8 ± 7.1	0.055 ± 0.001
32	-26.703	55.515	700	0.53 ± 0.03	1.43 ± 0.07	0.12 ± 0.01	0.42 ± 0.02	0.08 ± 0.00	0.018 ± 0.002	0.071 ± 0.003	0.010 ± 0.001	0.059 ± 0.003	0.011 ± 0.000	0.031 ± 0.003	0.0046 ± 0.0003	0.0286 ± 0.0012	0.0032 ± 0.0002	0.71 ± 0.04	282.1 ± 16.1	0.055 ± 0.002
32	-26.703	55.515	800	0.58 ± 0.02	1.57 ± 0.05	0.12 ± 0.00	0.42 ± 0.01	0.08 ± 0.01	0.027 ± 0.001	0.079 ± 0.002	0.011 ± 0.001	0.063 ± 0.003	0.012 ± 0.000	0.032 ± 0.003	0.0042 ± 0.0003	0.0281 ± 0.0006	0.0035 ± 0.0001	0.59 ± 0.02	316.1 ± 19.2	0.068 ± 0.002
32	-26.703	55.515	1000	0.56 ± 0.02	1.47 ± 0.05	0.11 ± 0.00	0.44 ± 0.02	0.07 ± 0.00	0.022 ± 0.001	0.082 ± 0.002	0.015 ± 0.001	0.066 ± 0.003	0.013 ± 0.000	0.035 ± 0.002	0.0049 ± 0.0002	0.0307 ± 0.0007	0.0034 ± 0.0001	0.85 ± 0.03	262.2 ± 12.3	0.056 ± 0.002
38	-31.266	58.843	10	4.90 ± 0.07	6.13 ± 0.10	0.37 ± 0.01	1.39 ± 0.03	0.25 ± 0.00	0.057 ± 0.002	0.274 ± 0.013	0.033 ± 0.001	0.188 ± 0.004	0.036 ± 0.001	0.100 ± 0.003	0.0124 ± 0.0003	0.0763 ± 0.0016	0.0091 ± 0.0003	2.17 ± 0.04	197.0 ± 4.1	0.037 ± 0.001
38	-31.266	58.843	20	2.73 ± 0.02	1.70 ± 0.01	0.50 ± 0.00	2.54 ± 0.02	0.36 ± 0.00	0.080 ± 0.001	0.420 ± 0.003	0.048 ± 0.000	0.271 ± 0.002	0.052 ± 0.000	0.138 ± 0.001	0.0183 ± 0.0001	0.1105 ± 0.0007	0.0138 ± 0.0001	2.94 ± 0.02	101.0 ± 0.7	0.040 ± 0.000
38	-31.266	58.843	40	1.67 ± 0.04	1.09 ± 0.02	0.35 ± 0.01	1.28 ± 0.03	0.24 ± 0.01	0.054 ± 0.001	0.217 ± 0.008	0.030 ± 0.002	0.169 ± 0.008	0.031 ± 0.001	0.087 ± 0.004	0.0108 ± 0.0006	0.0667 ± 0.0016	0.0089 ± 0.0003	1.83 ± 0.04	184.4 ± 6.4	0.135 ± 0.005
38	-31.266	58.843	60	0.61 ± 0.01	0.36 ± 0.01	0.12 ± 0.00	0.48 ± 0.01	0.10 ± 0.00	0.021 ± 0.000	0.084 ± 0.009	0.011 ± 0.000	0.068 ± 0.002	0.012 ± 0.000	0.032 ± 0.001	0.0046 ± 0.0002	0.0260 ± 0.0006	0.0025 ± 0.0001	0.68 ± 0.02	115.4 ± 2.6	0.111 ± 0.003
38	-31.266	58.843	80	0.44 ± 0.01	0.48 ± 0.01	0.07 ± 0.00	0.27 ± 0.01	0.06 ± 0.00	0.013 ± 0.000	0.054 ± 0.001	0.007 ± 0.000	0.043 ± 0.002	0.008 ± 0.000	0.022 ± 0.001	0.0030 ± 0.0002	0.0202 ± 0.0005	0.0020 ± 0.0001	0.37 ± 0.01	176.6 ± 6.2	0.018 ± 0.001
38	-31.266	58.843	100	0.38 ± 0.01	(3.17 ± 0.07)	0.07 ± 0.00	0.25 ± 0.01	0.05 ± 0.00	0.013 ± 0.000	0.050 ± 0.001	0.007 ± 0.000	0.040 ± 0.002	0.008 ± 0.000	0.022 ± 0.001	0.0032 ± 0.0002	0.0195 ± 0.0006	0.0021 ± 0.0001	0.34 ± 0.01	249.9 ± 7.9	0.020 ± 0.001
38	-31.266	58.843	120	0.41 ± 0.01	0.54 ± 0.02	0.07 ± 0.00	0.25 ± 0.01	0.06 ± 0.00	0.015 ± 0.001	0.053 ± 0.001	0.007 ± 0.000	0.042 ± 0.003	0.008 ± 0.000	0.021 ± 0.001	0.0030 ± 0.0002	0.0193 ± 0.0005	0.0015 ± 0.0001	0.42 ± 0.01	357.1 ± 13.5	0.060 ± 0.002
38	-31.266	58.843	140	0.45 ± 0.01	0.56 ± 0.01	0.07 ± 0.00	0.26 ± 0.01	0.05 ± 0.00	0.013 ± 0.000	0.053 ± 0.001	0.008 ± 0.000	0.046 ± 0.001	0.009 ± 0.000	0.025 ± 0.002	0.0036 ± 0.0001	0.0226 ± 0.0005	0.0025 ± 0.0001	0.39 ± 0.01	498.8 ± 12.0	0.023 ± 0.001
38	-31.266	58.843	160	0.75 ± 0.02	1.14 ± 0.03	0.11 ± 0.00	0.42 ± 0.02	0.08 ± 0.00	0.023 ± 0.001	0.077 ± 0.002	0.011 ± 0.001	0.062 ± 0.004	0.012 ± 0.000	0.034 ± 0.002	0.0050 ± 0.0004	0.0315 ± 0.0008	0.0036 ± 0.0002	0.66 ± 0.02	635.9 ± 25.1	0.108 ± 0.006
38	-31.266	58.843	180	0.49 ± 0.01	0.55 ± 0.01	0.08 ± 0.00	0.31 ± 0.01	0.07 ± 0.00	0.015 ± 0.000	0.075 ± 0.006	0.010 ± 0.000	0.055 ± 0.002	0.011 ± 0.000	0.031 ± 0.002	0.0040 ± 0.0003	0.0270 ± 0.0006	0.0030 ± 0.0001	0.50 ± 0.01	644.8 ± 15.6	0.031 ± 0.001
38	-31.266	58.843	200	0.47 ± 0.01	0.60 ± 0.01	0.09 ± 0.00	0.33 ± 0.01	0.07 ± 0.00	0.017 ± 0.000	0.066 ± 0.001	0.016 ± 0.000	0.057 ± 0.001	0.011 ± 0.000	0.029 ± 0.001	0.0042 ± 0.0002	0.0271 ± 0.0007	0.0030 ± 0.0001	0.52 ± 0.02	595.1 ± 16.7	0.026 ± 0.002
38	-31.266	58.843	300	0.58 ± 0.02	1.02 ± 0.03	0.12 ± 0.00	0.48 ± 0.02	0.10 ± 0.01	0.037 ± 0.002	0.098 ± 0.003	0.015 ± 0.001	0.082 ± 0.005	0.016 ± 0.000	0.044 ± 0.003	0.0060 ± 0.0003	0.0376 ± 0.0015	0.0043 ± 0.0002	0.75 ± 0.03	745.8 ± 26.9	0.052 ± 0.001
38	-31.266	58.843	400	0.86 ± 0.03	1.62 ± 0.05	0.20 ± 0.01	0.77 ± 0.03	0.15 ± 0.01	0.051 ± 0.002	0.154 ± 0.005	0.023 ± 0.001	0.132 ± 0.006	0.025 ± 0.001	0.068 ± 0.004	0.0092 ± 0.0005	0.0569 ± 0.0022	0.0069 ± 0.0003	1.34 ± 0.05	679.3 ± 27.0	0.068 ± 0.004
38	-31.266	58.843	500	0.83 ± 0.02	1.65 ± 0.04	0.20 ± 0.01	0.82 ± 0.03	0.18 ± 0.01	0.052 ± 0.002	0.197 ± 0.009	0.026 ± 0.001	0.151 ± 0.004	0.028 ± 0.001	0.078 ± 0.003	0.0103 ± 0.0005	0.0654 ± 0.0018	0.0081 ± 0.0003	1.42 ± 0.04	428.8 ± 16.3	0.063 ± 0.003
38	-31.266	58.843	600	1.15 ± 0.03	2.29 ± 0.05	0.24 ± 0.01	0.98 ± 0.04	0.21 ± 0.02	0.070 ± 0.003	0.203 ± 0.005	0.032 ± 0.001	0.175 ± 0.007	0.033 ± 0.001	0.091 ± 0.005	0.0125 ± 0.0006	0.0769 ± 0.0016	0.0098 ± 0.0003	1.54 ± 0.05	525.3 ± 19.7	0.107 ± 0.003
38	-31.266	58.843	700	0.93 ± 0.02	1.78 ± 0.04	0.20 ± 0.00	0.80 ± 0.02	0.24 ± 0.01	0.045 ± 0.001	0.160 ± 0.003	0.025 ± 0.001	0.138 ± 0.003	0.026 ± 0.000	0.074 ± 0.003	0.0095 ± 0.0003	0.0620 ± 0.0013	0.0077 ± 0.0001	1.42 ± 0.03	732.6 ± 20.0	0.080 ± 0.002
38	-31.266	58.843	800	2.19 ± 0.06	5.09 ± 0.15	0.34 ± 0.02	1.19 ± 0.03	0.15 ± 0.01	0.038 ± 0.001	0.148 ± 0.004	0.027 ± 0.002	0.124 ± 0.005	0.023 ± 0.001	0.064 ± 0.004	0.0082 ± 0.0004	0.0529 ± 0.0014	0.0065 ± 0.0002	1.04 ± 0.03	273.0 ± 9.5	0.070 ± 0.004
38	-31.266	58.843	1000	0.90 ± 0.02	1.77 ± 0.04	0.24 ± 0.01	0.97 ± 0.04	0.21 ± 0.01	0.056 ± 0.001	0.208 ± 0.005	0.032 ± 0.002	0.178 ± 0.006	0.033 ± 0.001	0.09 ± 0.004	0.0120 ± 0.0005	0.0751 ± 0.0016	0.0095 ± 0.0003	1.52 ± 0.04	244.6 ± 9.3	0.084 ± 0.003
44	-38.954	59.62	10	0.72 ± 0.02	0.59 ± 0.02	0.12 ± 0.01	0.45 ± 0.02	0.09 ± 0.00	0.025 ± 0.001	0.115 ± 0.004	0.025 ± 0.001	0.129 ± 0.01	0.029 ± 0.001	0.100 ± 0.007	0.0173 ± 0.0012	0.1376 ± 0.0040	0.0208 ± 0.0007	1.91 ± 0.07	115.4 ± 1.2	0.082 ± 0.003
44	-38.954	59.62	20	0.82 ± 0.03	0.48 ± 0.02	0.13 ± 0.01	0.56 ± 0.03	0.10 ± 0.00	0.029 ± 0.001	0.127 ± 0.004	0.021 ± 0.001	0.153 ± 0.008	0.035 ± 0.001	0.123 ± 0.007	0.0209 ± 0.0013	0.1716 ± 0.0036	0.0267 ± 0.0008	2.50 ± 0.08	95.4 ± 1.1	0.082 ± 0.002
44	-38.954	59.62	40	0.55 ± 0.02	0.48 ± 0.02	0.11 ± 0.00	0.44 ± 0.01	0.09 ± 0.00	0.025 ± 0.001	0.101 ± 0.003	0.020 ± 0.001	0.092 ± 0.003	0.019 ± 0.001	0.056 ± 0.002	0.0083 ± 0.0004	0.0571 ± 0.0018	0.0079 ± 0.0003	1.24 ± 0.05	282.4 ± 9.1	0.048 ± 0.001
44	-38.954	59.62	60	0.79 ± 0.03	0.80 ± 0.03	0.11 ± 0.00	0.39 ± 0.01	0.09 ± 0.00	0.02 ± 0.001	0.087 ± 0.003	0.012 ± 0.001	0.075 ± 0.002	0.015 ± 0.000	0.044 ± 0.002	0.0063 ± 0.0003	0.0442 ± 0.0013	0.0055 ± 0.0002	0.79 ± 0.03	287.5 ± 8.5	0.040 ± 0.001
44	-38.954	59.62	80	0.39 ± 0.01	0.91 ± 0.02	0.08 ± 0.00	0.29 ± 0.01	0.06 ± 0.00	0.015 ± 0.000	0.060 ± 0.001	0.008 ± 0.000	0.049 ± 0.002	0.009 ± 0.000	0.028 ± 0.001	0.0038 ± 0.0002	0.0246 ± 0.0006	0.0028 ± 0.0001	0.77 ± 0.02	432.5 ± 8.7	0.042 ± 0.001
44	-38.954	59.62	100	0.46 ± 0.02	0.72 ± 0.03	0.09 ± 0.00	0.34 ± 0.01	0.06 ± 0.00	0.020 ± 0.003	0.065 ± 0.003	0.009 ± 0.001	0.055 ± 0.003	0.011 ± 0.000	0.030 ± 0.002	0.0042 ± 0.0002	0.0272 ± 0.0010	0.0031 ± 0.0002	0.54 ± 0.03	429.0 ± 18.7	0.041 ± 0.002
44	-38.954	59.62	120	0.38 ± 0.01	1.81 ± 0.03	0.08 ± 0.00	0.30 ± 0.01	0.07 ± 0.00	0.015 ± 0.000	0.063 ± 0.001	0.009 ± 0.000	0.054 ± 0.002	0.010 ± 0.000	0.029 ± 0.001	0.0038 ± 0.0002	0.0257 ± 0.0005	0.0027 ± 0.0001	0.50 ± 0.01	436.4 ± 8.2	0.036 ± 0.000
44	-38.954	59.62	140	0.40 ± 0.01	0.61 ± 0.02	0.08 ± 0.00	0.31 ± 0.01	0.07 ± 0.00	0.025 ± 0.001	0.065 ± 0.002	0.008 ± 0.000	0.049 ± 0.002	0.009 ± 0.000	0.026 ± 0.001	0.0034 ± 0.0002	0.0230 ± 0.0007	0.0022 ± 0.0001	0.56 ± 0.02	435.3 ± 12.9	0.034 ± 0.001
44	-38.954	59.62	160	1.74 ± 0.06	3.25 ± 0.12	0.12 ± 0.00	0.40 ± 0.01	0.07 ± 0.00	0.018 ± 0.001	0.078 ± 0.003	n.d.	0.057 ± 0.002	0.011 ± 0.000	0.031 ± 0.002	0.0043 ± 0.0002	0.0260 ± 0.0009	0.0028 ± 0.0001	0.54 ± 0.03	517.9 ± 20.4	0.044 ± 0.001
44	-38.954	59.62	200	0.67 ± 0.01	1.16 ± 0.02	0.14 ± 0.00	0.49 ± 0.01	0.09 ± 0.00	0.018 ± 0.000	0.084 ± 0.002	0.012 ± 0.000	0.064 ± 0.002	0.012 ± 0.000	0.033 ± 0.001	0.0044 ± 0.0002	0.0281 ± 0.0007	0.0031 ± 0.0001	0.58 ± 0.02	663.8 ± 11.8	0.038 ± 0.001
44	-38.954	59.62	300	0.51 ± 0.01	1.08 ± 0.02	0.11 ± 0.00	0.40 ± 0.01	0.08 ± 0.00	0.021 ± 0.000	0.076 ± 0.002	0.012 ± 0.000	0.064 ± 0.001	0.012 ± 0.000	0.034 ± 0.001	0.0044 ± 0.0001	0.0290 ± 0.0006	0.0032 ± 0.0001	0.68 ± 0.02	715.1 ± 14.8	0.045 ± 0.001
44	-38.954	59.62	400	0.50 ± 0.01	0.92 ± 0.02	0.11 ± 0.00	0.40 ± 0.01	0.09 ± 0.00	0.021 ± 0.001	0.083 ± 0.003	0.011 ± 0.000	0.062 ± 0.002	0.012 ± 0.000	0.032 ± 0.001	0.0045 ± 0.0002	0.0268 ± 0.0005	0.0030 ± 0.0001	0.60 ± 0.02	718.7 ± 14.7	0.048 ± 0.001
44	-38.954	59.62	500	0.60 ± 0.02	1.21 ± 0.04	0.13 ± 0.00	0.45 ± 0.01	0.08 ± 0.00	0.026 ± 0.001	0.081 ± 0.002	n.d.	0.066 ± 0.002	0.012 ± 0.000	0.034 ± 0.001	0.0047 ± 0.0003	0.0298 ± 0.0008	0.0031 ± 0.0001	0.65 ± 0.03	643.5 ± 17.8	0.055 ± 0.001
44	-38.954	59.62	600	0.58 ± 0.01	1.15 ± 0.02	0.13 ± 0.00	0.45 ± 0.01	0.09 ± 0.00	0.019 ± 0.000	0.084 ± 0.003	0.014 ± 0.000	0.057 ± 0.002	0.01 ± 0.000	0.028 ± 0.002	0.0038 ± 0.0002	0.0233 ± 0.0005	0.0023 ± 0.0001	0.42 ± 0.01	482.3 ± 9.2	0.055 ± 0.001
44	-38.954	59.62	700	0.47 ± 0.01	0.82 ± 0.02	0.10 ± 0.00	0.34 ± 0.01	0.07 ± 0.00	0.019 ± 0.001	0.067 ± 0.002	0.009 ± 0.000	0.050 ± 0.002	0.009 ± 0.000	0.025 ± 0.001	0.0034 ± 0.0002	0.0208 ± 0.0006	0.0016 ± 0.0001	0.47 ± 0.02	657.9 ± 17.9	0.041 ± 0.001
44	-38.954	59.62	800	0.26 ± 0.01	0.47 ± 0.01	0.06 ± 0.00	0.19 ± 0.01	0.04 ± 0.00	0.010 ± 0.000	0.036 ± 0.001	0.009 ± 0.000	0.028 ± 0.001	0.005 ± 0.000	0.015 ± 0.001	0.0020 ± 0.0002	0.0127 ± 0.0004	0.0010 ± 0.0001	0.20 ± 0.01	484.9 ± 14.6	0.028 ± 0.001
44	-38.954	59.62	1100	0.57 ± 0.01	1.39 ± 0.03	0.12 ± 0.00	0.43 ± 0.01	0.09 ± 0.00	0.016 ± 0.000	0.084 ± 0.004	0.014 ± 0.000	0.064 ± 0.003	0.012 ± 0.000	0.034 ± 0.001	0.0045 ± 0.0003	0.0290 ± 0.0006	0.0027 ± 0.0002	0.49 ± 0.02	282.2 ± 5.9	0.060 ± 0.001
44	-38.954	59.62	1401	0.90 ± 0.03	1.85 ± 0.07	0.14 ± 0.01	0.51 ± 0.02	0.11 ± 0.00	0.046 ± 0.007	0.098 ± 0.004	0.013 ± 0.000	0.078 ± 0.003	0.015 ± 0.001	0.041 ± 0.002	0.0055 ± 0.0002	0.0342 ± 0.0011	0.0035 ± 0.0002	0.74 ± 0.04	296.4 ± 13.9	0.089 ± 0.004
51	-42.013	59.8	10	0.59 ± 0.15	0.41 ± 0.31	0.10 ± 0.05	0.38 ± 0.14	0.08 ± 0.02	0.020 ± 0.005	0.095 ± 0.018	n.d.	0.102 ± 0.019	0.022 ± 0.003	0.077 ± 0.012	0.0129 ± 0.0015	0.1113 ± 0.0070	0.0178 ± 0.0010	1.57 ± 0.21	120.0 ± 13.4	0.057 ± 0.021
51	-42.013	59.8	19	0.42 ± 0.24	0.52 ± 0.5	0.06 ± 0.08	0.21 ± 0.21	0.04 ± 0.03	0.011 ± 0.007	0.047 ± 0.025	0.008 ± 0.004	0.054 ± 0.025	0.012 ± 0.003	0.041 ± 0.014	0.0072 ± 0.0017	0.0567 ± 0.0098	0.0092 ± 0.0014	0.71 ± 0.50	61.4 ± 11.2	0.033 ± 0.041
51	-42.013	59.8	40	0.61 ± 0.14	0.50 ± 0.23	0.10 ± 0.03	0.37 ± 0.09	0.08 ± 0.02	0.020 ± 0.004	0.088 ± 0.013	0.013 ± 0.002	0.085 ± 0.013	0.017 ± 0.002	0.055 ± 0.007	0.0085 ± 0.0007	0.0656 ± 0.0043	0.0097 ± 0.0007	1.16 ± 0.13	166.4 ± 6.9	0.038 ± 0.015
51	-42.013	59.8	60	0.64 ± 0.09	0.49 ± 0.19	0.10 ± 0.02	0.50 ± 0.08	0.08 ± 0.01	0.020 ± 0.003	0.081 ± 0.01	0.012 ± 0.002	0.082 ± 0.009	0.017 ± 0.001	0.050 ± 0.005	0.0079 ± 0.0005	0.0574 ± 0.0030	0.0080 ± 0.0004	1.01 ± 0.08	179.1 ± 3.7	0.049 ± 0.014
51	-42.013	59.8	80	0.65 ± 0.15	1.50 ± 0.32	0.11 ± 0.04	0.42 ± 0.13	0.09 ± 0.02	0.025 ± 0.004	0.084 ± 0.015	0.012 ± 0.002	0.071 ± 0.013	0.013 ± 0.002	0.038 ± 0.007	0.0057 ± 0.0007	0.0391 ± 0.0042	0.0049 ± 0.0005	0.81 ± 0.15	242.6 ± 4.8	0.050 ± 0.018
51	-42.013	59.8	100	0.73 ± 0.20	1.11 ± 0.44	0.13 ± 0.06	0.46 ± 0.19	0.09 ± 0.03	0.022 ± 0.007	0.088 ± 0.021	0.017 ± 0.003	0.072 ± 0.02	0.014 ± 0.003	0.039 ± 0.012	0.0058 ± 0.0013	0.0401 ± 0.0068	0.0052 ± 0.0009	0.83 ± 0.19	298.5 ± 11.9	0.048 ± 0.028
51	-42.013	59.8	120	0.57 ± 0.16	1.39 ± 0.32	0.15 ± 0.05	0.52 ± 0.13	0.10 ± 0.02	0.031 ± 0.005	0.103 ± 0.017	0.014 ± 0.002	0.086 ± 0.015	0.016 ± 0.002	0.043 ± 0.008	0.0058 ± 0.0011	0.0362 ± 0.0062	0.0041 ± 0.0009	0.90 ± 0.17	185.9 ± 14.1	0.062 ± 0.019
51	-42.013	59.8	140	0.76 ± 0.18	1.44 ± 0.35	0.16 ± 0.06	0.55 ± 0.15	0.11 ± 0.02	0.026 ± 0.005	0.106 ± 0.016	0.013 ± 0.003	0.081 ± 0.021	0.015 ± 0.002	0.043 ± 0.009	0.0056 ± 0.0011	0.0383 ± 0.0040	0.0045 ± 0.0005	0.79 ± 0.14	279.4 ± 5.6	0.065 ± 0.028
51	-42.013	59.8	160	0.67 ± 0.02	1.35 ± 0.02	0.15 ± 0.00	0.53 ± 0.01	0.10 ± 0.00	0.025 ± 0.001	0.105 ± 0.004	0.014 ± 0.003	0.075 ± 0.005	0.014 ± 0.001	0.038 ± 0.004	0.0054 ± 0.0008	0.0340 ± 0.0037	0.0037 ± 0.0006	0.72 ± 0.06	261.0 ± 4.9	0.066 ± 0.002
51	-42.013	59.8	180	0.92 ± 0.01	1.83 ± 0.01	0.21 ± 0.00	0.73 ± 0.00	0.14 ± 0.00	0.034 ± 0.000	0.126 ± 0.001	0.017 ± 0.000	0.101 ± 0.002	0.018 ± 0.000	0.052 ± 0.002	0.0067 ± 0.0002	0.0446 ± 0.0008	0.0053 ± 0.0001	0.93 ± 0.01	248.3 ± 1.0	0.088 ± 0.001
51	-42.013	59.8	200	1.10 ± 0.02	2.31 ± 0.02	0.25 ± 0.00	0.89 ± 0.01	0.17 ± 0.00	0.045 ± 0.001	0.201 ± 0.003	0.025 ± 0.001	0.131 ± 0.005	0.024 ± 0.001	0.068 ± 0.003	0.0090 ± 0.0004	0.0576 ± 0.0024	0.0071 ± 0.0004	1.19 ± 0.05	350.5 ± 7.3	0.110 ± 0.001
51	-42.013	59.8	300	1.36 ± 0.02	2.47 ± 0.02	0.14 ± 0.01	0.54 ± 0.02	0.09 ± 0.00	0.029 ± 0.001	0.101 ± 0.008	0.015 ± 0.001	0.086 ± 0.005	0.017 ± 0.001	0.046 ± 0.003	0.0064 ± 0.0004	0.0400 ± 0.0018	0.0049 ± 0.0003	0.92 ± 0.04	462.1 ± 7.2	0.078 ± 0.001
51	-42.013	59.8	400	1.04 ± 0.02	2.11 ± 0.04	0.23 ± 0.01	0.83 ± 0.03	0.17 ± 0.04	0.041 ± 0.001	0.165 ± 0.003	0.021 ± 0.001	0.131 ± 0.003	0.024 ± 0.000	0.067 ± 0.003	0.0091 ± 0.0007	0.0588 ± 0.0013	0.0073 ± 0.0002	1.79 ± 0.03	426.0 ± 10.3	0.087 ± 0.002
51	-42.013	59.8	500	1.06 ± 0.02	2.60 ± 0.03	0.28 ± 0.00	1.03 ± 0.01	0.21 ± 0.00	0.054 ± 0.000	0.192 ± 0.003	0.027 ± 0.001	0.159 ± 0.003	0.029 ± 0.001	0.081 ± 0.003	0.0105 ± 0.0002	0.0669 ± 0.0014	0.0082 ± 0.0002	1.44 ± 0.03	321.8 ± 8.5	0.108 ± 0.001

Station	Longitude	Latitude	Depth [m]	La	Ce	Pr	Nd	Sm	Eu	Gd	Tb	Dy	Ho	Er	Tm	Yb	Lu	Y	Ba	Th
51	-42.013	59.8	600	0.44 ± 0.02	1.02 ± 0.05	0.10 ± 0.00	0.38 ± 0.02	0.08 ± 0.00	0.025 ± 0.001	0.077 ± 0.003	0.011 ± 0.001	0.065 ± 0.003	0.012 ± 0.000	0.034 ± 0.002	0.0046 ± 0.0003	0.0282 ± 0.0014	0.0029 ± 0.0002	0.93 ± 0.04	225.8 ± 5.7	0.040 ± 0.002
51	-42.013	59.8	700	0.50 ± 0.02	1.17 ± 0.04	0.12 ± 0.01	0.43 ± 0.02	0.08 ± 0.00	0.026 ± 0.001	0.088 ± 0.005	0.012 ± 0.001	0.074 ± 0.004	0.014 ± 0.001	0.040 ± 0.002	0.0057 ± 0.0002	0.0370 ± 0.0014	0.0046 ± 0.0002	0.87 ± 0.03	259.1 ± 8.5	0.050 ± 0.002
51	-42.013	59.8	800	0.74 ± 0.02	2.26 ± 0.04	0.20 ± 0.01	0.73 ± 0.02	0.15 ± 0.00	0.036 ± 0.001	0.143 ± 0.004	0.021 ± 0.001	0.119 ± 0.003	0.022 ± 0.000	0.061 ± 0.002	0.0081 ± 0.0002	0.0511 ± 0.0011	0.0063 ± 0.0001	1.12 ± 0.03	229.5 ± 8.1	0.073 ± 0.002
51	-42.013	59.8	1000	0.53 ± 0.03	1.28 ± 0.05	0.13 ± 0.01	0.48 ± 0.02	0.10 ± 0.00	0.029 ± 0.001	0.095 ± 0.003	0.013 ± 0.001	0.079 ± 0.004	0.014 ± 0.000	0.040 ± 0.002	0.0054 ± 0.0002	0.0334 ± 0.0011	0.0038 ± 0.0002	0.83 ± 0.03	171.6 ± 6.8	0.057 ± 0.002
53	-43.006	59.9	10	4.26 ± 0.04	8.33 ± 0.08	1.18 ± 0.01	3.88 ± 0.05	0.67 ± 0.01	0.152 ± 0.003	0.54 ± 0.022	0.073 ± 0.002	0.426 ± 0.011	0.077 ± 0.002	0.218 ± 0.006	0.0302 ± 0.0007	0.2112 ± 0.0035	0.0295 ± 0.0005	5.38 ± 0.06	334.9 ± 14.2	0.557 ± 0.005
53	-43.006	59.9	20	6.23 ± 0.03	12.58 ± 0.05	1.76 ± 0.00	5.52 ± 0.01	0.90 ± 0.00	0.180 ± 0.003	0.693 ± 0.002	0.095 ± 0.000	0.52 ± 0.002	0.095 ± 0.000	0.272 ± 0.001	0.0388 ± 0.0002	0.2776 ± 0.0008	0.0394 ± 0.0001	6.25 ± 0.02	254.6 ± 8.4	1.145 ± 0.001
53	-43.006	59.9	40	3.42 ± 0.04	5.68 ± 0.08	0.71 ± 0.01	2.36 ± 0.03	0.41 ± 0.01	0.094 ± 0.001	0.317 ± 0.006	0.044 ± 0.001	0.246 ± 0.005	0.044 ± 0.001	0.125 ± 0.003	0.0169 ± 0.0003	0.1175 ± 0.0020	0.0157 ± 0.0003	2.77 ± 0.08	156.7 ± 15.3	0.360 ± 0.003
53	-43.006	59.9	60	3.99 ± 0.02	8.78 ± 0.05	1.04 ± 0.01	3.40 ± 0.02	0.56 ± 0.00	0.125 ± 0.001	0.438 ± 0.008	0.058 ± 0.001	0.321 ± 0.003	0.056 ± 0.001	0.152 ± 0.003	0.0203 ± 0.0003	0.1277 ± 0.0011	0.0167 ± 0.0002	3.36 ± 0.03	149.1 ± 6.3	0.455 ± 0.001
53	-43.006	59.9	80	5.23 ± 0.02	11.36 ± 0.03	1.41 ± 0.00	4.47 ± 0.01	0.73 ± 0.00	0.161 ± 0.001	0.535 ± 0.002	0.067 ± 0.000	0.385 ± 0.002	0.067 ± 0.000	0.180 ± 0.002	0.0243 ± 0.0002	0.1518 ± 0.0010	0.0196 ± 0.0001	4.19 ± 0.04	156.4 ± 7.3	0.648 ± 0.001
53	-43.006	59.9	100	5.45 ± 0.02	11.50 ± 0.04	1.50 ± 0.00	4.76 ± 0.02	0.77 ± 0.00	0.174 ± 0.001	0.581 ± 0.003	0.074 ± 0.001	0.422 ± 0.003	0.075 ± 0.000	0.204 ± 0.002	0.0270 ± 0.0003	0.1774 ± 0.0013	0.0231 ± 0.0002	4.43 ± 0.05	268.5 ± 7.9	0.655 ± 0.002
53	-43.006	59.9	120	4.02 ± 0.02	7.63 ± 0.05	0.97 ± 0.01	3.27 ± 0.02	0.56 ± 0.00	0.130 ± 0.001	0.454 ± 0.003	0.059 ± 0.001	0.341 ± 0.004	0.061 ± 0.000	0.170 ± 0.002	0.0233 ± 0.0002	0.1557 ± 0.0009	0.0212 ± 0.0001	3.71 ± 0.03	303.7 ± 5.6	0.448 ± 0.001
53	-43.006	59.9	140	6.85 ± 0.02	14.59 ± 0.04	1.96 ± 0.00	6.08 ± 0.02	0.93 ± 0.00	0.208 ± 0.001	0.678 ± 0.003	0.086 ± 0.001	0.459 ± 0.003	0.08 ± 0.000	0.221 ± 0.002	0.0283 ± 0.0003	0.1854 ± 0.0013	0.0239 ± 0.0001	5.21 ± 0.03	198.1 ± 5.3	0.963 ± 0.002
64	-46.083	59.07	10	0.16 ± 0.01	0.20 ± 0.01	0.03 ± 0.00	0.09 ± 0.00	0.02 ± 0.00	0.004 ± 0.000	0.019 ± 0.001	0.003 ± 0.000	0.018 ± 0.001	0.004 ± 0.000	0.012 ± 0.001	0.0018 ± 0.0001	0.0155 ± 0.0005	0.0017 ± 0.0001	0.27 ± 0.02	52.4 ± 2.2	0.020 ± 0.002
64	-46.083	59.07	20	0.50 ± 0.02	0.68 ± 0.03	0.06 ± 0.00	0.20 ± 0.01	0.03 ± 0.00	0.006 ± 0.000	0.035 ± 0.001	0.006 ± 0.001	0.031 ± 0.001	0.006 ± 0.000	0.020 ± 0.002	0.0031 ± 0.0002	0.0240 ± 0.0008	0.0027 ± 0.0001	0.27 ± 0.02	112.9 ± 4.7	0.020 ± 0.001
64	-46.083	59.07	40	0.32 ± 0.01	0.31 ± 0.01	0.04 ± 0.00	0.15 ± 0.01	0.03 ± 0.00	0.006 ± 0.000	0.031 ± 0.001	0.004 ± 0.000	0.027 ± 0.001	0.005 ± 0.000	0.016 ± 0.001	0.0022 ± 0.0001	0.0163 ± 0.0007	0.0017 ± 0.0001	0.21 ± 0.01	74.6 ± 2.8	0.019 ± 0.001
64	-46.083	59.07	60	0.39 ± 0.01	0.29 ± 0.01	0.04 ± 0.00	0.15 ± 0.01	0.04 ± 0.00	0.008 ± 0.000	0.029 ± 0.001	0.005 ± 0.000	0.029 ± 0.002	0.006 ± 0.000	0.017 ± 0.002	0.0028 ± 0.0003	0.0174 ± 0.0007	0.0016 ± 0.0001	0.29 ± 0.02	86.3 ± 4.2	0.029 ± 0.003
64	-46.083	59.07	80	0.34 ± 0.01	0.34 ± 0.01	0.05 ± 0.00	0.20 ± 0.01	0.05 ± 0.00	0.010 ± 0.000	0.040 ± 0.003	0.006 ± 0.001	0.036 ± 0.002	0.008 ± 0.001	0.020 ± 0.002	0.0039 ± 0.0004	0.0202 ± 0.0007	0.0000 ± 0.0000	n.d.	138.3 ± 3.6	0.032 ± 0.002
64	-46.083	59.07	100	2.80 ± 0.05	3.98 ± 0.26	0.23 ± 0.00	0.75 ± 0.01	0.06 ± 0.00	0.013 ± 0.000	0.063 ± 0.001	0.008 ± 0.000	0.048 ± 0.001	0.009 ± 0.000	0.027 ± 0.001	0.0034 ± 0.0001	0.0242 ± 0.0005	0.0022 ± 0.0001	0.34 ± 0.01	214.7 ± 4.8	0.034 ± 0.001
64	-46.083	59.07	120	0.65 ± 0.02	1.16 ± 0.03	0.11 ± 0.00	0.38 ± 0.01	0.08 ± 0.00	0.021 ± 0.001	0.080 ± 0.002	0.012 ± 0.000	0.068 ± 0.002	0.013 ± 0.000	0.039 ± 0.002	0.0049 ± 0.0002	0.0339 ± 0.0007	0.0039 ± 0.0001	0.72 ± 0.02	353.8 ± 9.1	0.044 ± 0.001
64	-46.083	59.07	140	0.55 ± 0.02	4.26 ± 0.17	0.11 ± 0.00	0.39 ± 0.02	0.08 ± 0.00	0.020 ± 0.001	0.086 ± 0.004	0.011 ± 0.000	0.068 ± 0.003	0.013 ± 0.000	0.039 ± 0.002	0.0056 ± 0.0003	0.0378 ± 0.0014	0.0046 ± 0.0002	0.65 ± 0.03	400.6 ± 16.2	0.056 ± 0.002
64	-46.083	59.07	160	0.71 ± 0.02	1.39 ± 0.05	0.15 ± 0.01	0.56 ± 0.02	0.12 ± 0.00	0.027 ± 0.001	0.100 ± 0.003	0.016 ± 0.001	0.084 ± 0.003	0.015 ± 0.000	0.042 ± 0.003	0.0060 ± 0.0003	0.0376 ± 0.0013	0.0042 ± 0.0002	0.73 ± 0.03	369.0 ± 13.2	0.066 ± 0.002
64	-46.083	59.07	199	1.22 ± 0.02	2.11 ± 0.04	0.24 ± 0.00	0.95 ± 0.02	0.20 ± 0.01	0.045 ± 0.001	0.170 ± 0.005	0.031 ± 0.001	0.141 ± 0.004	0.027 ± 0.000	0.073 ± 0.003	0.0103 ± 0.0003	0.0635 ± 0.0013	0.0082 ± 0.0002	1.34 ± 0.03	485.7 ± 7.7	0.120 ± 0.002
64	-46.083	59.07	300	1.15 ± 0.05	2.47 ± 0.08	0.26 ± 0.01	0.94 ± 0.04	0.18 ± 0.01	0.046 ± 0.002	0.170 ± 0.005	0.023 ± 0.001	0.139 ± 0.006	0.026 ± 0.001	0.071 ± 0.004	0.0096 ± 0.0005	0.0599 ± 0.0021	0.0072 ± 0.0003	1.66 ± 0.08	369.7 ± 11.7	0.110 ± 0.004
64	-46.083	59.07	400	1.12 ± 0.04	2.68 ± 0.08	0.3 ± 0.01	1.09 ± 0.03	0.21 ± 0.01	0.050 ± 0.001	0.182 ± 0.005	0.025 ± 0.001	0.141 ± 0.004	0.026 ± 0.001	0.071 ± 0.003	0.0094 ± 0.0004	0.0588 ± 0.0018	0.0069 ± 0.0002	1.37 ± 0.05	265.7 ± 8.6	0.125 ± 0.004
64	-46.083	59.07	500	0.60 ± 0.02	1.06 ± 0.03	0.13 ± 0.00	0.45 ± 0.02	0.09 ± 0.00	0.022 ± 0.001	0.084 ± 0.003	0.012 ± 0.001	0.069 ± 0.003	0.013 ± 0.000	0.036 ± 0.002	0.0050 ± 0.0003	0.0304 ± 0.0011	0.0031 ± 0.0002	0.57 ± 0.03	495.7 ± 14.8	0.051 ± 0.002
64	-46.083	59.07	600	0.61 ± 0.02	1.09 ± 0.03	0.13 ± 0.01	0.48 ± 0.02	0.10 ± 0.01	0.000 ± 0000	0.093 ± 0.002	0.011 ± 0.001	0.077 ± 0.007	0.015 ± 0.000	0.036 ± 0.002	0.0061 ± 0.0003	0.0321 ± 0.0017	0.0039 ± 0.0002	0.95 ± 0.03	478.9 ± 18.0	0.065 ± 0.002
64	-46.083	59.07	700	0.47 ± 0.02	1.09 ± 0.03	0.11 ± 0.00	0.39 ± 0.02	0.05 ± 0.00	0.019 ± 0.001	0.075 ± 0.002	0.01 ± 0.001	0.06 ± 0.003	0.011 ± 0.000	0.031 ± 0.002	0.0042 ± 0.0002	0.0252 ± 0.0009	0.0024 ± 0.0001	0.48 ± 0.03	351.2 ± 11.0	0.047 ± 0.002
64	-46.083	59.07	800	0.64 ± 0.01	1.35 ± 0.03	0.15 ± 0.00	0.52 ± 0.01	0.10 ± 0.00	0.025 ± 0.001	0.096 ± 0.002	0.013 ± 0.000	0.078 ± 0.002	0.014 ± 0.000	0.040 ± 0.001	0.0053 ± 0.0003	0.0345 ± 0.0006	0.0038 ± 0.0001	0.71 ± 0.02	619.3 ± 12.6	0.065 ± 0.001
64	-46.083	59.07	900	0.63 ± 0.01	1.45 ± 0.03	0.16 ± 0.00	0.56 ± 0.01	0.11 ± 0.00	0.027 ± 0.001	0.102 ± 0.002	0.014 ± 0.001	0.082 ± 0.002	0.015 ± 0.000	0.041 ± 0.002	0.0054 ± 0.0002	0.0340 ± 0.0007	0.0036 ± 0.0001	0.68 ± 0.02	516.5 ± 10.8	0.065 ± 0.001
64	-46.083	59.07	1000	0.60 ± 0.01	1.19 ± 0.02	0.13 ± 0.00	0.46 ± 0.01	0.09 ± 0.00	0.022 ± 0.001	0.082 ± 0.002	n.d.	0.065 ± 0.002	0.012 ± 0.000	0.034 ± 0.002	0.0045 ± 0.0002	0.0281 ± 0.0007	0.0029 ± 0.0001	0.58 ± 0.02	473.9 ± 8.7	0.055 ± 0.001
69	-48.093	55.84	11	1.10 ± 0.03	1.38 ± 0.04	0.05 ± 0.00	0.16 ± 0.01	0.02 ± 0.00	0.006 ± 0.000	0.024 ± 0.001	0.004 ± 0.000	0.026 ± 0.002	0.006 ± 0.000	0.019 ± 0.001	0.0032 ± 0.0001	0.0255 ± 0.0006	0.0035 ± 0.0001	0.63 ± 0.02	47.0 ± 2.7	0.031 ± 0.002
69	-48.093	55.84	20	1.97 ± 0.04	1.45 ± 0.03	0.13 ± 0.01	0.48 ± 0.02	0.11 ± 0.01	0.026 ± 0.001	0.115 ± 0.004	0.025 ± 0.001	0.126 ± 0.005	0.028 ± 0.001	0.093 ± 0.006	0.0144 ± 0.0007	0.1243 ± 0.0035	0.0183 ± 0.0005	1.67 ± 0.04	172.9 ± 4.4	0.101 ± 0.003
69	-48.093	55.84	41	0.59 ± 0.02	0.87 ± 0.03	0.09 ± 0.00	0.32 ± 0.01	0.06 ± 0.00	0.014 ± 0.001	0.058 ± 0.002	0.008 ± 0.000	0.05 ± 0.002	0.009 ± 0.000	0.029 ± 0.002	0.0039 ± 0.0002	0.0302 ± 0.0010	0.0037 ± 0.0002	0.70 ± 0.03	145.4 ± 5.4	0.050 ± 0.002
69	-48.093	55.84	60	1.06 ± 0.04	1.52 ± 0.04	0.11 ± 0.00	0.39 ± 0.01	0.08 ± 0.00	0.017 ± 0.001	0.068 ± 0.002	0.011 ± 0.000	0.055 ± 0.002	0.011 ± 0.000	0.030 ± 0.002	0.0044 ± 0.0002	0.0295 ± 0.0009	0.0036 ± 0.0001	0.64 ± 0.03	159.6 ± 4.5	0.054 ± 0.002
69	-48.093	55.84	80	0.89 ± 0.04	2.99 ± 0.09	0.18 ± 0.01	0.62 ± 0.02	0.11 ± 0.00	0.026 ± 0.001	0.102 ± 0.004	0.013 ± 0.001	0.08 ± 0.003	0.015 ± 0.000	0.042 ± 0.002	0.0059 ± 0.0003	0.0378 ± 0.0013	0.0046 ± 0.0002	0.86 ± 0.04	291.5 ± 9.3	0.085 ± 0.003
69	-48.093	55.84	100	0.97 ± 0.03	1.59 ± 0.05	0.16 ± 0.01	0.58 ± 0.02	0.11 ± 0.01	0.029 ± 0.001	0.102 ± 0.002	0.016 ± 0.001	0.08 ± 0.007	0.015 ± 0.000	0.044 ± 0.003	0.0060 ± 0.0005	0.0396 ± 0.0011	0.0047 ± 0.0002	0.91 ± 0.03	399.7 ± 16.5	0.091 ± 0.002
69	-48.093	55.84	120	1.13 ± 0.04	1.98 ± 0.07	0.19 ± 0.01	0.67 ± 0.02	0.13 ± 0.00	0.029 ± 0.001	0.108 ± 0.004	0.015 ± 0.001	0.088 ± 0.003	0.016 ± 0.001	0.045 ± 0.002	0.0062 ± 0.0003	0.0402 ± 0.0014	0.0048 ± 0.0002	1.18 ± 0.06	401.3 ± 14.8	0.095 ± 0.003
69	-48.093	55.84	140	1.12 ± 0.02	1.94 ± 0.03	0.20 ± 0.01	0.78 ± 0.03	0.15 ± 0.00	0.035 ± 0.002	0.128 ± 0.007	0.025 ± 0.001	0.099 ± 0.005	0.019 ± 0.000	0.051 ± 0.002	0.0033 ± 0.0002	0.0393 ± 0.0011	0.0008 ± 0.0001	1.12 ± 0.02	437.1 ± 11.5	0.105 ± 0.003
69	-48.093	55.84	200	0.84 ± 0.02	1.56 ± 0.03	0.17 ± 0.00	0.56 ± 0.01	0.10 ± 0.00	0.023 ± 0.001	0.087 ± 0.002	0.011 ± 0.000	0.069 ± 0.002	0.013 ± 0.000	0.035 ± 0.002	0.0047 ± 0.0002	0.0307 ± 0.0006	0.0035 ± 0.0001	0.90 ± 0.02	509.7 ± 11.7	0.076 ± 0.001
69	-48.093	55.84	300	0.75 ± 0.02	1.24 ± 0.03	0.13 ± 0.00	0.49 ± 0.01	0.09 ± 0.00	0.025 ± 0.001	0.081 ± 0.002	0.011 ± 0.000	0.065 ± 0.003	0.012 ± 0.000	0.034 ± 0.002	0.0048 ± 0.0002	0.0304 ± 0.0008	0.0034 ± 0.0001	0.79 ± 0.02	582.6 ± 16.9	0.072 ± 0.002
69	-48.093	55.84	400	0.64 ± 0.02	1.37 ± 0.04	0.15 ± 0.00	0.52 ± 0.02	0.10 ± 0.00	0.024 ± 0.001	0.086 ± 0.003	0.012 ± 0.001	0.065 ± 0.003	0.012 ± 0.000	0.033 ± 0.002	0.0045 ± 0.0003	0.0287 ± 0.0010	0.0030 ± 0.0002	0.82 ± 0.04	542.3 ± 15.2	0.087 ± 0.003
69	-48.093	55.84	502	0.70 ± 0.01	1.32 ± 0.03	0.13 ± 0.00	0.47 ± 0.01	0.09 ± 0.00	0.019 ± 0.001	0.076 ± 0.001	0.010 ± 0.000	0.059 ± 0.002	0.011 ± 0.000	0.032 ± 0.001	0.0042 ± 0.0002	0.0258 ± 0.0010	0.0027 ± 0.0001	0.66 ± 0.01	577.1 ± 13.5	0.064 ± 0.001
69	-48.093	55.84	601	0.70 ± 0.03	1.44 ± 0.04	0.14 ± 0.00	0.49 ± 0.02	0.08 ± 0.00	0.022 ± 0.001	0.078 ± 0.002	0.011 ± 0.000	0.063 ± 0.002	0.012 ± 0.000	0.033 ± 0.002	0.0049 ± 0.0002	0.0294 ± 0.0010	0.0033 ± 0.0001	0.62 ± 0.03	642.9 ± 19.3	0.059 ± 0.002
69	-48.093	55.84	700	0.63 ± 0.01	1.48 ± 0.03	0.15 ± 0.00	0.51 ± 0.01	0.09 ± 0.00	0.021 ± 0.001	0.083 ± 0.002	0.011 ± 0.000	0.066 ± 0.002	0.012 ± 0.000	0.034 ± 0.001	0.0044 ± 0.0002	0.0287 ± 0.0008	0.0030 ± 0.0001	0.81 ± 0.02	637.8 ± 15.5	0.067 ± 0.001
69	-48.093	55.84	802	0.74 ± 0.03	1.70 ± 0.06	0.17 ± 0.01	0.6 ± 0.02	0.10 ± 0.00	0.046 ± 0.003	0.099 ± 0.003	0.013 ± 0.001	0.078 ± 0.003	0.014 ± 0.000	0.040 ± 0.002	0.0053 ± 0.0002	0.0332 ± 0.0010	0.0038 ± 0.0002	0.91 ± 0.04	629.3 ± 19.6	0.082 ± 0.002
69	-48.093	55.84	900	0.83 ± 0.03	1.73 ± 0.07	0.17 ± 0.01	0.59 ± 0.03	0.09 ± 0.01	0.031 ± 0.003	0.091 ± 0.005	0.015 ± 0.001	0.071 ± 0.006	0.013 ± 0.001	0.037 ± 0.003	0.0049 ± 0.0005	0.0308 ± 0.0019	0.0033 ± 0.0002	0.69 ± 0.04	505.1 ± 19.5	0.087 ± 0.034
69	-48.093	55.84	1001	0.62 ± 0.02	1.28 ± 0.04	0.14 ± 0.00	0.46 ± 0.01	0.09 ± 0.00	0.023 ± 0.001	0.076 ± 0.002	0.010 ± 0.000	0.06 ± 0.002	0.011 ± 0.000	0.030 ± 0.002	0.0038 ± 0.0002	0.0247 ± 0.0007	0.0025 ± 0.0001	0.60 ± 0.03	505.5 ± 13.8	0.066 ± 0.002
69	-48.093	55.84	1500	0.82 ± 0.02	2.07 ± 0.05	0.2 ± 0.00	0.71 ± 0.02	0.13 ± 0.00	0.026 ± 0.001	0.103 ± 0.002	0.013 ± 0.001	0.075 ± 0.002	0.013 ± 0.000	0.035 ± 0.001	0.0047 ± 0.0002	0.0297 ± 0.0008	0.0032 ± 0.0001	0.77 ± 0.02	403.5 ± 10.6	0.107 ± 0.002
69	-48.093	55.84	1501	0.74 ± 0.02	1.60 ± 0.03	0.15 ± 0.00	0.52 ± 0.01	0.10 ± 0.00	0.021 ± 0.000	0.098 ± 0.005	0.011 ± 0.000	0.067 ± 0.002	0.012 ± 0.000	0.033 ± 0.002	0.0044 ± 0.0001	0.0278 ± 0.0005	0.0029 ± 0.0001	0.87 ± 0.02	381.9 ± 7.8	0.066 ± 0.001
77	-51.095	52.99	10	1.75 ± 0.05	1.22 ± 0.03	0.16 ± 0.01	0.62 ± 0.02	0.14 ± 0.00	0.029 ± 0.001	0.134 ± 0.004	0.020 ± 0.001	0.131 ± 0.006	0.029 ± 0.001	0.095 ± 0.004	0.0145 ± 0.0007	0.1136 ± 0.0036	0.0166 ± 0.0006	1.23 ± 0.05	102.8 ± 2.6	0.057 ± 0.003
77	-51.095	52.99	20	1.56 ± 0.05	0.78 ± 0.02	0.17 ± 0.01	0.61 ± 0.02	0.14 ± 0.01	0.037 ± 0.001	0.154 ± 0.005	0.023 ± 0.001	0.151 ± 0.007	0.033 ± 0.001	0.110 ± 0.005	0.0171 ± 0.0007	0.1293 ± 0.0038	0.0193 ± 0.0007	1.68 ± 0.07	108.3 ± 3.3	0.059 ± 0.002
77	-51.095	52.99	39	1.66 ± 0.05	1.03 ± 0.03	0.25 ± 0.01	1.06 ± 0.03	0.24 ± 0.01	0.052 ± 0.002	0.258 ± 0.008	0.033 ± 0.001	0.206 ± 0.008	0.040 ± 0.001	0.130 ± 0.006	0.0194 ± 0.0008	0.1573 ± 0.0044	0.0146 ± 0.0008	1.22 ± 0.08	150.4 ± 5.0	0.082 ± 0.005
77	-51.095	52.99	60	1.08 ± 0.03	2.92 ± 0.08	0.20 ± 0.00	0.75 ± 0.02	0.18 ± 0.00	0.038 ± 0.001	0.175 ± 0.005	0.024 ± 0.001	0.149 ± 0.004	0.03 ± 0.001	0.098 ± 0.004	0.0155 ± 0.0005	0.1212 ± 0.0029	0.0204 ± 0.0005	2.01 ± 0.06	258.7 ± 6.6	0.060 ± 0.002
77	-51.095	52.99	80	0.78 ± 0.03	0.99 ± 0.03	0.14 ± 0.01	0.52 ± 0.02	0.11 ± 0.00	0.024 ± 0.001	0.103 ± 0.004	0.014 ± 0.001	0.087 ± 0.004	0.017 ± 0.001	0.055 ± 0.003	0.0080 ± 0.0003	0.0618 ± 0.0021	0.0097 ± 0.0004	0.96 ± 0.05	335.9 ± 11.0	0.059 ± 0.002
77	-51.095	52.99	100	0.92 ± 0.02	1.83 ± 0.04	0.18 ± 0.00	0.62 ± 0.01	0.12 ± 0.00	0.025 ± 0.001	0.102 ± 0.003	0.014 ± 0.000	0.084 ± 0.003	0.016 ± 0.000	0.047 ± 0.002	0.0068 ± 0.0003	0.0488 ± 0.0009	0.0069 ± 0.0002	1.55 ± 0.04	425.4 ± 8.4	0.080 ± 0.002
77	-51.095	52.99	120	1.08 ± 0.03	1.58 ± 0.04	0.17 ± 0.00	0.61 ± 0.02	0.11 ± 0.01	0.024 ± 0.001	0.085 ± 0.002	0.047 ± 0.001	0.071 ± 0.003	0.014 ± 0.000	0.039 ± 0.002	0.0056 ± 0.0004	0.0370 ± 0.0013	0.0043 ± 0.0002	0.56 ± 0.02	347.8 ± 11.3	0.085 ± 0.004
77	-51.095	52.99	140	1.09 ± 0.03	2.14 ± 0.05	0.20 ± 0.01	0.67 ± 0.02	0.12 ± 0.00	0.024 ± 0.001	0.093 ± 0.002	0.013 ± 0.000	0.071 ± 0.002	0.013 ± 0.000	0.038 ± 0.002	0.0052 ± 0.0003	0.0340 ± 0.0007	0.0043 ± 0.0001	0.66 ± 0.02	379.9 ± 9.2	0.105 ± 0.004
77	-51.095	52.99	160	1.00 ± 0.04	1.79 ± 0.07	0.19 ± 0.01	0.66 ± 0.04	0.12 ± 0.01	0.024 ± 0.002	0.096 ± 0.008	0.017 ± 0.001	0.071 ± 0.006	0.013 ± 0.001	0.037 ± 0.003	0.0050 ± 0.0004	0.0319 ± 0.0021	0.0036 ± 0.0003	0.55 ± 0.03	389.0 ± 15.9	0.102 ± 0.006
77	-51.095	52.99	200	1.27 ± 0.04	2.71 ± 0.08	0.26 ± 0.01	0.85 ± 0.02	0.15 ± 0.00	0.031 ± 0.001	0.115 ± 0.003	0.016 ± 0.001	0.084 ± 0.003	0.016 ± 0.000	0.044 ± 0.002	0.0057 ± 0.0003	0.0374 ± 0.0010	0.0044 ± 0.0001	0.76 ± 0.03	453.5 ± 13.4	0.130 ± 0.004
77	-51.095	52.99	300	0.79 ± 0.03	1.74 ± 0.06	0.17 ± 0.01	0.57 ± 0.02	0.10 ± 0.00	0.024 ± 0.001	0.091 ± 0.003	0.011 ± 0.000	0.065 ± 0.002	0.012 ± 0.000	0.034 ± 0.002	0.0044 ± 0.0002	0.0284 ± 0.0009	0.0031 ± 0.0001	0.67 ± 0.03	455.8 ± 15.4	0.087 ± 0.003
77	-51.095	52.99	401	0.72 ± 0.03	1.62 ± 0.04	0.16 ± 0.01	0.55 ± 0.02	0.10 ± 0.00	0.025 ± 0.001	0.110 ± 0.006	0.011 ± 0.000	0.064 ± 0.002	0.012 ± 0.000	0.032 ± 0.002	0.0041 ± 0.0002	0.0270 ± 0.0010	0.0030 ± 0.0002	0.69 ± 0.03	407.0 ± 11.0	0.078 ± 0.003
77	-51.095	52.99	500	1.03 ± 0.02	2.26 ± 0.04	0.22 ± 0.00	0.75 ± 0.01	0.13 ± 0.00	0.038 ± 0.001	0.101 ± 0.002	0.013 ± 0.000	0.078 ± 0.001	0.014 ± 0.000	0.039 ± 0.001	0.0052 ± 0.0002	0.0330 ± 0.0006	0.0036 ± 0.0001	0.89 ± 0.02	491.4 ± 10.0	0.107 ± 0.002
77	-51.095	52.99	601	1.63 ± 0.05	3.65 ± 0.11	0.20 ± 0.01	0.65 ± 0.02	0.12 ± 0.00	0.025 ± 0.001	0.094 ± 0.003	0.012 ± 0.001	0.069 ± 0.002	0.012 ± 0.000	0.034 ± 0.002	0.0048 ± 0.0002	0.0293 ± 0.0009	0.0032 ± 0.0001	0.56 ± 0.02	400.2 ± 11.2	0.086 ± 0.003
77	-51.095	52.99	700	0.99 ± 0.02	2.07 ± 0.05	0.22 ± 0.01	0.71 ± 0.02	0.13 ± 0.00	0.028 ± 0.001	0.111 ± 0.002	0.014 ± 0.000	0.085 ± 0.002	0.016 ± 0.000	0.043 ± 0.001	0.0060 ± 0.0002	0.0370 ± 0.0010	0.0043 ± 0.0001	0.75 ± 0.02	596.9 ± 11.7	0.109 ± 0.003
77	-51.095	52.99	800	0.68 ± 0.02	1.54 ± 0.05	0.17 ± 0.01	0.56 ± 0.02	0.10 ± 0.00	0.024 ± 0.001	0.095 ± 0.003	0.011 ± 0.000	0.061 ± 0.002	0.011 ± 0.000	0.031 ± 0.002	0.0041 ± 0.0002	0.0252 ± 0.0007	0.0026 ± 0.0001	0.51 ± 0.02	490.9 ± 13.8	0.085 ± 0.003
77	-51.095	52.99	901	1.05 ± 0.02	1.92 ± 0.04	0.19 ± 0.00	0.91 ± 0.02	0.17 ± 0.00	0.034 ± 0.000	0.093 ± 0.007	0.013 ± 0.001	0.073 ± 0.002	0.014 ± 0.000	0.037 ± 0.001	0.0049 ± 0.0003	0.0317 ± 0.0008	0.0035 ± 0.0001	0.67 ± 0.02	511.8 ± 14.0	0.085 ± 0.005
77	-51.095	52.99	1002	1.81 ± 0.07	3.97 ± 0.12	0.17 ± 0.01	0.55 ± 0.02	0.09 ± 0.00	0.029 ± 0.001	0.080 ± 0.003	0.013 ± 0.001	0.063 ± 0.002	0.011 ± 0.000	0.032 ± 0.002	0.0044 ± 0.0002	0.0272 ± 0.0010	0.0031 ± 0.0002	0.55 ± 0.03	437.3 ± 13.5	0.084 ± 0.003

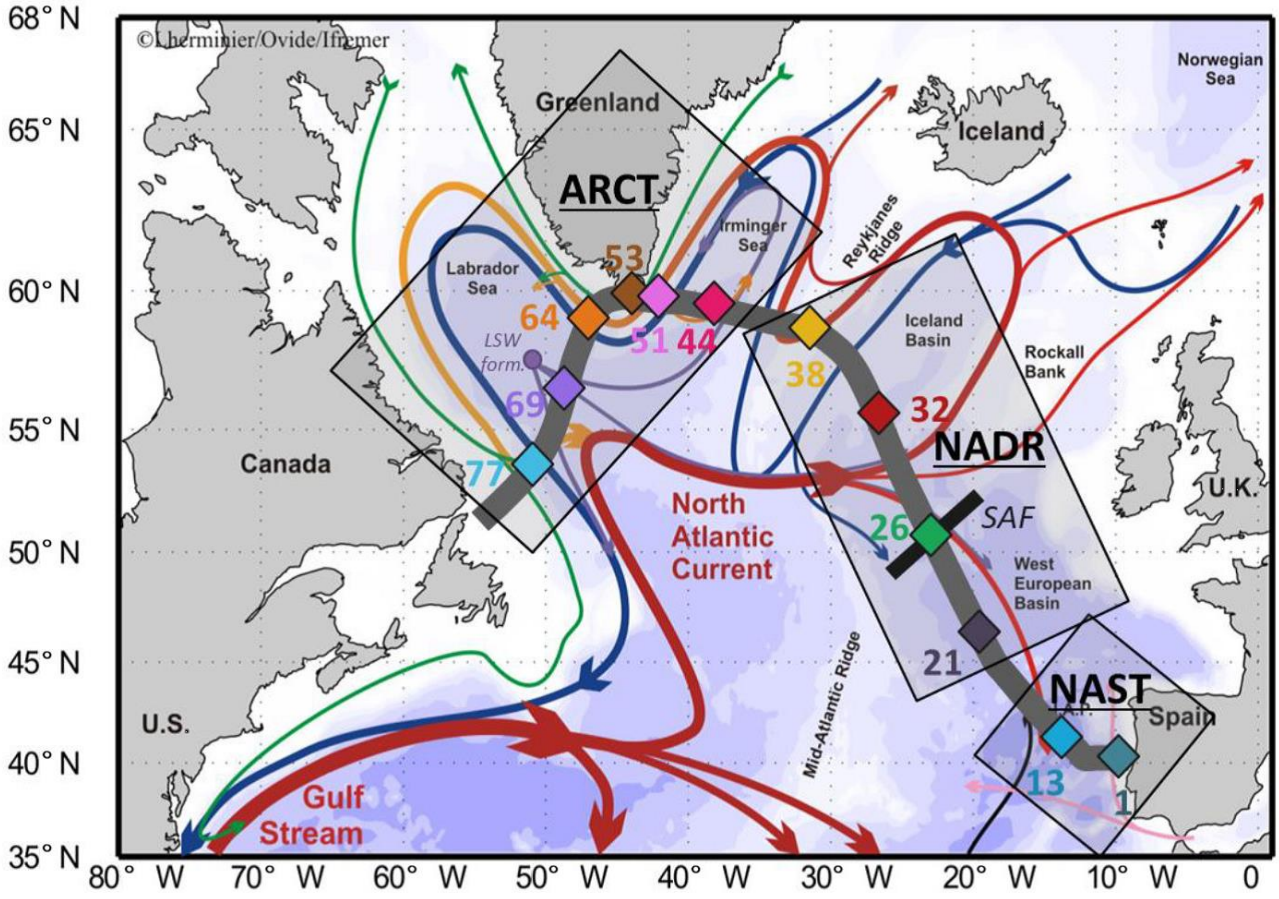

Figure 1: Map of the studied area (Subpolar North Atlantic, SPNA), including schematized circulation features, adapted from García-Ibáñez et al. (2015). Bathymetry is plotted in color with interval boundaries at 100 m, at 1000 m, and every 1000 m below 1000 m. Red and green arrows represent the main surface currents; pink and orange arrows represent currents at intermediate depths; blue and purple arrows represent the deep currents. Diamonds indicate station locations, in 3 distinct areas (grey squares): the North Atlantic Subtropical province (NAST), the North Atlantic Drift region (NADR), and the Arctic region (ARCT). The approximate locations of the subarctic front (SAF; black bar crossing station #26) and the formation site of the Labrador Sea Water (LSW form.) are also indicated. The section used in ODV figures is symbolized by the thick grey line. From (Lemaitre et al., 2018b).

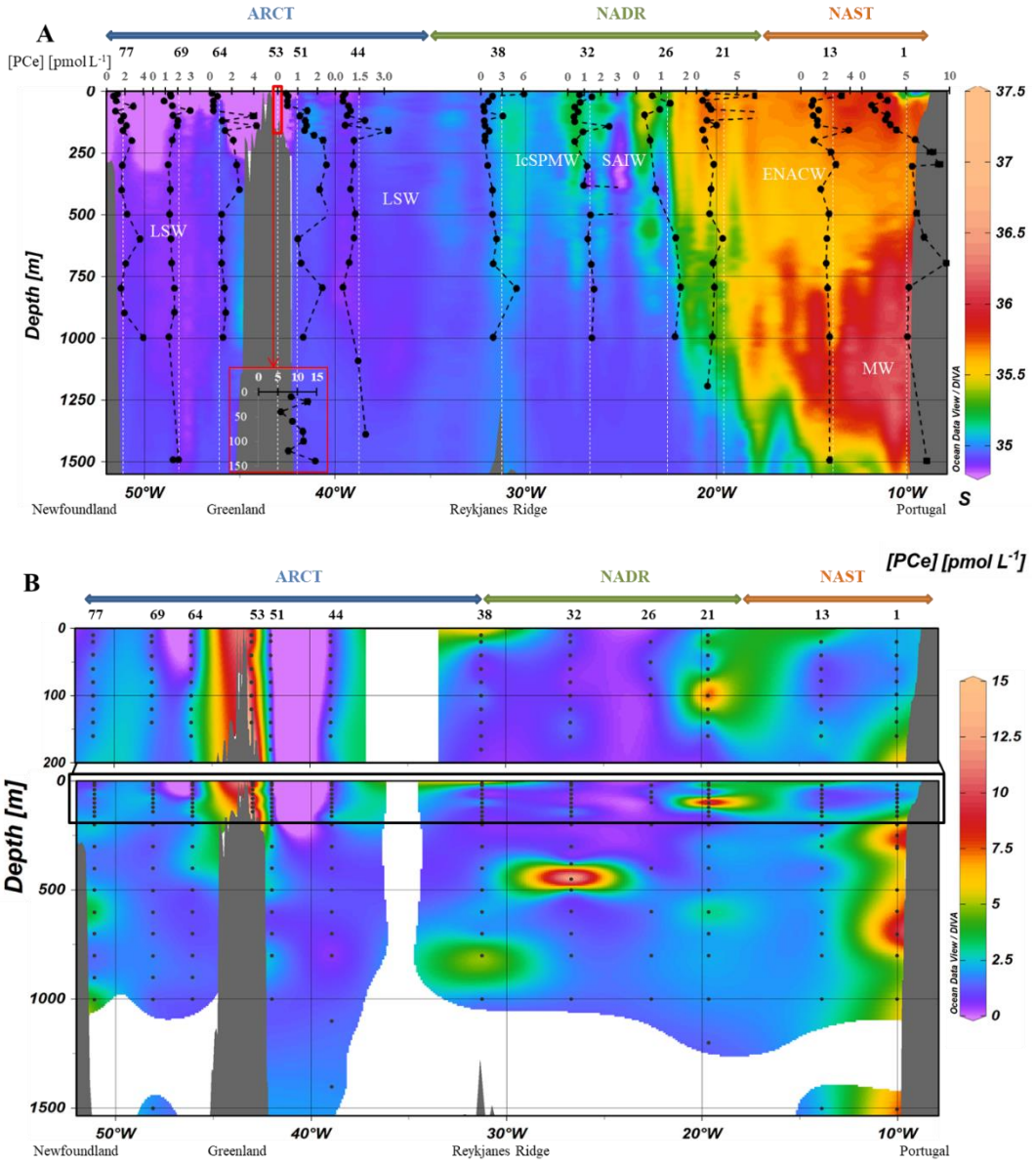

Figure 2: A. Vertical profiles of particulate [Ce] concentrations superimposed on salinity (S) measured by CTD at every GEOVIDE station (Lherminier and Sarthou, 2017); in white, the prevailing water masses characterized by a multiparametric (OMP) analysis: the Mediterranean Water (MW), the Subarctic Intermediate Water, the East North Atlantic Central Water (ENACW), the Subpolar Mode Water (SPMW), the Irminger Subpolar Mode Watern (IrSPMW) and the Labrador Sea water (LSW) (García-Ibáñez et al., 2018). For the station #53, profiles are shifted to the bottom at a lower scale because of the shallow depth of the station. This map and the following were created with the software Ocean Data View (Schlitzer, 2016). B. Particulate [Ce] concentrations interpolated with the DIVA gridding function of Ocean Data View along the section defined in Fig. 1, with a zoom in the first 200 m in the upper panel.

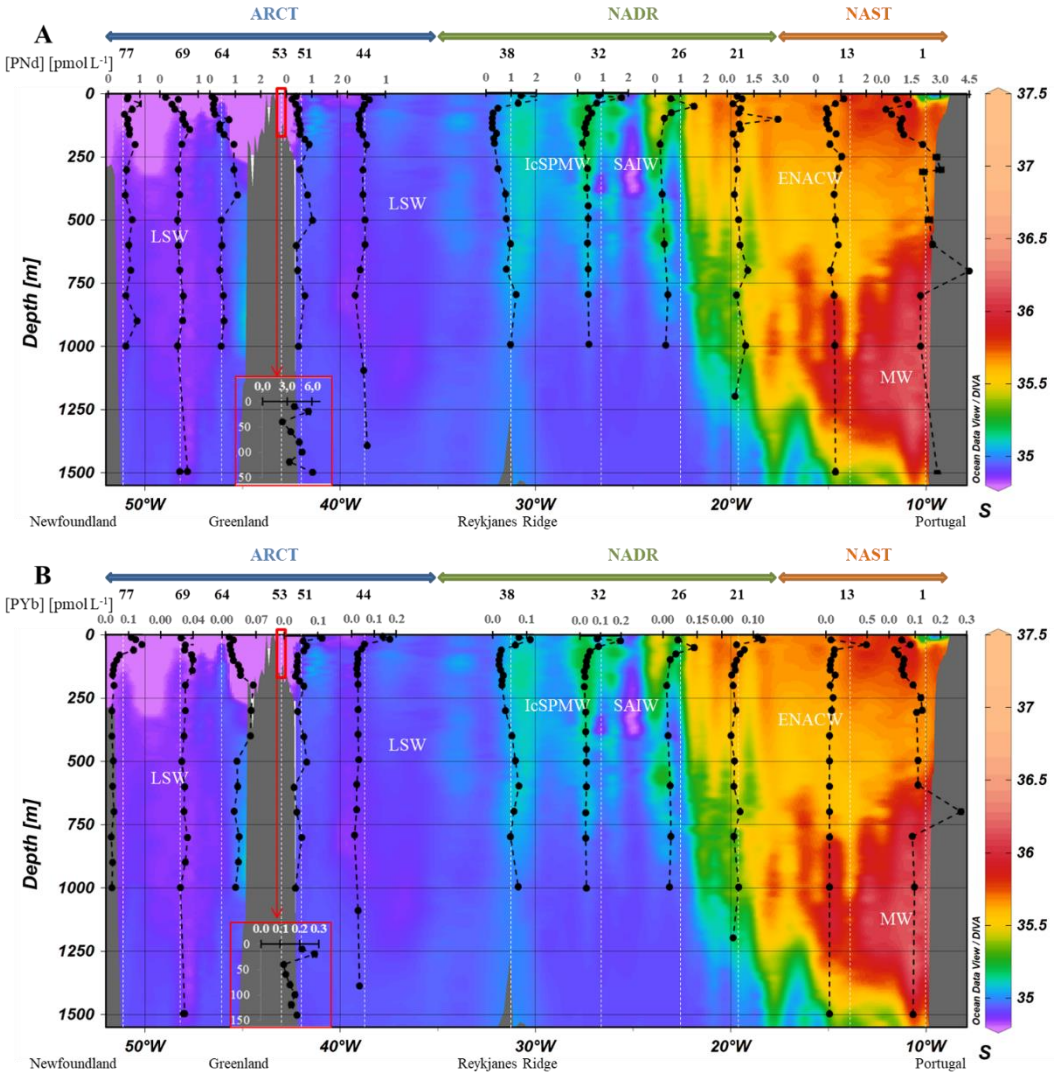
A
[PNd] [pmol L-1]
ARCT
NADR
NAST
77 69 64 53 51 44 38 32 26 21 13 1
Depth [m]
LSW
LSW
IcSPMW
SAIW
ENACW
MW
50°W
40°W
30°W
20°W
10°W
Newfoundland
Greenland
Reykjanes Ridge
Portugal
S
Ocean Data View / DIVA
B
[PYb] [pmol L-1]
ARCT
NADR
NAST
77 69 64 53 51 44 38 32 26 21 13 1
Depth [m]
LSW
LSW
IcSPMW
SAIW
ENACW
MW
50°W
40°W
30°W
20°W
10°W
Newfoundland
Greenland
Reykjanes Ridge
Portugal
S
Ocean Data View / DIVA

850

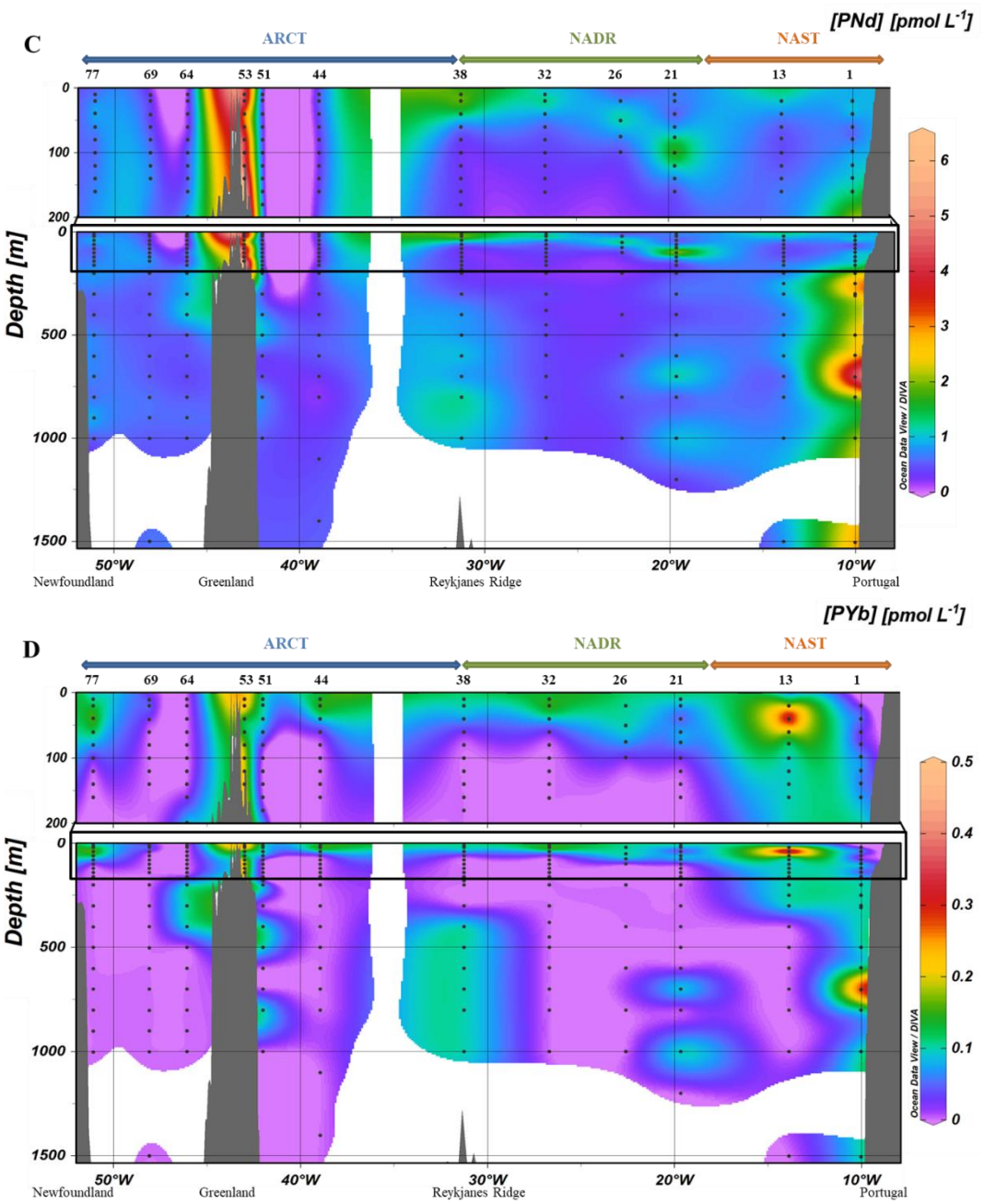

855 **Figure 3: A. Vertical profiles of particulate [Nd] and B. [Yb] concentrations superimposed on salinity (S) measured by CTD at every GEOVIDE station (Lherminier and Sarthou, 2017); in white, the prevailing water masses characterized by a multiparametric (OMP) analysis as in Fig. 2. At station #53, profiles are shifted to the bottom at a lower scale because of the shallow depth of the station. C. Particulate [Nd] and D. [Yb] concentrations interpolated with the DIVA gridding function of Ocean Data View along the section defined in Fig. 1., with a zoom on the first 200 m in the upper panel.**

860

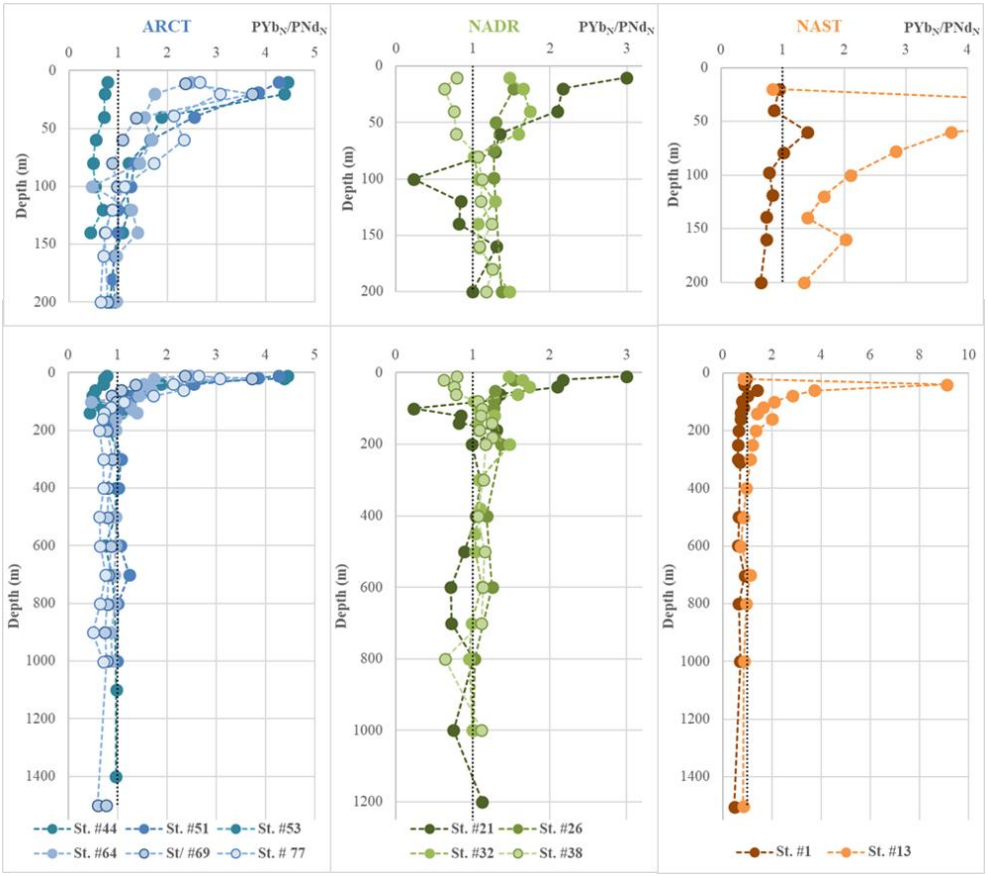

865 **Figure 4: Vertical profiles of PYb/PNd ratios normalized to PAAS in each biogeochemical province (ARCT, NADR, NAST). The upper panels present the first 200 m and lower panels all the data. The dashed black vertical line on each panel represents a ratio equal to the one of PAAS.**

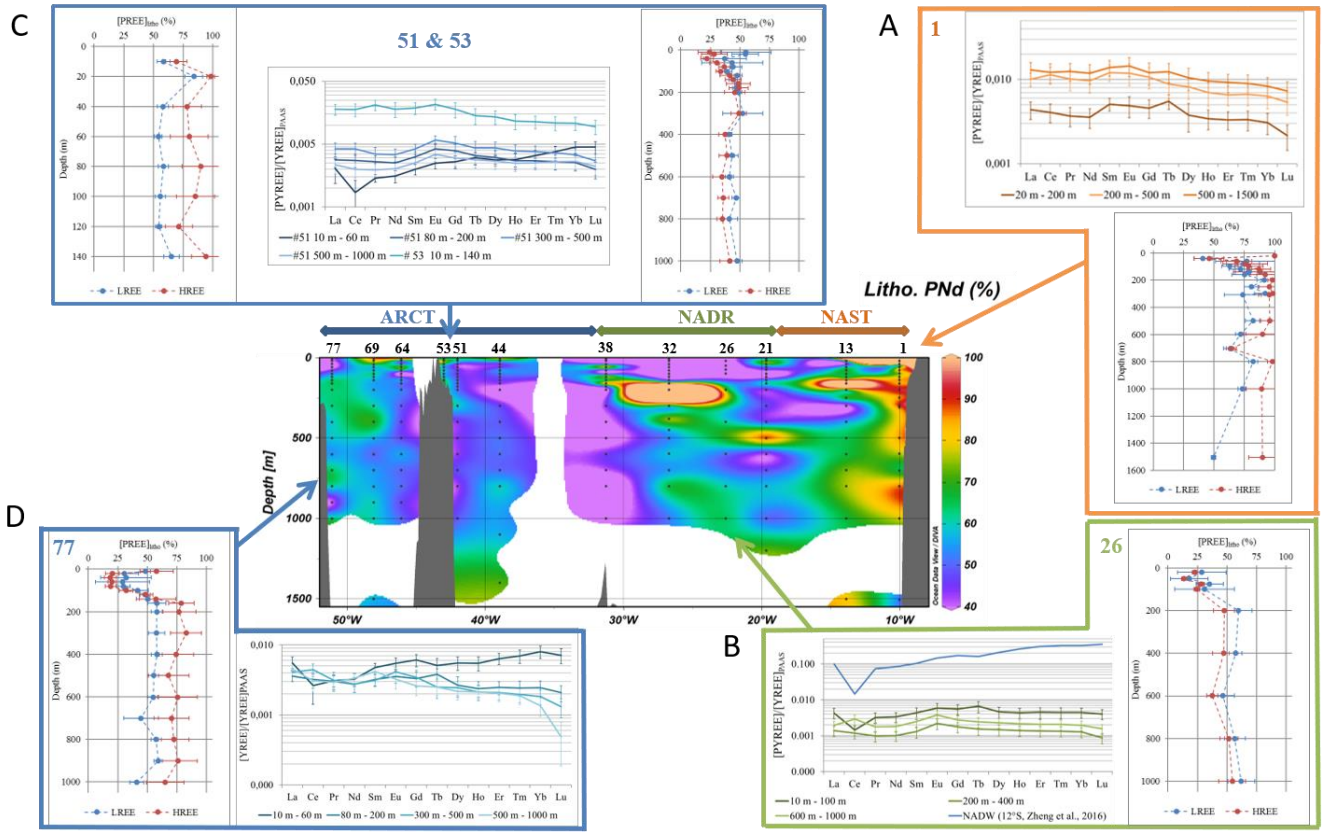

Figure 5: Center: fraction of lithogenic PNd along the GEOVIDE section (in %); Side plots: vertical profiles of the lithogenic fraction of LREE (except Ce, blue lines) and HREEs (red lines) and PAAS-normalized REE patterns of the total fraction at stations A. #1, B. #26 C. #51 and #53 and C. #77 Patterns are averaged by depth intervals displaying similar values. Error bars represent the standard deviation of the concentration series. A typical seawater pattern (NADW; 12°S, 2499m, Zheng et al., 2016) is represented along with patterns of station #26 with a blue line.

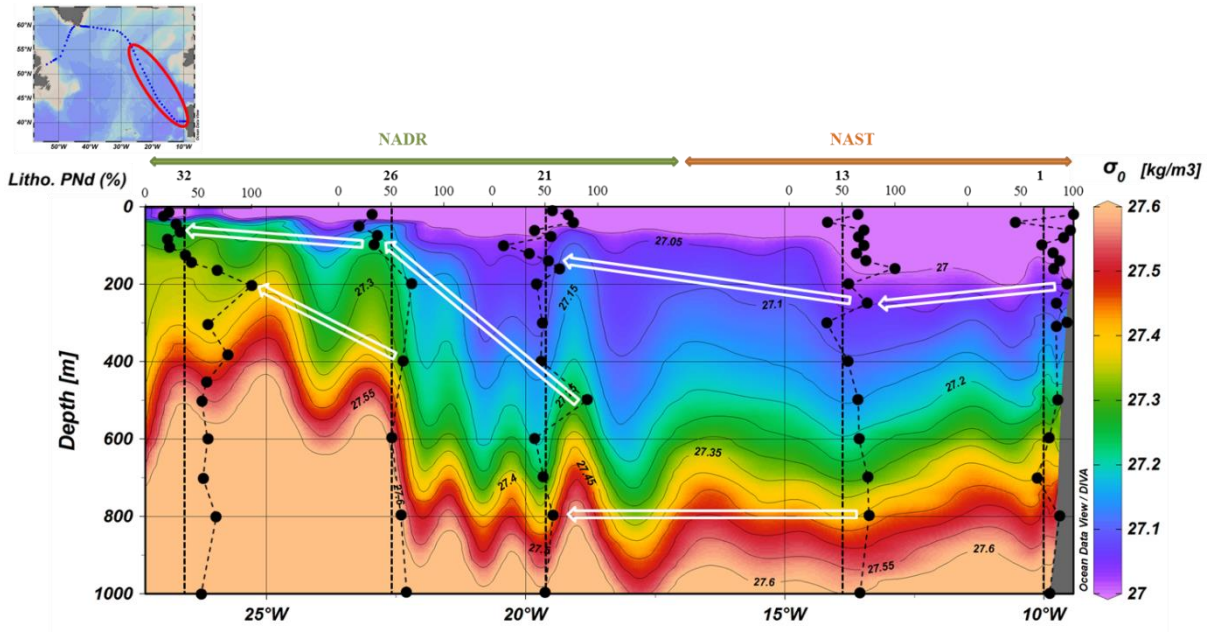

Figure 6: Estimated fraction of lithogenic PNd in the upper 1000m superimposed to density from station #1 to #32. White arrows follow the high lithogenic fractions spreading along the isopycnals σ_0=27.05 and σ_0=27.4.

880

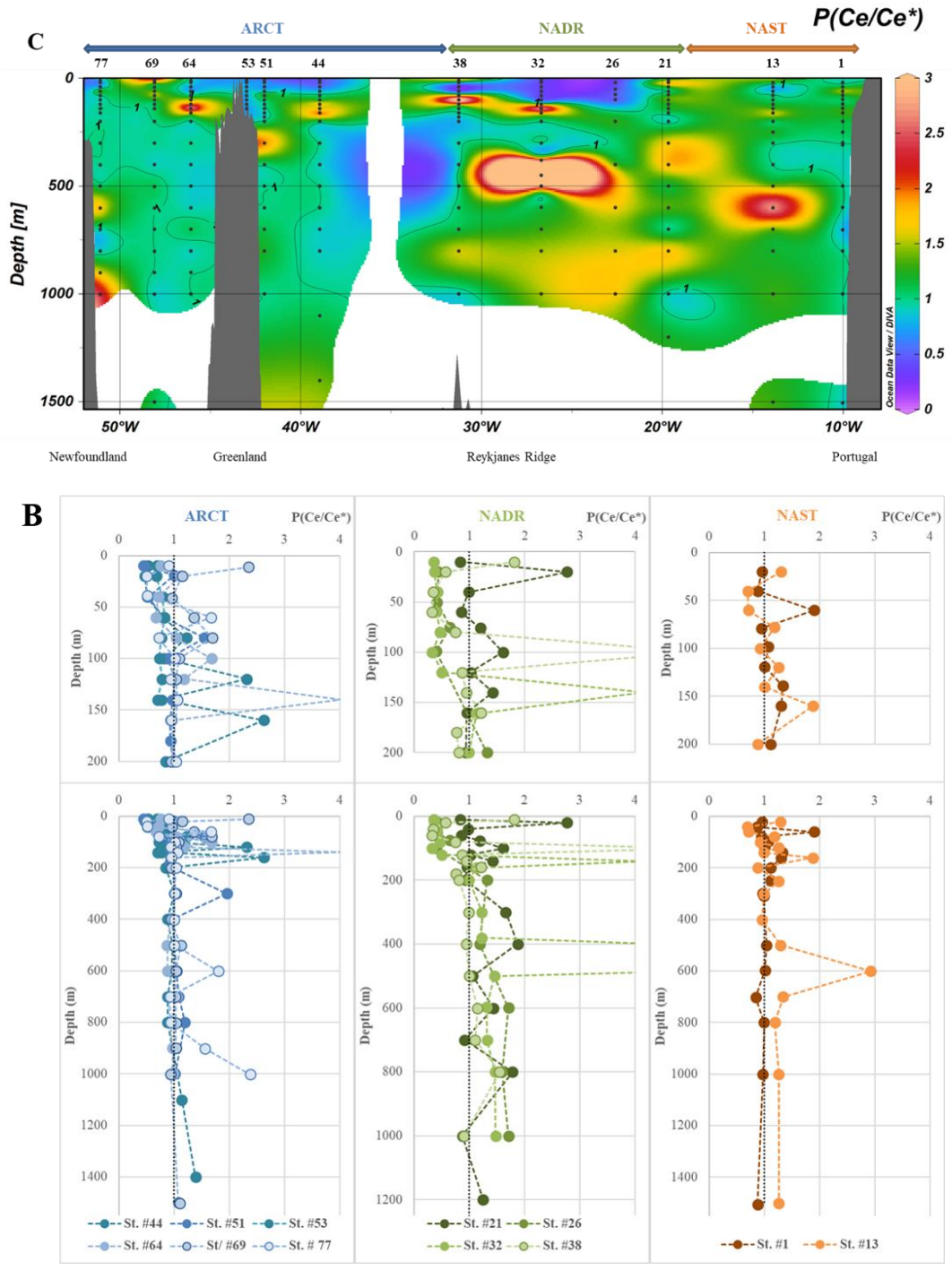

885 **Figure 7: A. Particulate Ce anomaly (Ce/Ce*) along the GEOVIDE section, interpolated with the DIVA gridding function of Ocean Data View and B. Ce/Ce* profiles grouped by biogeochemical provinces (ARCT, NADR, NAST). The upper panels present the first 200 m and lower panels all the data. Values above 2.5 are not represented. The dashed black vertical line on each panel represents the absence of anomaly (1).**

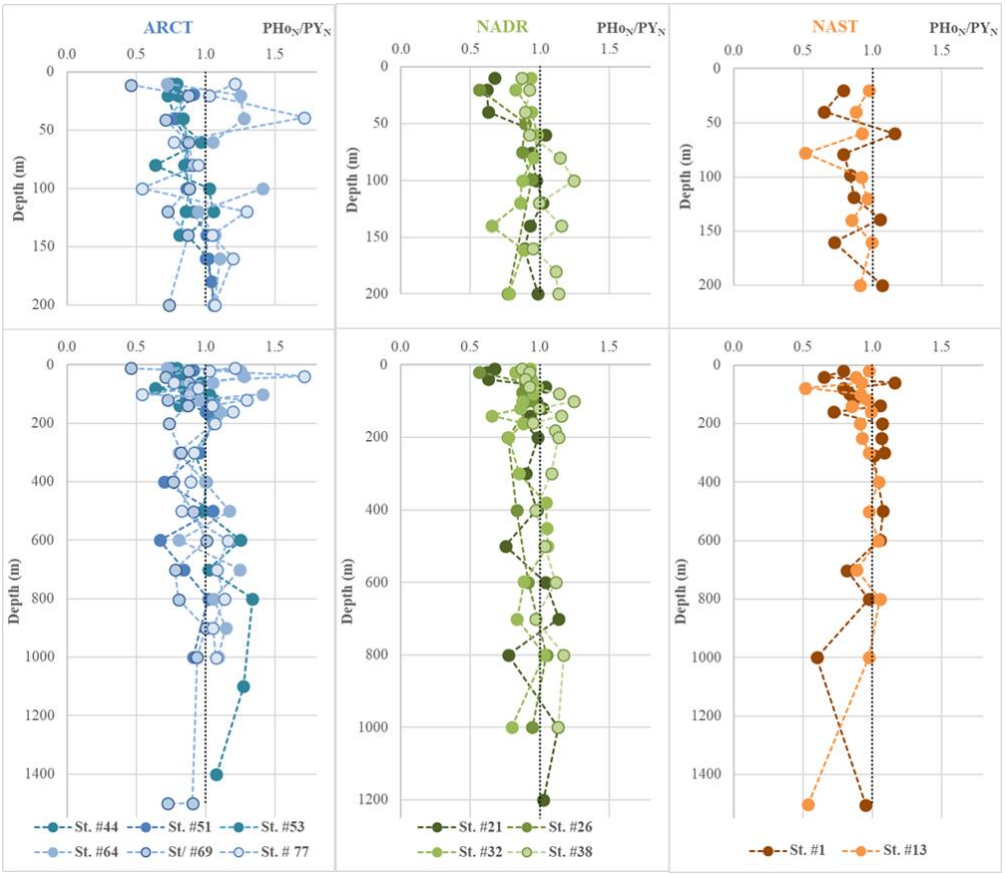

Figure 8: PAAS-normalized PHo/PY profiles grouped by biogeochemical provinces (ARCT, NADR, NAST). The upper panels present the first 200 m and lower panels all the data. The dashed black vertical line on each panel represents the PAAS-ratio (1).

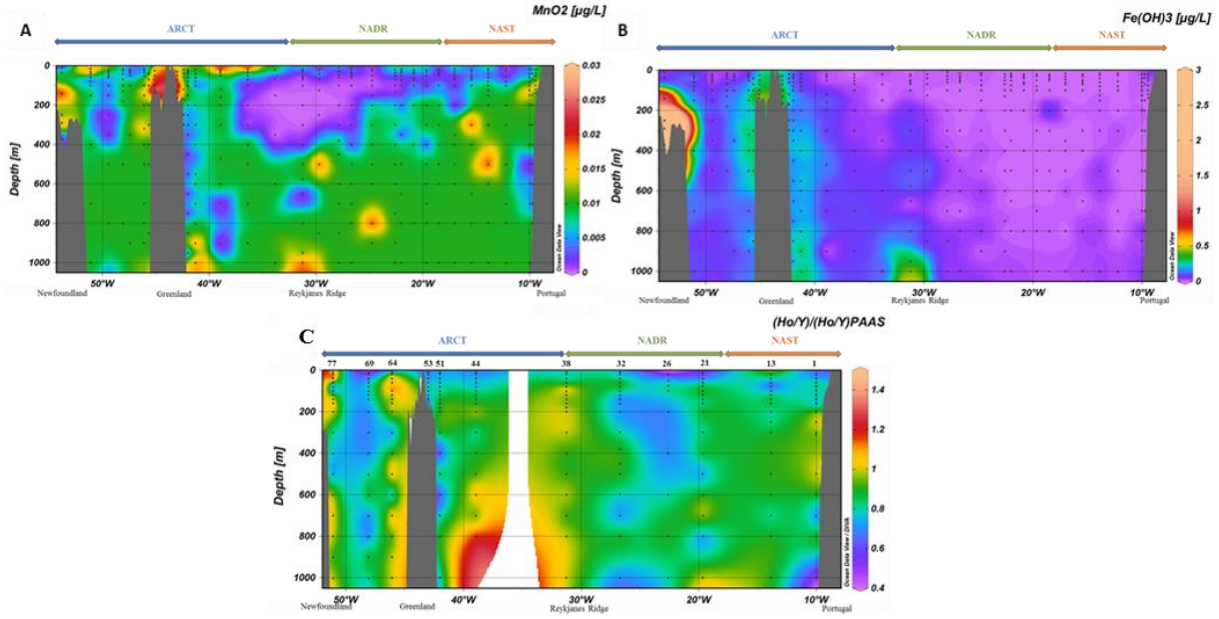

Figure 9: A. MnO_2 and B. $Fe(OH)_3$ concentrations (in $\mu g.L^{-1}$) calculated with the formula proposed by Lam et al. (2017) using particulate Mn, Fe and Al concentrations from Gourain et al. (2019). C. PHo/PY normalized to PAAS.

Author contribution

N.L. did the sampling during the cruise, helped by C.J and H.P. N.L. did the leaching on the PC filters and conducted first Ba measurements. C.J., M.B., M.G. and M.L. did REE measurements. M.L. wrote the manuscript, corrected by C.J., H.P., M.G., N.L. and P.L.

Competing interests

The authors declare that they have no conflict of interest.

Author's response to Referee #1

Dear Referee,

We would like to thank you for your careful reading and useful comments on our paper "Particulate Rare Earth Elements behavior in the North Atlantic". Our manuscript has greatly improved.

We carefully addressed all comments from the Referees. Referee #1's comments are reported in black font, and our responses are in blue font. New and/or modified line numbers are also provided. The modified parts in this new version of our manuscript appear in blue font.

We hope that you will find this manuscript suitable for publication.

Best regards.

In this manuscript, Lagarde and colleagues present a substantial dataset for suspended particulate REEs and Y from a 2014 cruise in the NE Atlantic. The authors are commended for publishing these data, as there are too few high-quality REE data sets for ocean particles, and the interpretations have the potential to greatly increase the understanding of biogeochemical processes in general, and the ocean chemistry of REEs in particular, relative to inferences from dissolved data alone. One liability to keep in mind is that the residence time of particulate phases is generally much shorter than that of the dissolved pool, so these kinds of datasets are much more like short-term "snapshots" of distributions, especially in the upper water column, than long-term averages of regional distributions. This difference might be worth pointing out explicitly in this paper.

We thank the reviewer for his/her detailed review and valuable comments. Regarding the "short-term snapshot" of the reported distributions of PREEs, we are now emphasizing it in the abstract and in the conclusion, lines 12-13 and 519-520.

Overall, the paper is well organized, and the figures are appropriate. This constitutes a substantive addition to the long history of effort to understand the processes affecting the distribution of REEs in the ocean, via inferences from (mostly dissolved) oceanic distributions, combined with laboratory studies that are not the focus of the current paper.

We thank the reviewer for this comment.

I do have a fairly long list of comments and criticisms, that in sum probably suggest major revision. I list these below, in order through the manuscript. Fortunately, only a couple of the comments refer to what I deem to be serious misinterpretations of the data. These are comments #25 and 26 below (marked with *).

Thank you for the careful reading of our paper and these comments. We answered to each one of them and reported the lines modified in the manuscript after your comments.

A substantial fraction of the other comments are related to clear wording, and confusions caused by vague or inaccurate use of words and phrases. These are very important, because they are relevant to the specific processes being discussed. I have also commented extensively through the first part of the manuscript (see attached marked-up pdf, looking carefully for the small Adobe editing marks), with numerous revisions of the English word use, syntax, or grammar. However, at some point I felt that there were too many editorial needs in the use of English, and I refrained from most revisions in the interest of time, simply marking the problematic spots in yellow highlight. I leave it to the more experienced authors with good command of English (e.g. Planquette) to spend a few hours carefully improving the writing to avoid incorrect word usage and awkwardness, with the goal of making this paper much more readable. The problems with the highlighted sections should be quite obvious. One tip is that the frequent use of "one" or "ones" in a comparative sentence almost always makes for awkward English.

Following this comment, we spent a lot of time rewording the manuscript.

Once the revisions to the main body of text are completed, the authors should re-consider the content of the Abstract. As it stands, it makes the point about the long-distance transport of INLs, which I argue below is not well substantiated, and it also ends on an unsatisfyingly uncertain note with regard to Ho/Y ratio observations. I suggest deleting this last part (and perhaps the final section of the paper – see below), to end the Abstract on a stronger note.

The patterns and the Ce anomaly clearly point out to a dominance of REE absorption processes in the first meters in contrast with scavenging processes at deeper depths. The abstract rephrased.

1. Line 100: Methods: Were Ba and Th-232 measured on samples taken from both kinds of sampling bottles? Were conventional bottles measured by one lab and GO-FLO samples by another lab? Later it says Y was used to compare the two procedures (but also the collection method?). Not clear starting at line 100. This should also be made clear in Table 2. The authors should state what exactly is being reported here vs. related results from the same cruise that are reported in other publications. I found this description of sample types and who measured what to be confusing.

Particulate Ba and ^{232}Th concentrations were first determined in particles collected with Niskin bottles at the Royal Museum for Central Africa, Tervuren, Belgium then at LEGOS, Toulouse, France on the remaining leaching solutions. Ba and Y concentrations were also determined in particles collected with Go-Flo bottles at LEMAR, Brest, France. The differences between the two methods and the results of the lab intercalibrations are provided in the Supplementary material (Fig. S4). The section was revised to make it clearer (lines 113-196).

2. Line 117: Samples were rinsed with MQ water. There is possible loss of adsorbed elements as water should have been pH 5.6 if equilibrated with air. Previous workers have used NH4OH to adjust pH of rinse water to~8-9 to avoid this potential loss of adsorbed elements. Can the authors argue that results were not biased by loss of material from the particulate samples?

As the reviewer pointed out, there is indeed possible desorption (or even adsorption) of elements when rinsing with Milli-Q water or any solution actually. However, this desorption process is element- and filter-dependent.

Concerning Y, we were able to perform a comparison between concentrations measured on samples collected with Niskin bottles and with Go-Flo bottles. Samples collected with GO-FLO bottles were not rinsed (see Gourain et al., 2019), the excess water being drawn off with a syringe. The agreement is very good (see answer to comments n°4 for more details).
Furthermore, a previous study conducted at LEGOS (Arraes-Mescoff et al., 2001) investigated the dissolution of REE and Th following the incubation of large particles filtered from seawater during 24 hours. Results showed that after 24h no dissolved REE could be measured (i.e. below detection limit) (their Fig. 2) and a slight increase in particulate ^{232}Th concentrations after 12h (their Table 3). They also showed that these concentrations did not exceed 0.4 ppb after 10 days, which remained less than 0.5% of the initial PREE concentrations (their Table 4).
The rinsing time during GEOVIDE was very short, and a volume of less than 5 mL was used (Lemaitre et al., 2018b), so the material loss is supposed to be negligible.

3. Line 127: Analytical Methodology: The text implies that 2.0mL from a 3.0mL total digest solution was used for REE, Y, Ba and Th analyses. But what was the dilution of this solution for analysis? Was HF included in this solution, and was an HF-compatible ICP-MS introduction system used?

The leaching solution was not diluted for most of the samples, only a few samples were diluted with HNO_3 0.32 mol L^{-1} (prepared from Merck nitric acid 65%, EMSURE® distilled again at LEGOS to get the purest product, regularly controlled) by a factor between 1.3 and 1.5, because the archive solution volume was too small to allow for ICPMS analysis that requires at least 2mL. HF was not included in this solution, therefore no specific introduction system was required. See lines 142-144 in the manuscript for details.

Were standard curve solutions match to the acid mixture and concentrations in the (diluted?) samples?

Yes, standards were prepared by dilution of a stock solution in 0.32 mol L^{-1} HNO_3 with ca. 0.1 ppb of In and of Re. This information is now included in lines 159-161.

What was the % correction for oxides for each of the REEs, especially those generated by Ba and the LREE?

Major interferences of Ba oxides and hydroxides affect the Eu and Gd isotope masses. BaO interferences represented a maximum of 0.4% and of 0.3% of the signals of the measured Eu and Gd isotopes respectively and occasionally reached 10% for Eu for seven samples. For the other REEs, oxides contributed to less than 0.1% of the signal. Hydroxide interferences are one order of magnitude less than oxide's interferences. This information is now provided in lines 155-156.

How were isobaric interferences avoided;

In low resolution, isobaric interferences were corrected by the software of the ICP-MS (Method Editor, Thermo Fischer Scientific), using another mass of the same element (not interfered, 161Dy in the

example below) to calculate the number of counts that are interfering the desired measurement. For example, for interferences of ^{161}Dy on ^{158}Gd, the correction is:

Counts(^{158}Gd) =counts(mass158)-counts(mass161) x abundance(^{158}Gd)/abundance(^{161}Dy)

They are listed together with the element interfered in the answer of the next comment. Note that the isotopes that we analyzed were selected to minimize these interferences. All the equations used for these corrections were checked in the method of the instrument before analyses, and that it is possible to custom the isotope used for correction.

it may be useful to list in a table the isotopes analyzed.

Done. Listed below are the isotopes analyzed. We did not consider relevant to add them in the main text; however, if the editor and referee wish, we could add them as supplementary material.

Y89
In115 (Sn115)
Sn118 (only used to correct In115 from Sn115 contribution)
Ba137
La139
Ce140
Pr141
Nd143
Nd146
Sm152 (Gd152)
Eu151
Eu153
Gd158 (Dy158)
Tb159
Dy162 (Er162)
Dy163
Ho165
Er166
Er167
Tm169
Yb172
Lu175
Re185
Th232
Dy161 (only used to correct Gd158 from Dy158 contribution)

What mass resolution settings on the HR-ICPMS were used for the various analytes?

All measurements were performed in low resolution mode (see line 151 of the corrected MS)

The reported 20-30% uncertainty in final PREE concentrations seems very high. What was the largest contributor to the uncertainty? Fig. S2A implies that the largest source of error was cutting the filter exactly in half (or sample heterogeneity on the filter surface). The highly variable and relatively large error associated with the measurement (Fig. S2A) is odd because cps should have been quite high given the sample volume and final digest volume, unless the primary digest solution was over-diluted (if so, why?).

Indeed, assuming a homogeneous filter loading, the largest contribution to the uncertainty is cutting the filter exactly in half, as shown in Fig. S2A. The different contributions are summed in the following table that replaced the Tab. S2 in the manuscript as Fig. S3.

Source of error	Determination	Mean % of the concentration
Volume of leachate	2sd calculated on the weight of all archive volume after 13 mL of HNO_3 0.32 M were added	0.6%
Volume taken for ICP-MS analysis	Average 2sd calculated on weighted replicates for a sample	0.005%
ICP-MS measurement	2sd calculated on 5 spectra measured for a sample	3.3%

Reading between the lines, one could guess that a dry-down step was not desired, so digests may have been diluted to acceptable acid concentrations for the ICP-MS introduction, leading to low counts per second and high uncertainties based on signal counting statistics. Alternatively, filter blanks may have been high and/or variable (this is not mentioned – what was the range of % filter blank?). This needs much more explanation, because 20-30% uncertainty is very high, and is be-lied by the relative smoothness of the profiles shown Fig. 3 for example. This stated measurement uncertainty should have yielded noticeably “bouncy” vertical profiles. I think the data are not as uncertain as the authors’ assessment, which may be more theoretical than empirical, since true sample replication was not practical.

There was a dry-down step and only few samples were diluted when there was not enough leaching solution left (see lines 145-146 in corrected MS). The chemical blanks represented 0.01% to 5% of the measured concentrations, rarely reaching 30% for Y, Lu and Th (lines 166-168 in corrected MS). Filter blank was determined by leaching an unused clean filter following the same protocol as for the samples. Taking your comment into account, we choose to not consider the contribution of the uncertainty on the fraction of filter analyzed to the final concentration error. The data set and the profiles are corrected. We provide additional information in lines 169-176.

4. Line 155: To compare concentrations between the two analytical labs, the regression slope is only partially helpful. Please give the mean % difference for all samples, and indicate if this % shows any trend with sample concentration (e.g. higher concentrations agree better?).

Following the reviewer's comment, we provide below the mean % difference for all samples:

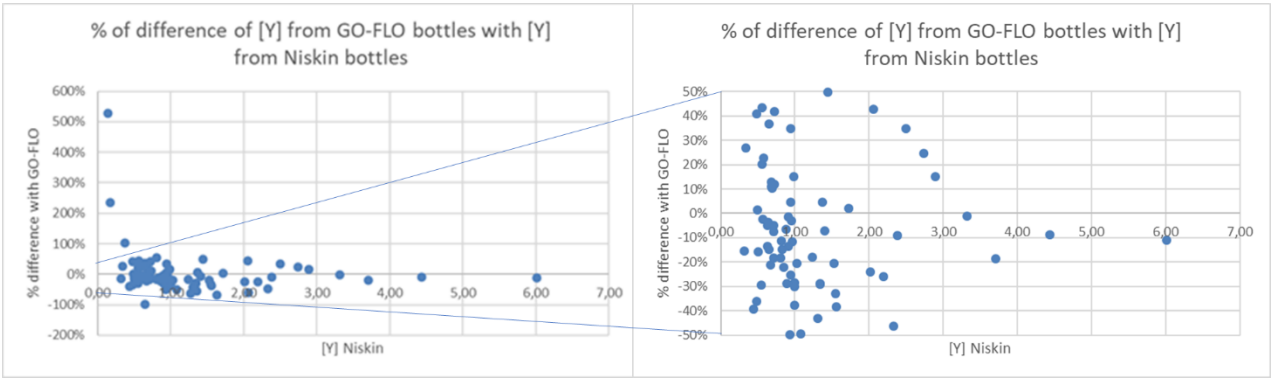

The figures above (twice the same plots, different scales) show that the highest concentrations agree better. Lowest concentrations of Y show the largest difference between the two labs. The median percentage of difference is 21%, for concentrations ranging between 0.3 pmol L^{-1} and 6 pmol L^{-1}. Four samples were excluded between the first and the second graph: one sample collected with a GO-FLO bottle (station #32 at 300 m) which had a concentration below 0.01 pmol L^{-1} and showed a difference of -100% with the sample taken at the same station at the same depth with a Niskin bottle. Three samples collected with Niskin bottles had significantly lower concentrations than samples from the GO-FLO bottles, below<0.3 pmol L^{-1}: at station #1 at 60m and at station #64 at 500 m and 900 m. These differences suggest an unidentified bias during the sampling and/or analytical protocols.

5. Line 159: Why did Y agree much better between the two sampling systems (and labs?) than Ba, which has much higher particulate concentrations? Was this related to the filter type used for each sampling effort, or differences in the digestion methods used by the two labs? This comparison is again quite unclear. If this cannot be explained in simple terms, please put all the information in a table, with columns of collection bottle type, filter used, digest method, analytical method, lab where analyses were made, and final results from each lab, etc.

A table is now provided in the supplementary material (Fig S4) and recaps the sampling systems, digestion procedures and intercomparison of measured concentrations.
Lemaitre et al. (2018a) explained the higher Ba concentrations measured in samples collected with Niskin bottles than in samples collected by GO-FLO bottles by the different filter types and the chemistry used. Samples collected with Niskin bottles were collected on 0.4 µm polycarbonate filters, while samples collected with GO-FLO bottles were collected on paired 0.45 µm polyethersulfone and 5 µm mixed ester cellulose filters. Different filters can lead to different concentrations even when the chemistry is the same (Planquette and Sherrell, 2012). Furthermore, a more concentrated HF solution was used for the chemistry on polycarbonate filters.
Although impossible to prove at this stage, it is possible that Y is less sensitive than Ba to the filter material, and/or to HF.

6. Line 167: "Ce oxidation onto particles" suggests a poor understanding of whether pCe is dominated by adsorbed Ce4+ or by an independent phase e.g. CeO2. If Ce forms or forms within an independent

oxidized authigenic mineral, then “prevents ad-sorption” is not the right phrase. Please clarify and expand this explanation of the unique behavior of Ce.

We carefully reworded this section. See lines 200-207:

The specific behavior of Ce is due to the occurrence of its IV oxidation state in addition to the III oxidation state common to all the REE. Two mechanisms for Ce oxidation have been proposed so far: a microbially mediated oxidation in seawater under oxic conditions that leads to formation of insoluble CeO_2, more particle reactive than Ce(III) (Byrne and Kim, 1990; Elderfield, 1988; Moffett, 1990, 1994; Sholkovitz and Schneider, 1991) and an oxidative scavenging onto Mn oxides particles (De Carlo et al., 1997; Koeppenkastrop and De Carlo, 1992). These two processes act in addition to the general scavenging process that affects all the trivalent REE by surface complexation, thus leading to the Ce enrichment in particles and its stronger depletion in the dissolved phase compared to other REE.

7. Line 171: This section describing pCe distributions is very hard to follow because no figures are referred to. Also the terms epipelagic and mesopelagic need to be re-defined by depth intervals as a reminder to the reader, so that “bottom of the epipelagic” can be understood relative to the depth scale of Figure 2.

We referred to Fig 2 at the beginning of the section (line 212), and added more references to each figure (PCe profiles on Fig. 2A and PCe section on figure 2B). Epipelagic refers to the depth range of 0-200 m while mesopelagic refers to the depth range of 200-1500 m (lines 117-118 and 220).

8. Line 184: The Station 44 maxima at 120m and 160m are defined by only one point each, so I think it is quite possible that they are uniquely contaminated with Ce, unless the contextual data can provide a clue as to a possible source in this region at those depths. See further related comment on Ce anomalies below.

At Station 44, PCe concentrations are 1.8 and 3.3. pmol L^{-1} at 120 m and 160 m, respectively. While higher compared to the concentrations above and below, they remain in the range of PCe concentrations measured along the section, and similar maxima are observed at station #32 at 140 m and at station #38 at 160 m. We investigated a possible carry-over contamination from the previous sample which cannot be excluded even if the Perspex systems were carefully rinsed between each sample. That said, station #38, which preceded Station #44 was not especially rich in PCe compared to other PREEs. Finally, when there is contamination with PCe other REEs are usually affected, like La for example. Looking at our dataset, a specific contamination in Ce seems very unlikely.

9. Line 200: Section 3.4 has a big problem because the heading says Nd/Yb but Fig.4 shows Yb/Nd, the inverse. One of these headings is wrong, and I suspect it is the section heading. I would expect that near-surface particles have a greater biogenic component and a smaller crustal component, so that Yb/Nd will be higher, reflecting the LREE-depleted seawater source for the particulate uptake, which is only partially compensated by preferential LREE removal by biological particle production, and by particle scavenging in general. In other words, I would expect PAAS-normalized REE patterns for particles in the euphotic zone to be “seawater-like”, but somewhat less LREE-depleted. Thus my guess is that Fig. 4 is correct, and the text throughout section 3.4 is wrong. Please correct this. The following two comments should be taken in this light.

Thank you for this comment. Indeed, the section heading was wrong. We corrected this mistake by harmonizing the use of Yb_N/Nd_N in the text and the figure (lines 239-250).

10. Line 202: I don't see any values of Yb/Nd of 0.01 in Fig. 4. Visually, it looks like the minimum value is about 0.2.

It has been corrected, see line 244.

11. Line 204: It is stated that the highest Yb/Nd value is in the epipelagic of Sta. 21, but Figure 4 shows a single subsurface value three times as high in the epipelagic of Sta.13. This needs to be corrected. The last sentence of this paragraph says that at this relative high Yb/Nd point at Sta. 21, four of the LREE are also at high concentration. This sounds odd, because high LREE would be expected to drive HREE/LREE, and thus Yb/Nd, to low ratios, not high. If this sentence is highlighting a surprising result (high HREE/LREE at high [LREE]) then this should be pointed out. I can see from Fig.2A that PCe has a single point maximum – is that single point the one that generates the high Yb/Nd?

The data point at station #13 at 40 m was categorized as an outlier at line 244. The last sentence of the paragraph is about the minimum at 100 m, it was specified line 248 to avoid confusion.

12. Line 231: "react preferentially with biogenic phases". Can the authors be more specific? Are they suggesting that Yb would be adsorbed preferentially to Nd on POM? On bSi? This phrase is too vague. Best to be more specific about the phase invoked, and to cite references appropriately.

This assumption is based on the work of Akagi et al. (2013), and is now detailed in lines 278-280 in the corrected manuscript:

In the Bering Strait, Akagi et al (2011) also observed a strong association between particulate HREE and biogenic silica collected in sediment traps. This specific BSi control on HREE behavior is discussed in section 4.6.

13. Line 241: This is the first place in the manuscript where I finally understood that the samples being discussed were collected in the standard Niskin bottles. This should be abundantly clear in the Methods. See comment above.

See answer to comment n°1, we provided more details in lines 113-196 and summarized the different sampling systems, chemistries on filters with the associated measured element in Fig. S4. We hope it is now clearer.

14. Line 244: Rock types in the crust are likely more variable in Th content than in Al content. A rough estimation of the uncertainty in the %Lithogenic fraction calculated in this manner should be presented. Are the uncertainties large enough that the %Lithogenic should be viewed only as a relative scale?

We did not want to use Al as lithogenic tracer because it was demonstrated that it could be incorporated in the biogenic silica. In addition, i) ^{232}Th is less soluble than Al, as shown by its shorter residence time

(25-55 years (Roy-Barman et al., 2019) versus 200 years (Hayes et al., 2018)); ii) PAl was not measured concomitantly to our samples, while ^{232}Th was; iii) ^{232}Th is less prone to contamination than Al. Moreover, previous observations allowed us to assume that ^{232}Th was relatively homogeneous in rocks and sediments: 1) Chase et al. (2001) showed that ^{232}Th concentration in lithogenic sediments sampled in the South Atlantic ocean was constant at around a value of 10 ppm 2) This value is close to the median concentration of 10,5 ppm of the upper crust reported in Rudnick and Gao, 2014 and used in this study 3) the GEOVIDE area is surrounded by shields and extended crust in majority of Caledonian fields (https://earthquake.usgs.gov/data/crust/type.html), with a relatively homogeneous geochemistry (Cocks and Torsvik, 2006; Rudnick and Gao, 2014). For all these reasons, we considered that ^{232}Th was a reliable tracer of the lithogenic fraction.

However, we also estimated the lithogenic contribution calculation using PAl concentrations measured in samples from the clean rosette and obtained a good agreement for most of the samples and stations. Discrepancies are discussed below.

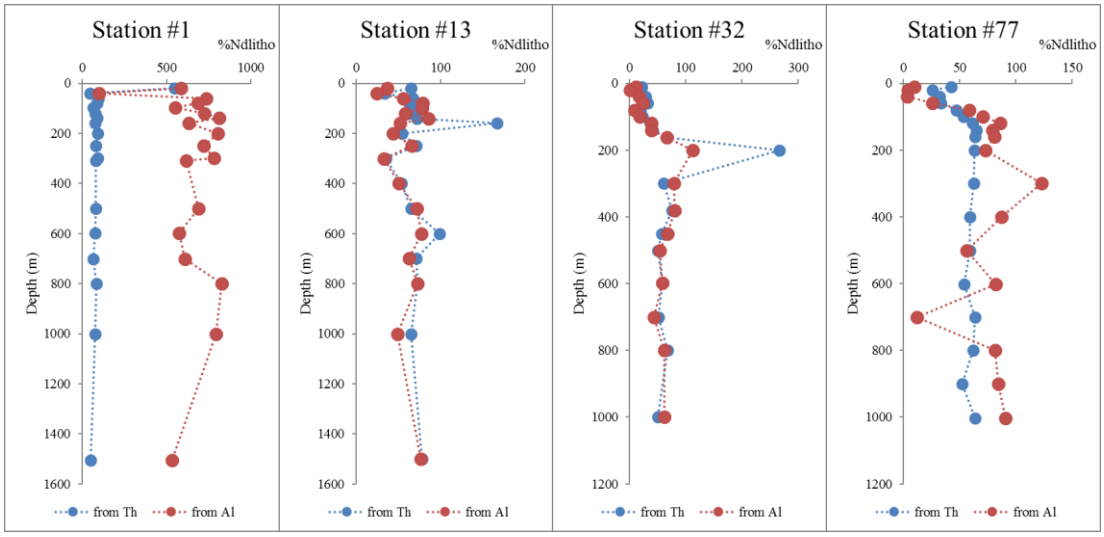

.

The error calculated on the lithogenic fraction varies from 0.7% to 6% when the error on the Th concentration only (3.3% on average) is considered. Propagating the error of ±0.5 ppm on Th concentrations in the upper crust increases this error to an average of 5.9% (ranging from 4.8% to 10.4%). Thus, overestimated lithogenic fractions below 106% are falling within this uncertainty (ie station #38 at 160 m). When the estimated lithogenic fraction was higher than 100%, we attributed it a value of 100%. Comparing with the lithogenic proportion calculated with Al shows that sometimes the use of Th overestimates the lithogenic fraction (for example at station #13 at 160m) but the calculation with Al also indicates a maximum at the same depth. At station #32 at 200 m, Al data are also significantly lower than Th data (113 % vs 200%), and allow us to assess a value of 100 % for the lithogenic fraction.

At stations #1 at 20 m, Th has likely been scavenged, and is present in authigenic fraction. Such “rapid Th scavenging” has already been reported by Hayes et al. (2015) in particles and by Robinson et al. (2008) in sediments. Hayes et al. (2015) proposed a correction using the partition coefficient of Th that is assumed to be the same for ^{232}Th and ^{230}Th, but we do not have data to do it, so we set the values to 100%. At the surface of station #77, where a diatom bloom occurred during the cruise, the lithogenic

fraction calculated from Al is lower than the one calculated from ^{232}Th (10% for Al and 40% for ^{232}Th), suggesting an authigenic source of Al.
To conclude, even if the used of ^{232}Th as a lithogenic tracer sometimes include a bias that can lead to an overestimation, it remains a better lithogenic tracer than Al for our data set. We added this discussion in lines 307-314 in the corrected MS.

15. Line 258: A finding of >100% lithogenic fraction using the Th-232 method suggests that ALL estimates of lithogenic fraction may be overestimates, and are at least probably not underestimates. This should be acknowledged in the text as a potential unidirectional bias in % lithogenic fraction.

We acknowledged it line 311.

16. Line 262: The patterns of PAAS normalized lithogenic fractions are called “flat” but the plots in Fig. S3 are on a log scale. This hides the fact that most of the patterns are MREE-enriched. Could the authors comment on this observation? I encourage plotting REE patterns on a linear scale whenever possible; this highlights the quality of the data and inter-element pattern details more clearly.

We agree with the reviewer regarding the MREE enrichment. Associated Gd and Eu anomalies were calculated. However, we decided to not present them in the manuscript because the associated errors prevent clear interpretation of the anomaly profiles. In consequence, we kept the “classical” pattern representation with a log scale, as used in the literature in the manuscript, and added the patterns with a linear scale in Fig. S7 B to the patterns represented with a logarithmic scale (Fig. S7 A in corrected supplementary).

17. Line 276: The enrichment in LREEs is interesting, and this enrichment appears larger where the absolute pREE concentration is higher (greater depths). The authors imply that this is because of the “lower solubility” of the LREE relative to the HREE, and that this depth difference in LREE enrichment is caused by the adsorbed fraction. Yet the % lithogenic increases with depth as well. Can the authors eliminate the possibility that the LREE-enrichment is a function of the difference in REE composition of source rocks (or the fraction of source rocks that survives chemical weathering) and PAAS? Also, as noted in comments on the pdf, “solubility” is not the right term to use to describe the LREE, if the process being referred to is adsorptive scavenging, not the solubility of a unique solid phase. Admittedly, this chemically inaccurate language is used often in the marine chemistry community.

We interpreted the increase of the lithogenic contribution with depth as an effect of remineralization, leading to a loss of authigenic material and by consequence an increase of the lithogenic fraction. As the preferential scavenging of LREEs relatively to HREE is a well-documented behavior in seawater, we assumed that the LREE enrichment observed in the particles is the symmetric of what happened in the dissolved pool of LREE (Garcia-Solsona et al., 2014; Tachikawa et al., 1999a).

18. Line 276: “these maxima”. It is not clear here that you are referring now to the Iberian margin maxima in % lithogenic fraction. This is because the start of the paragraph refers to BOTH margins. Please add words to make it clear that you are shifting your focus to the Iberian margin here. And the Fig. 6 caption needs to explain the white arrows in the figure.

We clarified this point in the text (line 335) and changed the Fig. 6 caption to provide information about the white arrow.

I think they are supposed to show a density similarity between relative maxima in the profiles from the various stations, but for Sta. 26, for example, the arrow from Sta. 21 does not point to a relative maximum; the maximum is one depth lower at 200m.
Similarly, the lower arrow pointing from Sta. 26 to Sta.32 shows the % lithogenic increasing from _60% (not a relative max) to _100% at Sta. 32. I don't see how the lithogenic fraction could increase unless biogenic particles are preferentially lost to sinking (not likely) or another source of lithogenic particles exists at Sta. 32. I suspect that these differences are all related to the uncertainties inherent in the Th-232 normalization. The authors need to do more work to justify their interpretation that Iberian margin suspended particles are advected NW along isopycnals. Where are currents going at various depths? What about the possible influence of the broad shelf-slope region around the British Isles?

The section is presented for Nd only, as an illustrative REE and because in the near-future we will be able to trace the sources of lithogenic material with its isotopic composition.
The point located at 200 m at station #26 is on the same isopycnal as the point located at 700 m at station #21 (σ_0= 27.25), and there is no datapoint on this isopycnal at station #1.
Our stations are located in currents that form the North Atlantic Current and are flowing northward (Zunino et al., 2017), preventing influence from the British Isles.
In addition, we are currently working on the mechanisms of sediment resuspension along the Iberian margin on one hand and on the propagation of these intermediate nepheloid layers on the other hand. In order to better quantify these mechanisms, we use a circulation model (NEMO with a resolution of 1/12° and 50 vertical layers) but interpreting them farther was beyond the scope of this paper. However, this work was presented at Ocean Sciences (San Diego), confirming that there is no influence of the British Isles.

19. Line 303: "no particular lithogenic contribution" is used to describe agreement between the PFe and PMn results from Gourain et al., as compared to the PREE results presented here. But Sta. 53 HREE have a substantially higher %lithogenic than Sta. 51 (Fig. 5), indicating that there IS in fact an increase in lithogenic fraction at Sta. 53 only. So the phrase in quotes does not represent an observation "in agreement with our results". This needs clarification and re-wording. The word "particular" is not clear in the above – do you mean "unusual"? Note also that authigenic contributions of Mn and Fe from shelf sediments may mask an increase in lithogenic Mn and Fe, when looking only at %lithogenic as a metric. This may be less true for REE, especially HREE, leading to the differences between Sta.'s 51 and 53 as noted above.

Regarding the reference to Gourain et al. (2019), we meant that the lithogenic contribution remains on the Greenland shelf and that no nepheloid layers were observed along the slope, in contrast with the Iberian margin. Correction is added in line 357.

20. Line 307: "At station #13 at 200m, no lithogenic maximum is identified". The authors need to clarify whether they are still referring to Ac-227 data or are now referring to REE data. Indeed, Fig. 6 shows this depth to be a relative min. in %lithogenic Nd, but there are relative max's just above and below. Please clarify language so it is fully clear which data you are referring to. Also, please use "lithogenic" and

"%lithogenic" appropriately. It is possible to have high lithogenic concentrations but low %lithogenic, for example near a margin where weathering particles might combine with higher biogenic particles resulting from high productivity. In the quote above, I think you mean "%lithogenic".

Yes, it is %lithogenic and not the absolute lithogenic concentration. It refers to ^{227}Ac, and this is indicated in line 362.

21. Line 308: "merging of the two maxima observed eastward". Please clarify where the two maxima are and do you mean eastward of Sta. 13 or some other station? Also, Fig. 4 does not show anything about isopycnals; should this be citing Fig. 6?

The two maxima we are referring to are those observed at station #1 (200 m and 240 m), and we are now directing the reader to Fig. 5 and Fig. 6. See line 335 for modified text.

22. Line 322: The concluding paragraph should sum up the REE results. As it stands, it restates more general processes at ocean margins that have been established through previous studies. It would be better to summarize the central findings related to REE marine geochemistry.

We are now summarizing the results in lines 375-377.

23. Line 327: "less prone to desorption". This phrase is not fully accurate because my understanding is that Ce, once oxidized, has a higher Kd, which describes an equilibrium state where adsorption and desorption rates are equal, but distribution of Ce is more strongly in favor of the solid surface. See for example Ohta and Kawabe, GCA, 2001. Also, the literature contains some discussion whether adsorption or coprecipitation best describes the association of Ce(IV) with authigenic Fe and Mn oxyhydroxides. The nature of the anomalous redox behavior of Ce deserves a more complete introduction here, including its relative Kd via adsorption to MnO2 and FeOOH, from abundant published experimental data. It is important to understand as well as possible which major authigenic mineral phase is most responsible for REE adsorption or coprecipitation, and for Ce oxidation.

This part has been rewritten with a more complete introduction on the Ce special behavior, see lines 379-391.

24. Line 329: "authigenic Ce adsorbed on". An adsorbed species must first be in solution, and "authigenic" usually refers to a mineral in solid phase, so this wording is incorrect. Whether Ce(III) is first adsorbed, then oxidized, or whether a discrete mineral (CeO2?) forms independently or in a co-precipitation process with a more abundant oxide is to my mind an open question, but the authors may wish to briefly summarize their understanding of the literature on this point. This reinforces the importance of the terminology referred to in the last comment.

To clarify these points, this part has been rewritten, see lines 379-391 for modified text.

25.* Line 338: The paragraph starting on this makes some assumptions that I think may not be true. First it is stated that Ce oxidation only occurs below the surface layer. In fact, without dissolved REE data, the authors cannot prove the Ce does not have a positive anomaly relative to the dissolved REEs.

The reviewer is perfectly right: the normalization to PAAS indicates that at the surface of productive areas a similar REE pattern to the seawater one is observed in particles, and then this is attenuated with depth. The observation of a more pronounced Ce anomaly below the surface layer does not necessarily mean that Ce oxidation did not occurred at lower depth. We are now softening this assumption in line 410.

The authors seem to have been caught in the trap of interpreting the Ce anomaly in absolute terms rather than in relation to the dissolved pool from which the REEs are adsorbed onto or absorbed into the biogenic particles. This dissolved pool has itself a very negative Ce anomaly throughout most of the ocean. Very likely then, the only way to achieve a positive Ce anomaly in marine suspended matter is via advection of sedimentary particles that have had very long time periods during which to undergo substantial REE cycling and fractionation, or as the authors suggest, preferential loss of the strictly trivalent REEs upon POM remineralization.

Thanks to your comment, we first noticed a mistake in our calculations of the Ce anomalies. Because of an error in the PAAS normalization, the presented Ce anomalies were larger than what they really are. The figure and the text of the manuscript were corrected. Please accept M. Lagarde sincere apologies for this mistake.
We do not agree on the ubiquity of the “very” negative Ce anomaly in the dissolved pool. Full depth published REE patterns show flatter shapes at the surface. More particularly, Greaves et al. (1994) and Tachikawa et al. (1999) reported surface patterns with quasi flat REE patterns (in particular no or slight HREE enrichment) following Saharan dust inputs.
Tachikawa et al. (1999b) also observed the formation of a positive Ce anomaly in suspended particles while settling through the water column. They explained this positive Ce anomaly by an adsorption of trivalent REE on newly formed Mn oxides (Moffett, 1994) without anomaly close to the surface. At greater depth, after particles began to settle, CeO_2 is adsorbed onto particles. This is consistent with a Ce oxidation slower than Mn oxidation (Moffett, 1994). These anomalies then increase with depth by desorption of strictly trivalent REEs. This mechanism is also discussed in detail in de Baar et al (2018).
For example, at the surface of station #32, there is a negative anomaly of 0.36. The observed increase of this anomaly to a value of 1.1 (at 160 m at the same station) requires to increase the PCe concentration of 0.7 pmol L^{-1} to a concentration of 2 pmol L^{-1}. At this station, dissolved Ce concentrations are higher than 6.3 pmol L^{-1} in the first 150 m, and below 5 pmol L^{-1} below 450 m (preliminary results of our ongoing work on GEOVIDE dissolved REEs). Thus, a positive anomaly of PCe is likely to happen.

The authors also suggest, however, that a strong (positive) Ce anomaly could result from high particle concentrations. But a higher concentration of reactive surfaces would affect all REEs similarly; I don’t see how high particle loads by themselves would lead to preferential Ce oxidation and retention on the particles.

This is only a suggestion. As the greatest positive anomalies occur in productive areas and identified lithogenic inputs, we suggest that higher particle concentration induces greater surface exchange and oxide formation.
It is possible that a higher bacterial activity enhances Ce oxidation (thereby forming CeO_2), in the areas of high productivity oxidation (de Baar et al., 2018; Moffett, 1990) and lead to high positive anomalies.

The authors assert that a positive Ce anomaly is not observed in the ARCT and NADR regions because export is strong and particle residence time is short, but Fig. 7 does show positive Ce anomalies at

various depths in these regions, so this assertion seems untrue and needs more thorough examination and explanation. If Ce is preferentially removed under all scavenging scenarios, then it is reasonable to expect that a productive region with rapid export would deplete dissolved Ce in the mixed layer in both absolute and relative terms, through the course of a weeks-long bloom, leading potentially to strongly negative Ce anomalies in the dissolved state and increasingly negative (though positive relative to the dissolved pool) in the near-surface particles sampled at some advanced bloom stage. I encourage the authors to examine whether this scenario has been shown or disproven in other productive regions.

Yes, the exact proposition is that a positive Ce anomaly is not observed at the surface in the ARCT and NADR regions (in the upper 100 m), because seawater-like patterns are observed in these areas. The hypothesis of a preferential scavenging of Ce is supported by the attenuation of the Ce anomaly with depth, until it is close to the absence of anomaly with a value close to 1 at 200 m. This scenario has been shown by Moffett (1990) who observed weaker anomalies where the particles export was more intense. He suggested that the kinetics of exchanges between the dissolved and the particulate pool rely on the time they are in contact. If particles are removed faster than the Ce oxidation occurs, the anomaly will be weaker than in areas where particle have a residence time closer to the equilibrium of the reactions that leads to preferential scavenging of Ce. This was included to the manuscript, lines 408-413.

Even if Ce oxidation were not favored in the sunlit ocean, I would guess that the dissolved REE pool would show a fairly strongly negative Ce anomaly, inherited during previous deep winter mixing. In sum, I would expect for most oceanic regions that Ce anomaly to be negative for biogenic particles in the euphotic zone in general, unless there were an admixture of authigenic particles (perhaps resuspended from shelf sediments) overwhelming the biogenic effect. The authors may be able to refute this idea based on published data, in which case this should be stated as part of the discussion in this section. These two particle sources are often mixed in highly variable ratios in ocean margins, and I would think that alone would make total particulate REE data difficult to interpret. I think this is the reason why the authors have so much trouble in the last few sentences of this paragraph seeing consistent correlations between Ce anomaly and Mn behavior, particle concentration, particle residence time, etc. Finally, I think the very sharp strong single-point maxima in Ce anomaly (Fig. 7A, B; e.g. Sta. 32, 440m and Sta. 13 600m) are very likely a result of Ce-specific contamination. Unless the authors can justify these oceanographically surprising features, those data points should be deleted from the graphs, and the data table values marked as likely contaminated values. See similar comments below.

1) We cannot exclude random contamination in Ce during the sampling, and we do not have a clear explanation. These data are not included in the graphs. They are reported under brackets in Table 2. See lines 437-440 in the revised MS.

26.* Line 360: The opening sentence of this paragraph seems incorrect to me, and gets the reasoning behind the interpretation of REE patterns in biogenic particles off on the wrong foot, affecting the rest of this discussion section. The LREE's likely have a larger lithogenic fraction than do the HREEs NOT because the LREE's are not preferentially taken up by (or onto) the biogenic particles, but simply because the surface seawater dissolved REE pool is so LREE-depleted relative to PAAS.
The degree of LREE-depletion cannot be known for the stations investigated here because no dissolved REE data are presented, but even with preferential LREE scavenging, a mixture of crustal minerals and biogenic surface particles would always show the observed larger lithogenic component for the LREE,

because the preferential LREE uptake on the biogenic particles cannot come close to compensating for how depleted the LREEs are in the dissolved pool.
This depletion might be especially true for a surface layer that has already seen substantial growth and export in the preceding weeks, which could cause the surface layer to be even more LREE-depleted than it was immediately following winter mixing. I encourage the authors to "borrow" dissolved REE data from elsewhere in the Atlantic (no one measure them on GEOVIDE??), assume a degree of preferential LREE uptake based on published laboratory adsorption experiments or papers showing both dissolved and particulate data for euphotic zones in other regions, and do the calculation themselves. Without looking exhaustively at the literature, it is evident from dissolved REE data near Bermuda (see deBaar et al., GCA, 2018, Fig. 10) that dissolved Nd/Yb decreases from deep water up to the surface. In sum, a "seawater-like" pattern does not necessarily imply a unique LREE/HREE fractionation, or absorption vs. adsorption, it simply means short-term uptake from a very LREE-depleted pool, without significant admixture of authigenic minerals or refractory lithogenic particles, which are so important to the total PREE patterns below the surface layer. I think it is a mistake and is misleading to refer to "HREE enrichment" because PAAS-normalization has little relevance for biogenic marine particles, and this term implies preferential HREE uptake, relative to LREE. I also think that the speculations about REE patterns implying some kind of control by biogenic carbonate vs. Silica is poorly reasoned and not convincing; I would argue that the vast majority of REEs in biogenic particles (mostly living cells in productive surface waters) is associated with organic matter, as is true for nearly all trace metals. In sum, I strongly disagree with the interpretations in section 4.4 and I urge the authors to reconsider and rewrite this entire section. As a related side observation, I see from Fig. 5 that the REE pattern of near-surface particles from Sta. 53 shows high concentrations (relative to Sta. 51) and strong LREE-enrichment (shown log scale). This station was dismissed in the first sentence of the section as distinct from most other stations which form the basis of the discussion in Section 4.4. But the question remains how this LREE-enrichment might occur. Is this a result of preferential LREE scavenging from a "flat" dissolved REE pattern, or does it reflect mineral particles from sediments or the continent that are already LREE-enriched, for example the authigenic products of previous long-term particle-seawater interactions?

At the surface, even if LREE are depleted by comparison to PAAS, LREE concentrations are still higher than HREE concentrations due to their natural abundance (de Baar et al., 2018; Fig. 10). We also know that dissolved REE concentrations are higher than particulate REE concentrations which represent only 5% of the total Nd (Jeandel et al., 1995). We are currently performing the analyses on dissolved REE samples collected during GEOVIDE. Preliminary results also confirm that dissolved Nd concentrations are 5 to 65 times higher than particulate Nd concentrations. Particulate LREE represent 3% to 5% of total LREE pool (data for stations #1 to #32, ongoing work). Therefore, a short-term uptake mechanism would be in favor of LREE at the surface if the REE distributions are driven by adsorption processes. With depth, the dissolved patterns show a decrease of the DNd/DYb ratio, by preferential adsorption of LREE on oxides and hydroxides on particles. In addition, lithogenic inputs by dust or resuspended sediments can lead to an LREE enrichment in surface waters (Greaves et al., 1991, 1994; Tachikawa et al., 1999a for dusts, station #53 and #1 are an example for lithogenic inputs).
The association of REE with biogenic silica and calcium carbonates is still under debate in the literature (de Baar et al., 2018 and references therein; Patten and Byrne, 2017). The link between biogenic matter and REE is mostly established by the observation of a correlation between REE and major nutrients (de Baar et al., 2018). However, only few works are documenting the REE concentrations in the different particulate fractions yet: Akagi, (2013) and Akagi et al. (2011) suggest a main control by the biogenic silica, while de Baar et al. (2018) are in favor of a control by the soft material (traced by P and N).

This incorporation of REE in particles with a seawater-like pattern by association with soft tissue is what we observed in the NADR region, where a coccolithophorids bloom occurred during the cruise. Yet, the PYb_N/PNd_N ratio observed in the ARCT area is contrasting with the PYb_N/PNd_N ratio of the NADR region. This ratio is maximum where the diatom bloom occurred, while the REE patterns in the Labrador Sea (ARCT) are less similar to a seawater pattern than in the NADR region. This could be explained if one assumes that the bloom is senescent and the lithogenic inputs are higher. Then, HREE seems more particle-reactive at the surface of the ARCT region than at the surface of the NADR region, when LREE seems to be less depleted at the surface due to a higher lithogenic component. This is consistent with the theoretical work of Akagi (2013), and seems to indicate that HREE are more linked to Si cycle than LREE.

Station #53 is dismissed at the beginning of the section as it is not considered as an "open-sea" station because it is located on the Greenland shelf and subject to high particles inputs from Greenland that results in a dominant lithogenic signal. This lithogenic fraction is not as high as at station #1 and is higher for HREE than for LREE. LREE are found in higher proportion than HREE in the authigenic fraction, suggesting a preferential scavenging of LREE, unlike what happens at the stations discussed in this section. The roughly constant Ce anomaly around 1 confirms that a lithogenic origin is more probable than LREE-enriched authigenic products.

27. Line 426: The meaning of "dynamic scavenging" used here and above, and how it can generate a positive Ce anomaly, should be explained further. My understanding of the authors' meaning is that that successive cycles of adsorption and desorption accompanied by progressive Ce oxidation, can increase the Ce anomaly until it is strongly positive. But could remineralization of organic matter, and loss of the associated REE, leaving MnO2 and other authigenic oxyhydroxides as a greater fraction of the overall particulate REE, have the same effect, as long as refractory lithogenic particles (no Ce anomaly) were not an important part of the mix? This is not the same process as repeated cycles of adsorption and desorption on a constant particle population.

The reviewer understanding is right, we meant that a positive Ce anomaly was generated by successive cycles of adsorption/desorption of REE, with less desorption for Ce. A remineralization of organic matter would not prevent a preferential adsorption of Ce on oxides and hydroxides to occur. The amount of adsorption sites would modify the intensity of the Ce anomaly and depends on the particle modification through time. Remineralization would modify the intensity of the anomaly too, with a decrease of the negative Ce anomaly imprinted by organisms from seawater, but cannot generate a positive Ce anomaly without adsorption of Ce on particles.

28. Line 429: "and then a stronger scavenging of REEs". It is not clear what this phrase means. Is this proposed to be the second step occurring at this depth interval, after "intensive exchanges", or does "then" mean further down the water column. I'm not clear how ones achieves the combination of high PHo enrichment and strong positive Ce anomaly. Could the responsible processes be occurring independently, involving different particle types within the suspended particle mixture? Overall, it seemed to me that this section dutifully follows a pattern of discussion points in other REE papers from the senior author's group, and is interesting on theoretical grounds, but did not advance understanding of the relative behavior of Ho and Y in the ocean to a significant degree.
The variations in Fig. 8 seem barely interpretable in any cohesive way. The authors should reconsider whether this section truly adds to the impact of the paper. To my reading, it makes the paper end on a somewhat vague note.

Following this comment and the previous ones, this section has been entirely reworded. We agree that Fig. 8 does not bring important information and we deleted it. Instead, we proposed a general conclusion in lines 516-547.

References

Akagi, T.: Rare earth element (REE)–silicic acid complexes in seawater to explain the incorporation of REEs in opal and the "leftover" REEs in surface water: New interpretation of dissolved REE distribution profiles, Geochim. Cosmochim. Acta, 113, 174–192, doi:10.1016/j.gca.2013.03.014, 2013.

Akagi, T., Fu, F., Hongo, Y. and Takahashi, K.: Composition of rare earth elements in settling particles collected in the highly productive North Pacific Ocean and Bering Sea: Implications for siliceous-matter dissolution kinetics and formation of two REE-enriched phases, Geochim. Cosmochim. Acta, 75(17), 4857–4876, doi:10.1016/j.gca.2011.06.001, 2011.

Arraes-Mescoff, R., Roy-Barman, M., Coppola, L., Souhaut, M., Tachikawa, K., Jeandel, C., Sempéré, R. and Yoro, C.: The behavior of Al, Mn, Ba, Sr, REE and Th isotopes during in vitro degradation of large marine particles, Mar. Chem., 73(1), 1–19, doi:10.1016/S0304-4203(00)00065-7, 2001.

de Baar, H. J. W., Bruland, K. W., Schijf, J., van Heuven, S. M. A. C. and Behrens, M. K.: Low cerium among the dissolved rare earth elements in the central North Pacific Ocean, Geochim. Cosmochim. Acta, 236, 5–40, doi:10.1016/j.gca.2018.03.003, 2018.

Byrne, R. H. and Kim, K.-H.: Rare earth element scavenging in seawater, Geochim. Cosmochim. Acta, 54(10), 2645–2656, doi:10.1016/0016-7037(90)90002-3, 1990.

Chase, Z., Anderson, R. F. and Fleisher, M. Q.: Evidence from authigenic uranium for increased productivity of the glacial subantarctic ocean, Paleoceanography, 16(5), 468–478, doi:10.1029/2000PA000542, 2001.

Cocks, L. R. M. and Torsvik, T. H.: European geography in a global context from the Vendian to the end of the Palaeozoic, Geol. Soc. Lond. Mem., 32(1), 83–95, doi:10.1144/GSL.MEM.2006.032.01.05, 2006.

De Carlo, E. H., Wen, X.-Y. and Irving, M.: The Influence of Redox Reactions on the Uptake of Dissolved Ce by Suspended Fe and Mn Oxide Particles, Aquat. Geochem., 3(4), 357–389, doi:10.1023/A:1009664626181, 1997.

Elderfield, H.: The oceanic chemistry of the rare-earth elements, Philos. Trans. R. Soc. Lond., A(325), 105–126, 1988.

Garcia-Solsona, Esther, Jeandel, Catherine, Labatut, Marie, Lacan, François, Vance, Derek, Chavagnac, Valérie and Pradoux, Catherine: Rare earth elements and Nd isotopes tracing water mass mixing and particle-seawater interactions in the SE Atlantic, Geochim. Cosmochim. Acta, 125, 351–372, 2014.

Greaves, M. J., Rudnicki, M. and Elderfield, H.: Rare earth elements in the Mediterranean Sea and mixing in the Mediterranean outflow, Earth Planet. Sci. Lett., 103(1–4), 169–181, doi:10.1016/0012-821X(91)90158-E, 1991.

Greaves, M. J., Statham, P. J. and Elderfield, H.: Rare earth element mobilization from marine atmospheric dust into seawater, Mar. Chem., 46(3), 255–260, doi:10.1016/0304-4203(94)90081-7, 1994.

Hayes, C. T., Anderson, R. F., Fleisher, M. Q., Vivancos, S. M., Lam, P. J., Ohnemus, D. C., Huang, K.-F., Robinson, L. F., Lu, Y., Cheng, H., Edwards, R. L. and Moran, S. B.: Intensity of Th and Pa scavenging partitioned by particle chemistry in the North Atlantic Ocean, Mar. Chem., 170, 49–60, doi:10.1016/j.marchem.2015.01.006, 2015.

Hayes, C. T., Anderson, R. F., Cheng, H., Conway, T. M., Edwards, R. L., Fleisher, M. Q., Ho, P., Huang, K.-F., John, S. G., Landing, W. M., Little, S. H., Lu, Y., Morton, P. L., Moran, S. B., Robinson, L. F., Shelley, R. U., Shiller, A. M. and Zheng, X.-Y.: Replacement Times of a Spectrum of Elements in the North Atlantic Based on Thorium Supply, Glob. Biogeochem. Cycles, 32(9), 1294–1311, doi:10.1029/2017GB005839, 2018.

Jeandel, C., Bishop, J. K. and Zindler, A.: Exchange of neodymium and its isotopes between seawater and small and large particles in the Sargasso Sea, Geochim. Cosmochim. Acta, 59(3), 535–547, doi:10.1016/0016-7037(94)00367-U, 1995.

Koeppenkastrop, D. and De Carlo, E. H.: Sorption of rare-earth elements from seawater onto synthetic mineral particles: An experimental approach, Chem. Geol., 95(3), 251–263, doi:https://doi.org/10.1016/0009-2541(92)90015-W, 1992.

Lemaitre, N., Planquette, H., Sarthou, G., Jacquet, S., García-Ibáñez, M. I., Gourain, A., Cheize, M., Monin, L., André, L., Laha, P., Terryn, H. and Dehairs, F.: Particulate barium tracing of significant mesopelagic carbon remineralisation in the North Atlantic, Biogeosciences, 15(8), 2289–2307, doi:10.5194/bg-15-2289-2018, 2018.

Moffett, J. W.: Microbially mediated cerium oxidation in sea water, Nature, 345(6274), 421–423, doi:10.1038/345421a0, 1990.

Moffett, J. W.: The relationship between cerium and manganese oxidation in the marine environment, Limnol. Oceanogr., 39(6), 1309–1318, doi:10.4319/lo.1994.39.6.1309, 1994.

Patten, J. T. and Byrne, R. H.: Assessment of Fe(III) and Eu(III) complexation by silicate in aqueous solutions, Geochim. Cosmochim. Acta, 202, 361–373, doi:10.1016/j.gca.2016.12.004, 2017.

Planquette, H. and Sherrell, R. M.: Sampling for particulate trace element determination using water sampling bottles: methodology and comparison to in situ pumps, Limnol. Oceanogr. Methods, 10(5), 367–388, doi:10.4319/lom.2012.10.367, 2012.

Robinson, L., Noble, T. and Mcmanus, J.: Measurement of adsorbed and total 232Th/230Th ratios from marine sediments, Chem. Geol., 252(3–4), 169–179, doi:10.1016/j.chemgeo.2008.02.015, 2008.

Roy-Barman, M., Thil, F., Bordier, L., Dapoigny, A., Foliot, L., Ayrault, S., Lacan, F., Jeandel, C., Pradoux, C. and Garcia-Solsona, E.: Thorium isotopes in the Southeast Atlantic Ocean: Tracking scavenging during water mass mixing along neutral density surfaces, Deep Sea Res. Part Oceanogr. Res. Pap., 149, 103042, doi:10.1016/j.dsr.2019.05.002, 2019.

Rudnick, R. L. and Gao, S.: Composition of the Continental Crust, in Treatise on Geochemistry, pp. 1–51, Elsevier., 2014.

Sholkovitz, E. R. and Schneider, D. L.: Cerium redox cycles and rare earth elements in the Sargasso Sea, Geochim. Cosmochim. Acta, 55(10), 2737–2743, doi:10.1016/0016-7037(91)90440-G, 1991.

Tachikawa, K., Jeandel, C. and Roy-Barman, M.: A new approach to the Nd residence time in the ocean: the role of atmospheric inputs, Earth Planet. Sci. Lett., 170(4), 433–446, doi:10.1016/S0012-821X(99)00127-2, 1999a.

Tachikawa, K., Jeandel, C., Vangriesheim, A. and Dupré, B.: Distribution of rare earth elements and neodymium isotopes in suspended particles of the tropical Atlantic Ocean (EUMELI site), Deep Sea Res. Part Oceanogr. Res. Pap., 46(5), 733–755, doi:10.1016/S0967-0637(98)00089-2, 1999b.

Zunino, P., Lherminier, P., Mercier, H., Daniault, N., García-Ibáñez, M. I. and Pérez, F. F.: The GEOVIDE cruise in May–June 2014 reveals an intense Meridional Overturning Circulation over a cold and fresh subpolar North Atlantic, Biogeosciences, 14(23), 5323–5342, doi:10.5194/bg-14-5323-2017, 2017.

Author's response to Referee #2

Dear Editor, dear Referee,

We would like to thank you for your careful reading and useful comments on our paper "Particulate Rare Earth Elements behavior in the North Atlantic". Our manuscript has greatly improved.

We carefully addressed all comments from the Referees. Referee's comments are reported in black font, and our responses are in blue font. New and/or modified line numbers are also provided. The modified parts in this new version of our manuscript appear in blue font.

We hope that you will find this manuscript suitable for publication.

Best regards

The manuscript by Lagarde et al. presents a unique sampled section for particulate YREE. Data like this are really of great value and are need to better understand the marine cycle of YREE. Although I appreciate the dataset itself, there are some issues in the manuscript that need to be addresses and clarified prior to acceptance.

We thank the referee for these useful comments.

Minor comments

- There are quite a few orthographic and grammatical impurities. I suggest to avoid the use of 'being' and abbreviations in the beginning of sentences. The word 'one' is also often used inappropriately.

We carefully checked the orthograph and grammar.

- Figures should be reorganised and it is not always clear to which figure the captions relate. I would also suggest to make use of isolines instead of plotting 4 sections with 3 parameters. Draw salinity isolines and colour code the REE values, instead of plotting the profiles in the section. I would also strongly encourage to enlarge the upper 200m to show the features. This is the interesting depth range for most of your parameters. Also the interpolation is done differently when comparing Figure 6 and 2 A/B for which the former are without gaps while the latter section plots show white gaps.

We thank the reviewer for this comment.

We preferred to plot 4 sections with three parameters to display together the profiles and a description of the prevailing water masses using the salinity. We did try to add isolines but it rapidly came out that the figure was less readable (see examples below). The quality of the interpolations directly depends on the density of dataset. The depth and longitudinal resolutions for salinity and density are better than for PREE concentrations, so it is more rigorous to leave the gaps when PREE profiles are too distant from each other. The interpolation of Fig. 7A was revised to be the same as on Fig. 2B, 3C and 3D. We added a panel that enlarges the upper 200 m on Fig. 2B, 3C, 3D, 4, 7B and 8. For Fig. 6, the y axis is not the

same because this figure shows a part of the section.

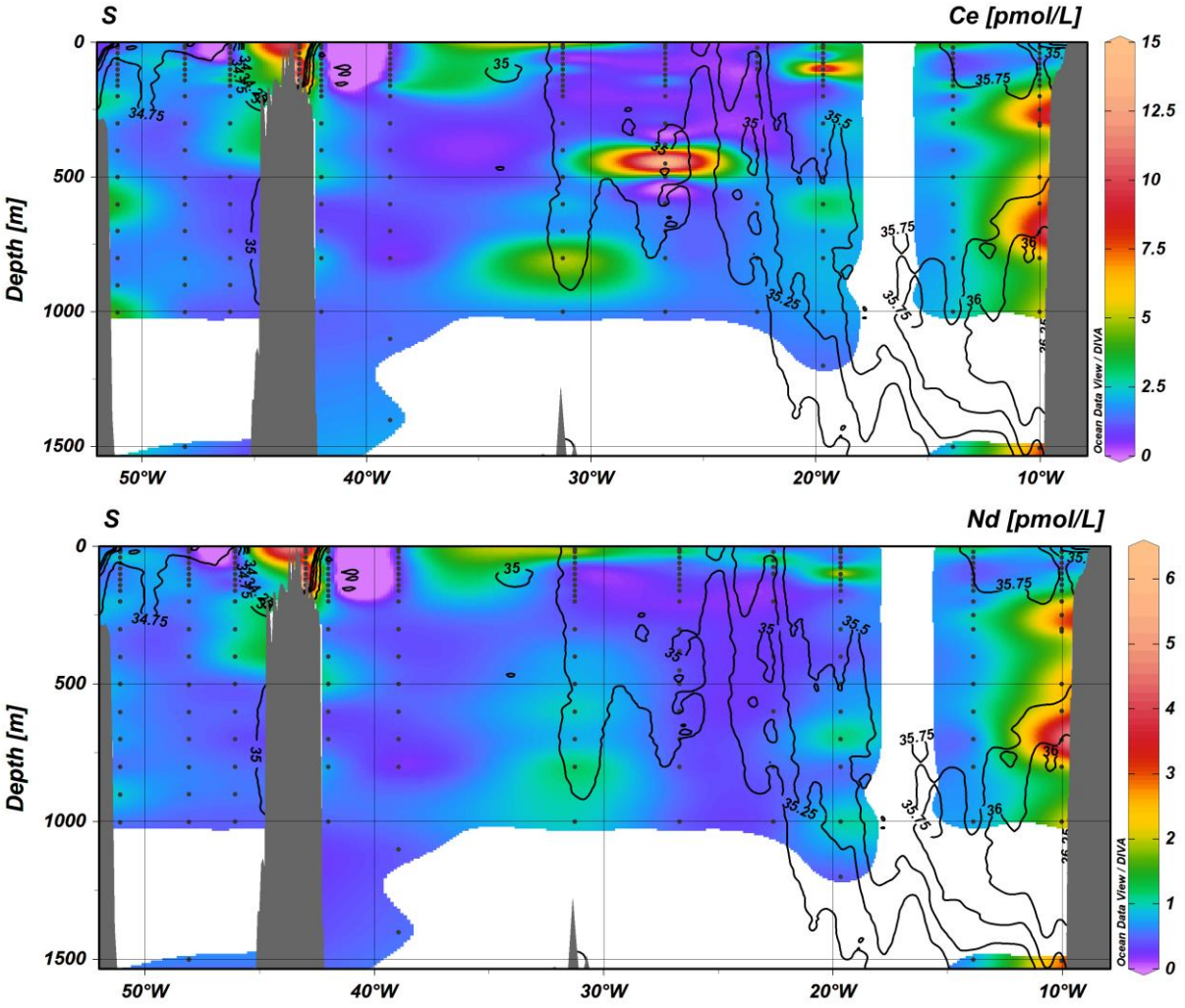

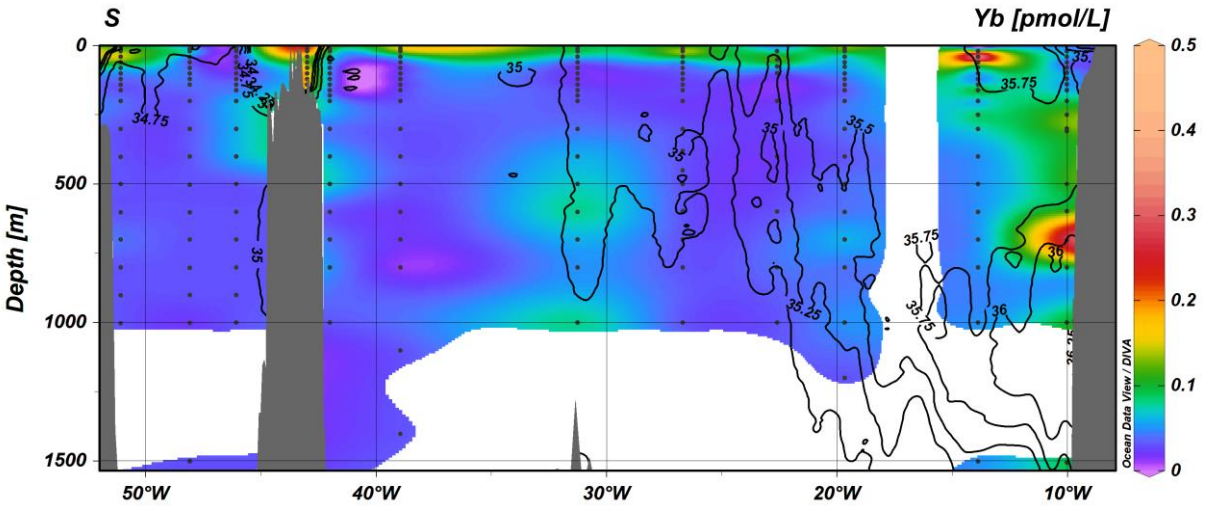

- the tables do not have units

Units were added in the table 2 and in the caption, line 821.

-some data, eg. Ac data, are not shown and not trackable by the reader, so discussions cannot be verified by the reader. For instance in lines 257-259 and 263-264.

Indeed. We are now referring to Emilie Le Roy's thesis, line 359. This work is available online.

- There are many places with missing citations. These are highlighted in the pdf.

Thank you. Citations were added when required, see revised MS.

- Parts of the discussion is found in figures in the supplement. It is awkward for the reader to keep having the supplement at hand to follow the discussion.

Figures were reorganized to prevent this. In particular, the section dealing with Ce anomalies was re-written and does not refer to the supplementary material anymore.

- The paper does not come to any conclusions is that intended in this format?

This is a mistake, we now provide a conclusion: see revised MS lines 516-547.

Detailed comments

L22: This needs to be formulated more clearly why this connection is drawn. Also, be consistent with PREE: When you use just REE or HREE without the 'P' it could be interpreted that your are not referring to particles.

Done, see revised abstract (lines 10-26).

L24 These 2 sentences appear out of place and attempt to state what has not been mentioned up to here. Please provide more information or leave them out.

We added more information, see revised abstract.

L29 what does this number refer to? Particle concentration, dust, algae?

It refers to particle concentration, it is now specified line 31.

L31 I know what you mean here, but this needs to be rephrased. Maybe start with "Elemental concentrations are..."

It was rephrased, see lines 36-37.

L39 Either formulate this as a hypothesis or provide a citation.

References were added line 36.

L41-49 This paragraph needs citations. There is not a single one

Citations were added, see lines 42-50.

L53 How does this quantification work then? What would be the approach using REE?

Precisions about the use of REEs were added lines 52 to 61.

L60 What does 'SP' then stand for. I assume Sub Polar - this should be added.

Yes, it is, it was added line 72.

L71 Please list them here.

The biogeochemical provinces are listed, see line 83-84.

L72 It is not clear how this diversity has been catergorised. The figure does not really show the distribution of water masses. There are only labels and the reader is let to find the actual extend of the water masses.

The biogeochemical features of each region are developed in the paragraphs following L72 (line 86 in the revised manuscript). We choose to stay concise when describing features since they are described in details in Lemaitre et al. (2018b) and Longhurst, (1995). The labels represent the dominant water mass, it is specified in the manuscript lines 85, and the meaning of the labels was added to the caption and to the abbreviation table (lines 836-840). We do not provide information of the extension of the water

masses because this is beyond the scope of a work discussing the PREE distributions. We are currently measuring the dissolved REE which will allow discussing dissolved and particulate data regarding the water masses.

L80 Please remind the reader where this region is geographically.

It is reminded at the beginning of the paragraph, line 93.

L101 This pool is not presented here (unfortunately).

It is a work in progress (see responses to Reviewer 1 as well).

L104 should be defined to be consistent

It is now defined lines 114 and 116.

L108 not shown in this figure.

It is now shown on the Fig. S4 in supplementary.

L110 be more precise. REE are trace metals too

Fe and Zn were given as examples, see line 181.

L113 the range given in the introduction is only 1 km wide.

This has been corrected, line 117-118.

L114 pressurised with what? Normal air? filtered air? Nitrogen gas?

It was normal air.

L115 Link? Not everybody is familiar with the GEOTRACES cookbook and its content.

The link was added line 119.

L118 was this buffered?

No, it was not buffered.

L121 Nevertheless, it should be briefly summarised here.

This section has been rewritten and clarified lines 130-136 and 188-191. We also provided a table in Fig. S4 to summarize the differences between the two sampling systems and analytical procedures performed on the filters. Results of this comparison are also provided graphically.

L126 Was the filter fully digested after this step?

Yes, it was fully digest. It was added line 142.

L141 Please give some more details

Details are provided in lines 164-165, and Fig. S2 was added in supplement to show the percentage of difference between replicates for each element analyzed.

L144 Were those values revised accordingly?

Yes, the blank was subtracted to the measured concentrations, it was added line 168.

L149 I do acknowledge that error propagation was not disregarded, however figure S2 does not provide any details, nor does the supplement.

The error propagation was reconsidered, and this part has been rewritten, see lines 169-176 and Fig. S3.

L150 what is the evidence of this 'apparent consistency'?

Particles seem to have a homogenous repartition on the filters to the naked eye. That said, we do not discuss more the hypothesis of homogeneity since we cannot quantify a difference between the two parts of a filter.

L154 It would be good to provide the reader with the main differences of the 2 methods.

This section was reworded for clarification, see lines 130-136, 188-191 and Fig S4.

L157 I do not know in which context the two studies are. What are the similarities? what are the differences?

See the rewritten section in lines 177-194 and Fig. S4.

L164 Do you really need to provide the isotope number of natural Th? Until now there are no other Th isotopes mentioned. You can state in the beginning that you will discuss 232Th which will be termed 'Th' throughout the text. Just a suggestion...

We prefer to keep it in, for sake of clarity.

L166 Please avoid abbreviations in the beginning of sentences.

An effort was made to delete abbreviations at the beginning of sentences.

L167 This is a bit over-simplified and lacks citations.

This short introduction to the specific behavior of Ce was completed, see lines 200-207.

L170 That is very ambiguous. Could you be more specific?

Precisions were added lines 209-210.

L174 You will need to increase the resolution of the pots to verify this as reader.

The upper 200 m were enlarged on Fig. 2B, 3C and 3D.

L176 terminology: the figure refers to sub-arctic front instead.

This is the sub-arctic front, it was revised, see line 218.

L179 provide depth range to remind the reader where this bottom is. Particularly, because you have change the range from the introduction

The depth ranges were added, see line 220.

L187 There are only PAAS normalised patterns for other PREE in the supplementary, no concentrations.

A reference to table 2 is now added in line 196. Normalized concentrations allow a comparison between concentrations. We show that they are higher close to the Iberian margin, so we decided to keep the reference to the patterns.

L197 remind the reader at which depth we are.

It is reminded, see line 237.

L208 I suggest to summarise these in a table and/or figure

It is summed in a table, added in Fig. S5.

Reference	Location	Sampling method	Nd (pmol L^{-1})	Ce (pmol L^{-1})	Yb (pmol L^{-1})
Kuss et al. (2001)	Along the 20°W meridian between 30°N and 60°N	Samples pumped and centrifuged from several m^3 of water at a depth of 7 m (n=24)	0.17 to 2.16 Average 0.67	0.2 to 4.9 Average 0.82	0.03 to 0.47 Average 0.13
Tachikawa et al. (1999)	Tropical northeastern Atlantic	*In-situ* pumps at 3 stations (an eutrophic (E), a mesotrophic (M) and	E: 0.7 to 10.5 M: 0.3 to 2.6	E: 2.5 to 24.6 M: 1.0 to 5.5	E: 0.04 to 0.5 M: 0.02 to 0.09

	(20°N, 18-31°W)	an oligotrophic (O) sites), filtration of 30 to 995 L	O: 0.1 to 0.5	O: 0.4 to 1.1	O: 0.05 to 0.03
This study	Subpolar North Atlantic (40-60°N,10-55°W)	Niskin bottles	0.1 to 6.1	0.2 to 16.3	0.01 to 0.50

L213 This is a bit confusing to me. Your transect within this region is rather meridional. Do you mean the southern part by 'to the east'? Please clarify. Also while checking this in your table, I noticed that you did not provide any units.

South east would be more exact, it is specified line 258. Units are provided in Table 2.

L214 This is not a discussion. This is just a comparison of 2 different studies in two different regions. Tachikawa's study is more than 20 degrees further south than your southernmost station. If you want to compare the studies, you have to be more thorough in explaining the differences from your study. As it is now, it reads as if theses study areas are very lose to each other actually comparable.

It seemed interesting to us to compare our results to this study because it described PREE behavior in three very different contexts, with a station located in an eutrophic area, another one in an mesotrophic area and the last one at an oligotrophic site. These authors highlighted differences in PREE distributions and Ce anomaly profiles between the three sites, revealing different processes depending on the type of the station. It provides a wide range of concentrations to compare our data. Our stations can be compared to eutrophic/mesotrophic/oligotrophic types, and we discuss our results in the light of these sites, especially in the part about the Ce anomaly, because comparable features are observed. Finally, to our knowledge, even located 20° south of our most southernmost station, this study is the closest study dealing with PREE in the literature. For all these reasons, it seemed important to us to provide details about the study at the beginning of the discussion.

L230 Can you explain the reader, why this fractionation might occur? You missed to explain the reader a bit on REE chemistry in the introduction (e.g free metal vs stable complex)

Information about REE chemistry in seawater were added in the introduction, lines 52-60.

L233 Which phases do you mean. Please repeat, because you have introduce a couple of more phases in lines 230 and 231.

It was repeated, see line 282.

L245 it's not yet percent unless you multiply by 100. Like this, I would term it 'fraction'

It was multiplied by 100, see line 297.

L246 you cannot subtract concentrations in different pools from each other. You have to factor them by the lithogenic fraction. In this case [REE]authi = ([REE]total - F x [REE])/(1-F). Or the other way around the [REE]total = F x [REE]lith + (1-F)x[REE]authi

It was revised, see lines 295-297.

L250 not correct - see comment on equation (3)

It was revised, see line 300.

L252 What does this mean. You only chose LREE without Ce? This is is OK, but (1) explain why and (2) you don't need to write '...on the one hand ...on the other hand...'

We choose not to take Ce into account because of its distinctive behavior. It was added line 303-304, and '...on the one hand ...on the other hand...' was deleted.

L257 by how much is this excess? It is not visible in the figure.

This excess is of a few per cent most of the time, and can be up to 550 % at the surface of station 1. The excess of a few per cent is within the uncertainties, when higher excess suggests authigenic Th. We developed the discussion about it lines 308-314.

L261 this is correct and you need to point out - assuming you talk about concentrations in the water column - that you can only compare the pattern, but not the absolute numbers.

Yes, only patterns were compared, not absolute concentrations.

L262 They're flat because you determined your lithogenic REEs via UCC, which is pretty much PAAS in the distribution pattern.

This is right, that part was deleted. Instead, we used the total flat patterns of station #1 and #13 to assess the validity of the UCC as a lithogenic source (lines 325).

L263 where do you show that?

It is not shown here as it was done by Rudnick and Gao (2014).

L265 Of course, as you compare dust from a specific region with your data I would not expect matching patterns.
Also if you would have determined your lithogenic REE via dust normalisation the pattern would be flat too. I think this is a circular argument.

We deleted this argument and replaced it : we use the UCC as a lithogenic reference because the GEOVIDE are is surrounded by shields and extended crust, and dust inputs were not significant during the GEOVIDE cruise (Shelley et al., 2017). See lines 325-328.

L270 Will you discuss about this?

Details were added lines 319-322

L276 Which maxima do you refer to? You talked about little LREE enrichment, but not about maxima (of what?).

It was specified line 336.

L278 bracketing and where were these samples taken from? The same region? What the values?

Samples were collected during the same cruise with the clean sampling system (samples used for the comparison in 2.3.2). For PFe, the values were also 100%. For PMn they were about 40% between 200 m and 250 m, and ranged between 60% and 75 % from 500 m to 1000 m.

L281 You do not have the data to prove that. station 53 is above the shelf. Station 51 to the east - still close to the continent - does not show this enrichment. To the west station 64 is already far away from the shelf. Or what do you mean by eastern end of the section?

This is a comparison with the intermediate nepheloid layers observed along the slope at station #1, at the south east of the section. It was reworded lines 358.

L291 where are these fractionated patterns to find and which 'other processes are at play'?

These are the patterns of station #77 presented in Fig. 5, and the other processes are discussed in the following parts. Fractionation by diatoms and precipitation of Fe and Mn hydroxides were added here as examples, lines 352-353.

L293 This paragraph jumps geographic regions and compares them amongst each other but differences are not discussed at all.

This paragraph was deleted as it was not helpful for the discussion.

L295 I'm confused here. Why do you have flat patterns in figure S3 and fractionated patterns in fig. 5?

Patterns were flat in Fig. S3 because they represent the lithogenic fraction, the patterns for total PREE were represented on Fig. 5.

L306 It is rather consistent with the high lithogenic fraction, but not really visible in PREE data.

This has been corrected, see line 362.

L310 You talk about data that the reader has no access to - therefore difficult to verify

See answer to minor comment 4.

L325 This section is very vague and not convincing. I am not sure what the aim of this discussion is.

L335 was it?

L338 You should show that and convince the reader that there is a relationship

L349 where do you have the residence time from?

L352 This is basically a discussion about supplementary material. Why is this not shown in the main paper?

For the five previous comments: the section was completely rewritten, see lines 379-441.

L360 there are a few statements in this paragraph without back up of citations.

Citations were added, see lines 442-483.

L647 Suggestion: Combine pMe and sal in one section plot using isolines for one parameter. You can still show your stations by slightly increasing the sample dots. I would also stronlgy encourage to zoom into the upper 250m where you have the highest variation in pMe.

See the answer to the second minor comment.

L661 Same here: Please zoom into the dynamic upper layer

The upper 200 m were enlarged on Fig. 2B, Fig.3C and D, Fig. 7B and Fig. 8.